The role of the inwardly rectifying potassium channel Kir5.1 in the distal convoluted tubule

DISSERTATION

ZUR ERLANGUNG DES DOKTORGRADES DER NATURWISSENSCHAFTEN (DR. RER. NAT.) DER FAKULTÄT FÜR BIOLOGIE UND VORKLINISCHE MEDIZIN DER UNIVERSITÄT REGENSBURG

Vorgelegt von

Catarina Isabel Rina Quintanova

aus Vila Franca de Xira, Portugal

Im Jahr

2017

Das Promotionsgesuch wurde eingereicht am: 05.12.2017

Die Arbeit wurde angeleitet von: Prof. Dr. med. Richard Warth

Unterschrift:

_____

(Catarina Quintanova)

Table of Contents

1. Introduction

1.1 Distal Convoluted Tubule

The kidney plays an important role in maintaining body electrolytes and fluid balance, blood pressure and in the regulation and maintenance of systemic acid-base balance. The nephron is the structural and functional unity of the kidney (Figure 1). This functional unit filters the blood, reabsorbs the filtered electrolytes, solutes and fluid and excretes excessive electrolytes and water.[1]

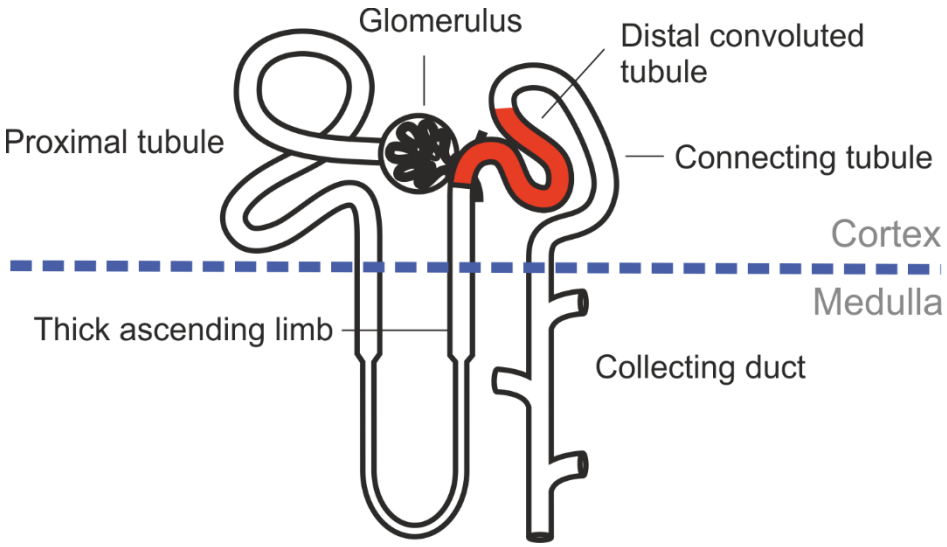

Figure 1. Schematic representation of a single nephron.
The nephron is the microscopic structural and functional unit of the kidney. It is composed of a renal corpuscle and a renal tubule. In the glomerulus, ultra-filtrate is continuously generated by filtration of the blood. In the adherent renal tubule, certain substances and water are either reabsorbed or secreted. The ultra-filtrate first reaches the proximal tubule—the main side of reabsorption—followed by the U-shaped loop of Henle including the thick ascending limb, where the filtrate is concentrated. Fine-tuning of the urine composition takes place in the distal convoluted tubule (red) and in the collecting ducts.

The distal convoluted tubule (DCT) is the shortest segment of the nephron and is the portion of the nephron that is immediately downstream from macula densa and ends in the connecting tubule/collecting duct system (CD). Despite its size, DCT plays an important role in regulating the extracellular fluid volume and electrolyte homeostasis in a variety of homeostatic processes that include sodium (Na^+) reabsorption, potassium (K^+) secretion, calcium (Ca^{2+}) and magnesium (Mg^{2+}) handling (Figure 2). The DCT can be further divided into two sub-segments, DCT1 and DCT2, which are distinguished by their response to the mineralocorticoid aldosterone. Aldosterone is a steroid hormone that is released from the adrenal glands in response to hyperkalemia and volume depletion. DCT2 is more sensitive to aldosterone due to the expression of an enzyme called 11-β hydroxysteroid dehydrogenase 2 (11-βHSD2) that metabolizes cortisol. Cortisol has a structure similar to

aldosterone, therefore by metabolizing cortisol to cortisone the enzyme 11-βHSD2 prevents the binding to the mineralocorticoid receptor expressed in the DCT2. The enzyme 11-βHSD2 is also expressed in connecting tubule (CNT) and CCD making these three segments known as the aldosterone sensitive distal nephron.[2,3,4,5,6]

DCT is morphologically unique since its extensive basolateral membrane has numerous deep infoldings and the cells are particularly rich in mitochondria. Because of very high rates of transcellular ion transport, the DCT requires a considerable amount of ATP high activity of Na^+/K^+-ATPase to maintain ionic gradients. It is therefore, not surprising that DCT cells possess the highest density of Na^+/K^+-ATPase along the nephron.[7,8]

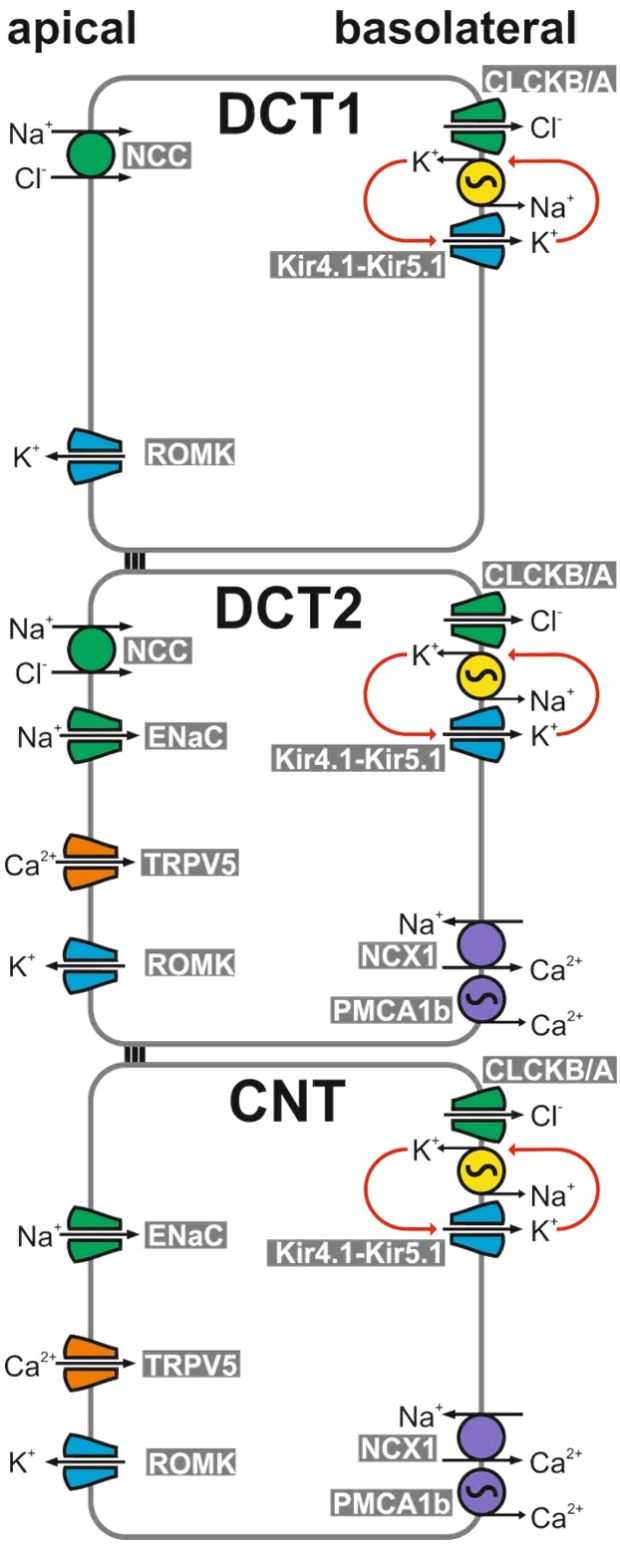

Figure 2. Schematic model of distal convoluted tubule and connecting tubule.
In the early DCT (DCT1), apical Na^+ reabsorption is exclusively mediated by NCC, whereas in the late DCT (DCT2) and connecting tubule (CNT). Na^+ reabsorption is also mediated by the epithelial Na^+ channel ENaC. Na^+ transport by ENaC is coupled to the activity of the renal outer medullary K^+ channel (ROMK) mediating K^+ secretion into the urine. The Na^+/K^+-ATPase mediates basolateral Na^+ efflux and K^+ uptake. The latter is functionally coupled to K^+ recycling through Kir4.1-Kir5.1. Apical Ca^{2+} transport is mediated by TRPV5 in the late DCT and connecting tubule. In the cytosol, Ca^{2+} is bound by calbindin and then transported out of the cell by NCX1 or plasma membrane Ca^{2+} ATPases (PMCA).

1.1.1 Reabsorption of Na^+ in the DCT

Regulation of Na^+ excretion is essential to control and maintenance of extracellular fluid balance and blood pressure control. Na^+ is mainly reabsorbed by proximal tubules (PT) and thick ascending limbs (TAL) with fine-tuning occurring in the distal convoluted tubule (DCT), connecting tubule (CNT) and collecting ducts (CD). The DCT cells are responsible for reabsorbing 5-10% of the filtered Na^+ and chloride (Cl^-) from the filtrate. The uptake of Na^+ in the DCT is mediated through the action of the NaCl cotransporter (NCC). NCC, also known as thiazide-sensitive Na^+ and Cl^- cotransporter, is localized in the apical membrane of DCT1. This process is electroneutral, since for one Na^+ cation one Cl^- anion enters the cell. NCC inhibition by thiazides, a class of diuretics, is used in the clinical setting for the treatment of arterial hypertension and edema. Thiazides inhibit Na^+ reabsorption by blocking NCC thereby decreasing the workload for the Na^+/K^+-ATPase. In parallel, urinary Na^+, K^+ and Mg^{2+} excretion increases. However, Ca^{2+} is less excreted (hypocalciuria). Hypocalciuria was postulated to be generated by two different mechanisms: either by increased active Ca^{2+} uptake via the vanilloid transient receptor potential channel 5 (TRPV5) in the DCT, or by thiazide-induced hypovolemia resulting in enhanced passive Ca^{2+} uptake in the proximal convoluted tubule.[9] Since the $TRPV5^{-/-}$ mice still developed hypocalciuria when given thiazide diuretics, an increased uptake of Ca^{2+} in the DCT seems less likely.[2,9–14]

Besides Na^+ uptake through NCC, Na^+ can also be taken up in DCT2 by the amiloride-sensitive epithelium Na^+ channel (ENaC). ENaC, mediates Na^+ influx and causes a depolarization of the apical membrane. This depolarization enhances the driving force for K^+ secretion across the apical membrane through the "renal outer medullary K^+ channel" (ROMK). The reabsorbed Na^+ is extruded at the basolateral side by the Na^+/K^+-ATPase. The activity of the Na^+/K^+-ATPase fuels further Na^+ transport across the tubular cells by keeping the intracellular Na^+ concentration low and the K^+ concentration high (Figure 2). [6,15]

1.1.2 Regulation of DCT K^+ transport

As mentioned above, sustained reabsorption of Na^+ by either NCC or ENaC requires basolateral Na^+ extrusion via the Na^+/K^+-ATPase. For ongoing activity of Na^+/K^+-ATPase, that exchanges three Na^+ for two K^+, the basolateral availability of K^+ can become a limiting factor, especially at high transport rates and when the basolateral space is narrow, i.e. in the basolateral infoldings of the plasma membrane. Therefore, basolateral K^+ channels serve two important functions: i) they hyperpolarize the membrane (which is important for voltage-dependent processes such as Cl^- exit through channels) and ii) the recycle of K^+

thereby allowing the ATPase to run at high transport rates. The functional coupling of the ATPase and the basolateral K^+ conductance (K^+ leak) is called "pump-leak coupling".[2,6,8,16]

Recently, a more prominent role of the DCT in the regulation of K^+ homeostasis was suggested by Terker and co-workers.[17] They hypothesized that DCT cells can actively sense changes in plasma [K^+] and indirectly modify K^+ secretion in CNT and CCD through regulation of the NCC. Reduced NCC activity leads to an enhanced Na^+ flux to CNT and CCD where Na^+ is then replaced by K^+. They suggested, that the plasma K^+ sensor Kir4.1 (and Kir4.1-Kir5.1) that senses increases in plasma [K^+] by translating it into a depolarization of DCT cells. This depolarization, in turn results in increased intracellular [Cl^-] by reducing the driving force for Cl^- efflux via ClC_{kb} channels. Increased intracellular [Cl^-] then was proposed to lead a decrease in phosphorylation of NCC via the inhibition of the Cl^--sensitive WNK-SPAK/OSR1 kinase pathway ultimately leading to decreased Na^+ reabsorption in the early DCT (Figure 3).[17,18] The resulting elevated luminal Na^+ ions would be reabsorbed in more distal segments via ENaC leading to ROMK-mediated secretion of K^+ and normalization of elevated plasma K^+ levels.

Narrow regulation of plasma K^+ between 3-6 mM concentrations is vital for life. Depending on plasma K^+ levels, the kidney can vary the fraction excretion of K^+ from 1% (net reabsorption) to 200% (net secretion) meaning that the kidney is a main contributor to K^+ homeostasis. This flexibility is a property of the aldosterone-sensitive distal nephron including collecting ducts. In the early DCT, secretion of K^+ is low and increases along the distal tubule parallel to the increase in lumen-negative transepithelial voltage observed in the late DCT. ROMK mediated K^+ transport depends on the driving force for K^+ secretion which is mainly determined by the aldosterone-regulated ENaC-mediated Na^+ reabsorption. The increased activity of ENaC depolarizes the apical membrane, which is a stimulus for K^+ efflux through ROMK. Other channels may be involved in K^+ secretion Maxi-K^+ channels (BK channels). BK channels are triggered in states of high urinary flow (during diuretic use, for example) leading to an increase of K^+ secretion under these conditions.[2,5,19]

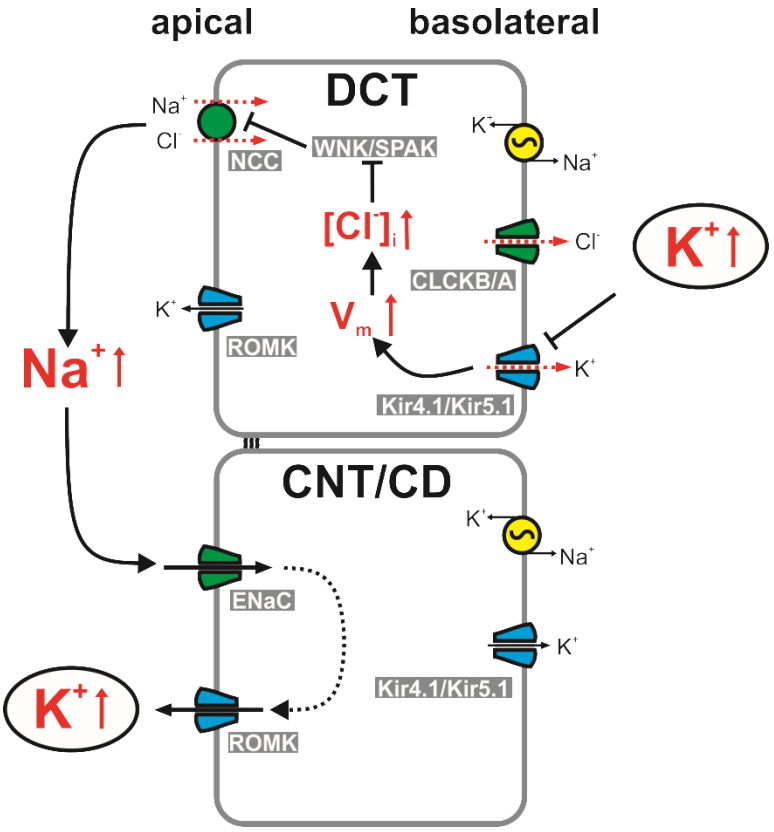

Figure 3. Model of K^+ sensing and regulation in the distal tubules.
In the distal convoluted tubule DCT, elevated plasma K^+ levels are sensed by heteromeric Kir4.1-Kir5.1 channels leading to depolarization of the basolateral membrane potential (V_m), which in turn inhibits Cl^- efflux via ClC_{KB} channels. The resulting increased intracellular [Cl^-] blocks the Cl^--dependent kinases in the WNK/SPAK pathway, which in turn inhibits the activity of the Na^+/Cl^--cotransporter (NCC) resulting in elevated luminal Na^+ levels. Apical Na^+ is reabsorbed in the more distal connecting tubule (CNT) and collecting duct (CD) by the epithelial Na^+ channel (ENaC) ultimately leading to K^+ efflux via the renal outer medullary K^+ channel (ROMK) effectively correcting the elevated plasma K^+ levels.

1.1.3 Ca^{2+} reabsorption in the DCT

Extracellular Ca^{2+} is tightly regulated and serves as intracellular messenger in numerous essential cellular events such as immune response, muscle contraction, hormone secretion and regulation of enzymes. Ca^{2+} is regulated in the renal tubules by several calciotropic hormones including parathyroid hormone (PTH), 1,25-dihydroxyvitamin D3 (vitamin D3), calcitonin and Ca^{2+} itself. PTH and vitamin D3 are known to increase Ca^{2+} reabsorption in TAL, DCT and CNT. Plasma Ca^{2+} also controls renal Ca^{2+} absorption through altered PTH secretion and by binding to the Ca^{2+}-sensing receptor (CaSR) in the TAL. To facilitate paracellular Ca^{2+} reabsorption along renal tubules, transepithelial voltage difference needs to be favorable paracellular Ca^{2+} passage, meaning a positive voltage in the apical side. For transcellular reabsorption, Ca^{2+} can enter through apical channels and needs to be extruded in an energy consuming process on the basolateral side.[9,20–22]

In the kidney, transcellular Ca^{2+} reabsorption is restricted to the late DCT and CNT. Only 5-10% of filtered Ca^{2+} is absorbed in DCT in a three-step process. In the DCT, the transport of Ca^{2+} is passively mediated by TRPV5 channels on the apical membrane. The reabsorbed Ca^{2+} is then bound to cytosolic calbindin-D_{28K}, which is involved in transcellular Ca^{2+} diffusion and buffers cytosolic Ca^{2+} to maintain a low intracellular concentration. Ca^{2+} then is basolaterally extruded by secondary active transport through Na^+/Ca^{2+} exchanger (NCX1) and across Ca^{2+}-ATPase (PMCA 1-4). NCX1 controls intracellular Ca^{2+} levels by extruding Ca^{2+} from the cell. In the kidney, NCX1 is expressed in the basolateral membrane of DCT2 and CNT and actively transport Ca^{2+} back to basolateral side due to electrochemical gradient created by Na^+/K^+-ATPase playing a key role in the process of renal transcellular Ca^{2+} reabsorption.[10,12,20,23,24]

1.2 DCT disorders

Mutations in renal ion transport systems can lead to distinct salt-losing nephropathies, which demonstrate the kidneys' crucial role in fluid and electrolyte homeostasis.

1.2.1 Gitelman's syndrome

Gitelman's syndrome mimics the effect of long-term thiazide treatment and is an autosomal recessive salt-wasting kidney disease characterized by hypokalemia, hypomagnesemia, decrease of Ca^{2+} in urine and elevated blood pH (metabolic alkalosis). The disorder is caused by genetic mutations resulting in improper function of the thiazide-sensitive NCC in the DCT.[6,10] In more than 80% of the cases, Gitelman's syndrome can be linked to inactivating mutations in SLC12A3 that encodes the NCC. Due to inactivation of the NCC, the reabsorption of Na^+, Cl^- and Mg^{2+} is reduced in the DCT while proximal Ca^{2+} reabsorption is increased as discussed earlier (Section 1.1.1).[13,25] The CNT and CD compensate the loss of Na^+ by activation of ENaC to some extend leading to secretion of K^+ and H^+. Ultimately, Na^+, K^+, H^+, Mg^{2+} and Cl^- are wasted into the urine leading to the above-mentioned symptoms of hypokalemia, hypomagnesemia, hypocalciuria and alkalosis. Additionally, the loss of Na^+ leads to hypovolemia with secondary increased aldosterone levels. [3,13,26,27]

1.2.2 Familial hyperkalemic hypertension (Gordon syndrome)

Familial hyperkalemic hypertension (FHHt) is a rare monogenic hypertensive disease also called pseudohypoaldosteronism type II. FHHt results from mutations in the genes encoding the WNK kinases (serine/threonine kinases) or regulatory proteins and is characterized by hyperkalemia and hypertension and hyperchloremic metabolic acidosis.[28,29] The common result of all mutations is the modulation of NCC activity. For example, WNK4 inhibits the

activity of NCC, while mutations in SPAK and OSR1 activate those kinases, which results in phosphorylation and activation of the NCC and other cotransporters, thereby increasing Na^+ reabsorption and K^+ secretion by ROMK. However, other WNK4 mutation can have a stimulatory effect on NCC by reducing its inhibitory effect on NCC trafficking and increasing NCC surface expression (Figure 3). Another kinase, WNK1 can inhibit wildtype WNK4 and activate SPAK and OSR1 stimulating NCC surface delivery and phosphorylation.[2,5,18,28]

Recent models suggests that the DCT senses changes in plasma [K^+] that affects NCC activity. Increases in plasma [K^+] depolarizes the basolateral membrane, which leads to an increase of intracellular [Cl^-]. Afterwards, Cl^- binds to WNK kinases decreasing phosphorylation of NCC and therefore impairing NCC activity.[18,26]

1.2.3 EAST/SeSAME syndrome

To date, EAST/SeSAME syndrome is the only clinical distal tubular disorder known to affect a basolateral K^+ channel. Multiple loss-of-function mutations of KCNJ10 were found to cause EAST/SeSAME syndrome. The electrophysiological consequences of over 120 coding-region single nucleotide polymorphisms (SNPs) reported in publicly accessible genome databases still remain to be examined.[2,30,31]

The medical relevance is underlined by the pathophysiology of the EAST/SeSAME syndrome, a disorder in which an inwardly rectifying K^+ channel causes a hereditary form of renal salt wasting tubulopathy. The tubulopathy is characterized by hypokalemia, metabolic alkalosis, hypomagnesemia and hypocalciuria – a pattern reminiscent of the symptoms in Gitelman's syndrome. In contrast to Gitelman's syndrome, in which only the kidneys are affected, the EAST/SeSAME syndrome is a pleiotropic disease. The acronym "EAST" stands for epilepsy, ataxia, sensorineural deafness and tubulopathy. The acronym "SeSAME" stands for seizures, sensorineural deafness, ataxia, mental retardation and electrolyte imbalance. Both acronyms refer to the same genetic disease and are caused by loss-of-function mutations of Kir4.1 (encoded by the KCNJ10 gene).

Kir4.1 is a basolateral K^+ channel in DCT, CNT and cortical CD. The disease-causing mutations diminish or completely abolish its function and, therefore impair transcellular electrolyte transport in those nephron segments. [16,30,32–37]

1.3 Classification and function of K^+ channels

K^+ channels are located in most cell membranes and control transportation of K^+ ions efflux from and influx into cells. They play crucial roles in excitable and non-excitable cells. K^+ channels have two to six transmembrane domains (TMs) spanning the lipid bilayer. Based

on the structure and function, the channels are categorized into three major classes: the voltage-gated (Kv) (six TMs), inwardly rectifying (Kir) (two TMs), and tandem pore domain (K2P) (four TMs) channels.[38,39]

K^+ channels have a similar structure that does not dependent on which class they belong. The common protein structure can be divided into two parts: the pore-forming domain and the regulatory domain. The pore-forming domain is responsible for transportation of K^+ ions and its structure is similar in all types of K^+ channels. The regulatory domain senses diverse stimuli and its structure differs among the classes. The basic organization of K^+ channels is a tetramer with each monomer containing one pore-forming domain. Four pore-forming domains comprise a pore through which the ions are transported. K^+ channels are highly selective and about 10 000 times more permeant for K^+ than Na^+ and are tightly regulated. K^+ channels usually can be found in different opening states: resting, activated, and inactivated. In the resting state, the channels are closed and can be opened after activation stimuli, followed by turning to the nonconductive states.[5,38,39]

1.3.1 Inwardly rectifying K^+ channels

Inwardly rectifying K^+ channels (Kir) were firstly described as anomalous rectifier K^+ currents. The Kir channels, under physiological conditions generate large K^+ conductances at negative potentials close to K^+ equilibrium potential and have the ability to maintain the resting membrane potential. The unique feature of Kir channels is that they conduct K^+ ions on hyperpolarization, rather than on depolarization as in other K^+ channels.[38,40,41]

Kir channels basic molecular structure is common to all Kir, it includes two putative membrane-spanning domains (TM1 and TM2) linked by an extracellular pore-forming region and cytoplasmic amino (NH2-) and carboxyl (COOH-) terminal domains. The C-terminal cytosolic domain is rich in β-sheets and is located below the pore-forming domain, extending the ion conduction pathway. The cytosolic domain also forms a binding site to interact with diverse intracellular regulatory mediators. Multiple ion binding sites in this domain are conserved and are critical to inward rectification. To form functional Kir channels, four subunits with two TM domains each are necessary to complete an ion channel in a tetrameric complex. [38,40,42,43]

Kir channels have diverse physiological functions in the cell, depending on their type and location and are modulated by various mediators, such as ions, phospholipids, and binding proteins. Several Kir subunit genes were identified and can be classified into seven subfamilies (Kir1.x–Kir7.x, where x is the number of each member) that belong to four functional groups: classical Kir channels, G protein-gated Kir channels, ATP-sensitive K^+

channels and K^+-transport channels. Kir4.1 (encoded by KCNJ10) and Kir5.1 (encoded by KCNJ16) belong to the K^+-transport channels and will be further discussed.[38,40,44] The homology between the Kir channels permits homomeric and heteromeric combinations to form functional channels. Usually, heteromerization occurs between members of the same subfamily as with Kir4.1 and Kir5.1.[38–40]
Kir channels are involved in maintenance of a negative resting membrane potential, potassium buffering, extracellular glutamate clearance, myelination, cell volume regulation and control of excitablility.[31,41]

1.3.1.1 KCNJ10 (Kir4.1)

KCNJ10 was first cloned from a rat brain cDNA library and as a member of the Kir family and requires four subunits to form a functional channel. Kir4.1 can be found as a homomeric or heteromeric channel complex. Kir4.1 expression was found in the brain, inner ear, retina (Müller cells) and kidneys. In kidneys, Kir4.1 is specifically localized in the basolateral membrane of renal tubules from TAL, DCT and CCD.[36,39,40,45]

In the brain, Kir4.1 is involved in K^+ homeostasis and maintenance of membrane potential. Studies with Kir4.1$^{-/-}$ mice revealed that in glial cells the resting membrane potential is less negative suggesting that Kir4.1 may be essential to K^+ recycling.[39] In the inner ear, Kir4.1 channels are expressed as a homomeric channels in the stria vascularis and contributes to the formation and maintenance of the endocochlear potential. It has been suggested that mutations in KCNJ10 impair K^+ secretion and alter composition and potential of the endolymph.[46,47]

In the kidney, Kir4.1 subunits were prominently expressed along TAL, DCT and more distal segments.[31,48] In these nephron segments, Kir4.1 is necessary for K^+ recycling across the basolateral membrane maintaining the gradient necessary for the activity of Na^+/K^+-ATPase. Kir4.1 is also involved in maintaining the electrolyte transport in the DCT, documented by the loss-of-function mutations in Kir4.1.[16,30,41,49]

Kir4.1 channels expressed in heterologous expression systems are characterized by a high open probability (P_o ~ 0.9) and a single channel conductance of around 20 pS and a rather weak sensitivity to changes of the intracellular pH around physiological values.[30,50,51] Recent studies reported that the major contributor to the basolateral membrane conductance in DCT cells is an inward channel with single channel conductance between 40-45 pS. It has been proposed that the channel is composed by Kir4.1 and Kir5.1, a heteromeric Kir channel.[39,52–55]

1.3.1.2 KCNJ16 (Kir5.1)

Kir5.1, like all other Kir family members, requires four subunits to form a functional channel. The channel may be either homo- or heteromeric, however homomeric Kir5.1 channel complexes do not produce detectable K^+ currents in expression systems.[56] KCNJ16 is localized in the brain, kidney, spleen, adrenal glands and cochlea.[10,39,40]

Even though homomeric Kir5.1 does not seem to form functional channels, expression of Kir5.1 was observed in fibrocytes in the spiral ligament of the lateral wall of the cochlea (Figure 4). The distribution of Kir5.1 is distinct from that of Kir4.1 in the inner ear. Since homomeric Kir5.1 is likely not forming a functional channel, the localization of Kir5.1 without the presence of Kir4.1 is puzzling, although a role of Kir5.1 in the hearing process was suggested.[40,46] Besides heteromerization with Kir4.1, Kir5.1 might form heteromeric channel complexes with its close homologue Kir4.2. Kir4.2 is encoded by KCNJ15 and its expression was found in kidney, brain, lungs, liver and pancreas. In pancreas, Kir4.2 is involved in the resting membrane potential of β-cells, preventing membrane depolarization.[39] The co-expression of Kir5.1 and Kir4.2 affects the sensitivity of Kir4.2 to intracellular pH and changes the rectification properties and stability of heteromeric complexes. The formation of Kir4.2-Kir5.1 heteromers may form in tissues where Kir4.1 is not expressed, for example in the pancreas.[39,57,58]

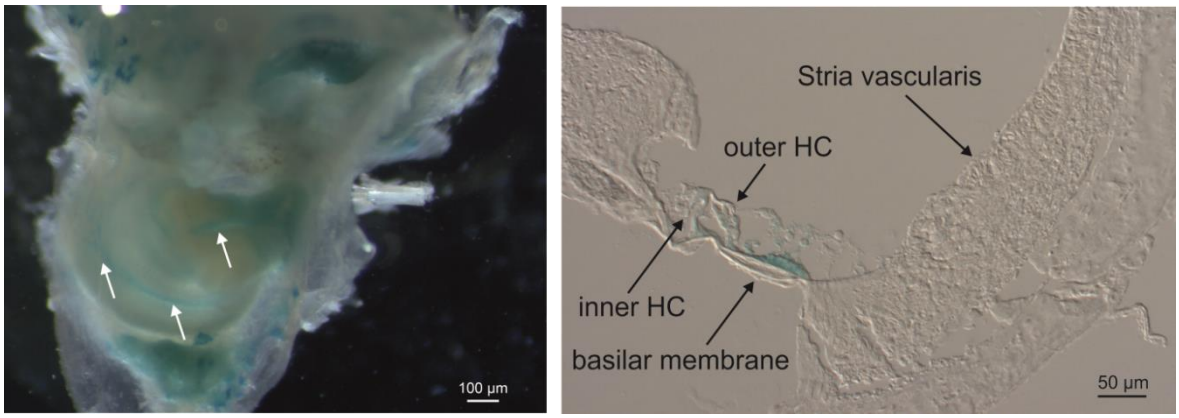

Figure 4. Kir5.1 promotor-driven X-Gal staining of mouse cochlea.
Blue staining indicates promotor-driven X-gal staining in transgenic Kir5.1$^{-/-}$ mice carrying the LacZ gene within the gene locus. The spiral shaped blue color of positive cells was observed in the turns of Kir5.1$^{-/-}$ cochlea (white arrows on the left). Positive staining on a cochlea section was visible in the organ of Corti and hair cells (black arrows on the right). Abbreviation: HC, hair cells; X-Gal, 5-bromo-4-chloro-3-indolyl-β-D-galactopyranoside; LacZ, lactose operon.

Expression of Kir5.1 in the kidney is mainly found in the distal nephron segments that consists of TAL, DCT and CNT/CCD where it co-localizes with Kir4.1. Due to the nature of Kir5.1, it most likely associates with Kir4.1. Heteromeric Kir4.1-Kir5.1 have been shown to have pH sensitivity in the physiological intracellular range (pKa ~ 7.45). Kir5.1 seems to

confer an enhanced sensibility to intracellular pH to Kir4.1-Kir5.1 channels.[36,39,55,59] The pH sensitivity of Kir4.1-Kir5.1 heteromeric channels in the physiological pH range has led to the assumption that Kir4.1-Kir5.1 might be a good candidate for CO_2 chemoreception. The pKa of 7.4 might allow those channels to regulate membrane potentials in response to modest changes in pCO_2. Cui et al. discovered that in the oocyte expression system heteromeric Kir4.1-Kir5.1 channels were modulated by changes in pCO_2 leading to changes of the membrane voltage. Therefore, the cells could detect states of hyper- and hypocapnia and translate it into a modified membrane excitabiliy. However, the precise contribution of Kir4.1-Kir5.1 to chemosensation is still a matter of debate, since the loss of Kir5.1 appeared to be compensated thereby leaving the ventilatory responses intact.[60–62]

In Kir5.1$^{-/-}$ mice, it was observed that in the absence of Kir5.1 the remaining K^+ channel present in DCT had a conductance of ~25pS instead of ~50pS observed in control animals. This smaller single channel conductance is typical for homomeric Kir4.1 channels indicating that the physiological K^+ channels in mouse DCTs are heteromeric Kir4.1-Kir5.1 channel complexes. Co-expression of Kir4.1 and Kir5.1 subunits lead to the formation of a 40-60 pS single channel K^+ conductance and a lower open probability (P_o ~ 0.4) when compared with homomeric Kir4.1. [50,51,54] The expression of heteromers in the basolateral membrane of the distal tubule was suggested to be involved in the recycling of the K^+ across the basolateral membrane, necessary for maintenance of the activity of Na^+/K^+-ATPase.[31,50,51,53,59] Deletion of KCNJ16 in mice led to a renal phenotype characterized by hypokalemia, hyperchloremic metabolic acidosis with hypercalciuria.[54] The authors concluded that disruption of KCNJ16 induces a severe renal phenotype that, apart from hypokalemia, is the opposite of the phenotype seen in EAST/SeSAME syndrome. This phenotype was attributed to increased mean basolateral K^+ conductance mediated by the remaining homomeric Kir4.1 channels in the distal nephron.[54,60,61,63]

For KCNJ16, unlike KCNJ10, no mutations have yet been associated with human pathologies. However, our collaborator Prof. Dr. Konrad Martin in Münster identified a patient, who suffers from renal salt wasting, hypokalemia and acidosis and has the c.104G>A mutation (NCBI Reference Sequence: NM_001291625.1) within the KCNJ16 gene (unpublished data). This mutation leads to the missense mutation p.Arg35Gln (R35Q) in KCNJ16 (UniProt: Q9NPI9), replacing the charged aliphatic arginine (R) to the neutral and polar amino acid glutamine (Q) (Figure 5). This mutation is located at the N-terminal region of the protein.

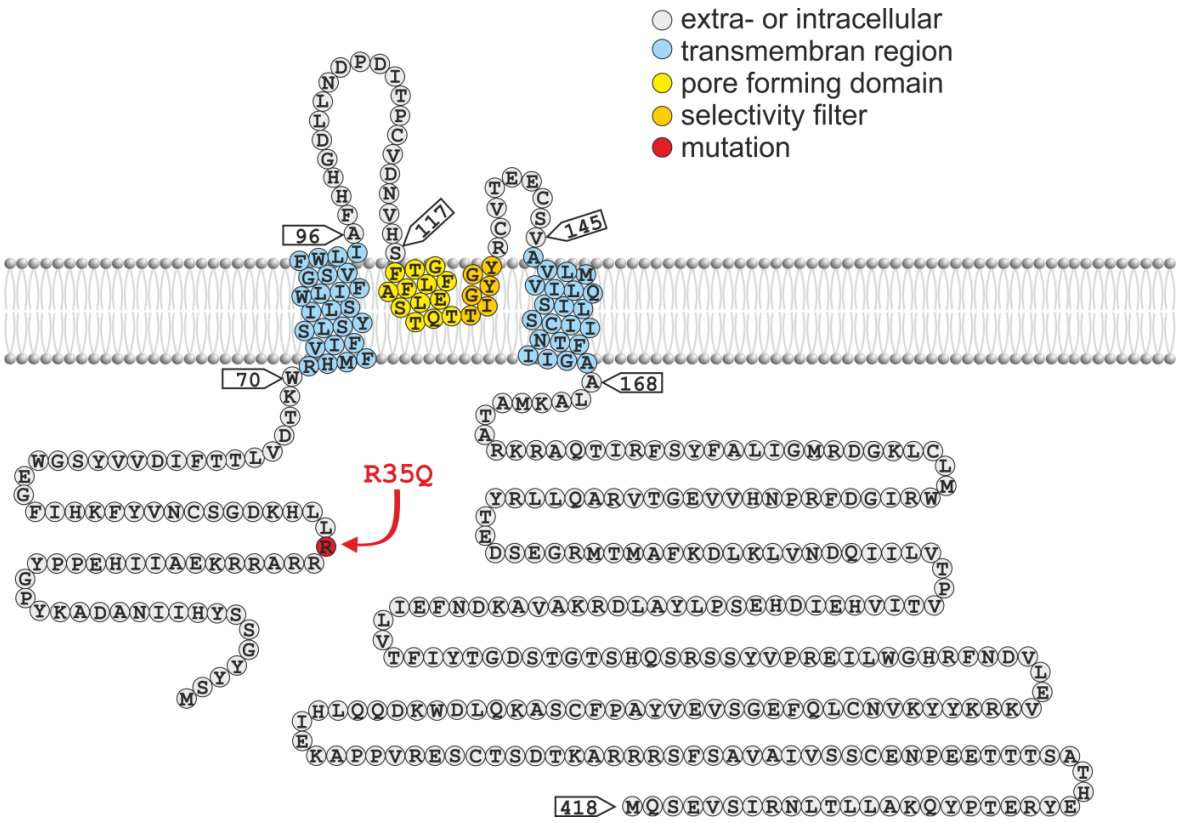

Figure 5. Schematic topology of human Kir5.1 (UniProt Q9NPI9).
Kir5.1 is an inwardly rectifying K^+ channel containing two transmembrane regions and a pore-forming region in between the two regions. The missense mutation p.Arg35Gln (R35Q) found in one patient with hypokalemic acidosis is located in the N-terminal region of the protein.

2. Objectives

Kir5.1 (KCNJ16) potassium channels are strongly expressed in the kidney. Previous work by Paulais and co-workers suggested that Kir5.1 together with Kir4.1 forms a basolateral K^+ conductance in distal convoluted tubules (DCT).[54] Moreover, these authors provided evidence that genetic inactivation of Kir5.1 leads to disturbed renal salt handling and hypokalemia. Surprisingly and in contrast to the alkalosis observed after inactivation of Kir4.1, knockout mice for Kir5.1 displayed metabolic acidosis. So far, no human disease has been linked to mutations of Kir5.1. Our collaborator Prof. Konrad, Münster, identified in a patient with hypokalemia and acidosis a homozygous missense mutation of Kir5.1 (R35Q) and he asked our group in Regensburg to test if this Kir5.1 mutant can be disease-causing or if it is only a rare variant.

Therefore, my thesis aimed at testing the hypothesis if i) the mutation R35Q leads to impaired channel function and ii) inactivation of Kir5.1 disturbs salt transport in the kidney, especially in the DCT, thereby creating a renal tubulopathy similar to the one observed in Prof. Konrad's patient.

To investigate the functional consequence of the R35Q mutant, I co-expressed Kir5.1 and Kir4.1 in a heterologous expression system and studied the subcellular localization of Kir5.1 and the electrophysiological properties in those transfected cells.

In the second part of my thesis, I studied the consequences of the Kir5.1 gene inactivation in mice *in vivo* with the focus on renal salt handling, pH homeostasis, K^+ induced Ca^{2+} signaling in DCT cells and respiratory control.

With these sets of experiments, I hoped to gain insights into the pathophysiology of a potentially novel human disease and to establish - or falsify - a genotype/phenotype correlation.

3. Materials and Methods

3.1 Material

3.1.1 Instruments

Instruments	Manufacturer
Blood Gas Analyzer pHOx plusM	Nova Biomedical, Rödermark, Germany
Cryostar NX70	Thermo Fisher Scientific, Dreieich, Germany
Cryostat Leica CM3050	Leica, Wetzlar, Germany
EPC 10 Amplifier Patch-Clamp	HEKA Elektronik Dr. Schulze GmbH, Pfalz, Germany
Gas mixer for Isoflurane-Vaporizer	MFI Föhr Medical Instruments GmbH, Seeheim, Germany
Incubator	Heraeus Instruments, Osteode, Germany
Inverted Microscope Axiovert 10	Zeiss, Jena, Germany
Inverted Microscope Axiovert 200	Zeiss, Jena, Germany
Inverted Microscope Observer Z.1	Zeiss, Jena, Germany
Ion Chromatography ICS-1600 Dionex	Thermo Fisher Scientific, Dreieich, Germany
Isoflurane-Vaporizer	MFI Föhr Medical Instruments GmbH, Seeheim, Germany
Laminar Flow	Thermo Fisher Scientific, Dreieich, Germany
Light-Cycler LC480	Roche, Mannheim, Germany
Microcentrifuge	Hettich, Tuttlingen, Germany
Microtome (Rotary microtome RM2165)	Leica, Wetzlar, Germany
Millicell® ERS-2 Voltohmmeter	Merck, Darmstadt, Germany
Mini Trans-Blot Cell	Bio-Rad, Munich, Germany
Mini-PROTEAN Tetra Vertical Electrophoresis Cell	Bio-Rad, Munich, Germany
NanoDrop 2000c Spectrophotometer	Thermo Fisher Scientific, Dreieich, Germany
NOVOstar Microplate reader	BMG Labtech, Ortenberg, Germany
NOVOstar Microplate reader	BMG Labtech, Ortenberg, Germany
O_2 sensor Oxydig	Dräger, Ultra Medical GmbH, Saarbruecken-Gersweiler, Germany
Paraffin incubator	Modell 300, Memmert, Schwabach, Germany
PatchStar Micromanipulator	Scientifica, United Kingdom
Perfusor	Precidor 902681, Infors AG, Bottmingen, Switzerland
Peristaltic perfusion system PP52	Multichannel systems MCS GmbH, Reutlingen, Germany
pH electrode	Schott Geräte, Mainz, Germany
Plethysmography chamber	EMKA Technologies Company, USA
PowerLab 4/30	ADInstruments Ltd., United Kingdom
PowerPac Basic Power Supply	Bio-Rad, Munich, Germany
Roller pump	Ismatec SA., Zurich, Switzerland
Scale (EK-600)	A&D Instruments Ltd, Tokio, Japan
Sound-attenuated chamber	Industrial Acoustics, Niederkrüchten, Germany

Surgery instruments	FST, Bad Oeynhausen, Germany
Thermomixer 5436	Eppendorf GmbH, Hamburg, Germany
Warm plate for mouse operations	Dr. J. Barhanin, Nizza, France
Warm plate for paraffin	HI 1220, Leica, Wetzlar, Germany
Water bath	Modell W13, Haake, Karlsruhe, Germany

3.1.2 Laboratory Material

Products	Manufacturer
0.5 ml Insulin-syringe	BD Micro-Fine+, BD Consumer Healthcare, Heidelberg, Germany
96-well plate	Nuclon Surface, Nunc A/S, Roskilde, Denmark
96-well Polymerase chain reaction (PCR) Plate, white	Nerbe Plus GmbH, Winsen/Luhe, Germany
Blood gas capillary	Hirschmann Labor geräte GmbH & Co. KG, Eberstadt, Germany
Cell culture flasks (T-25, T-75)	Nuclon Surface, Nunc A/S, Roskilde, Denmark
Cell Culture Inserts, 0,4µm PCF, 12mm diameter	Merck Millipore, Darmstadt, Germany
Cell culture plates (6-well, 12-well, 24-well)	Nuclon Surface, Nunc A/S, Roskilde, Denmark
Cell scraper	TPP Techno Plastic Products AG, Trasadingen, Switzerland
Coverslips	A. Hartenstein GmbH, Würzburg, Germany
DePeX mounting medium	Serva Electrophoresis GmbH, Heidelberg, Germany
Epoxy embedding medium	Sigma, Taufkirchen, Germany
Eppendorf microplestle for 1,2 – 2 mL tubes	A. Hartenstein GmbH, Würzburg, Germany
Eppendorf Tubes (0,2 ml, 0,5 ml, 1,5 ml, 2 ml)	Eppendorf AG, Hamburg, Germany
Falcon tubes (15 ml, 50 ml)	Greiner bio-one, Frickenhausen, Germany
Filter paper	GE Healthcare Life Sciences, Buckinhamshire, UK
GeneRuler™ DNA Ladder (50 bp, 100 bp, 1 kb)	MBI Fermentas GmbH, St. Leon-Rot, Germany
Latex gloves	Kimberly-Clark, Roswell, USA
Light-Cycler Capillaries	Roche, Mannheim, Germany
Millex-GP Syringe Filter Unit, 0.22 µm, polyethersulfone, 33 mm, gamma sterilized	Merck Millipore, Darmstadt, Germany
Millicell® Cell Culture Inserts, 0,4 µm	Merck, Darmstadt, Germany
Mortar	Rosenthal Technik, Tostedt, Germany
Nanosep Centrifugal	VWR International, Darmstadt, Germany
Non-fluorescent Glycergel mounting medium	DakoCytomation, Dakato North America Inc., Carpinteria, USA
Pasteur pipettes	Brand, Wertheim, Germany
Pestle	Rosenthal Technik, Tostedt, Germany

Petri dishes (p35, p60, p100 mm)	Nuclon Surface, Nunc A/S, Roskilde, Denmark
Pipette tips (10 µl, 200 µl, 1000 µl)	Sarstedt, Nümbrecht, Germany
Polysine microscope adhesion slides	Kindler, Freiburg, Germany
Polyvinylidene difluoride (PVDF) membrane	GE Healthcare GmbH, Freiburg, Germany
Serological Pipettes	Nerbe Plus GmbH, Winsen/Luhe, Germany
Tissue cassettes for paraffin blocks	A. Hartenstein GmbH, Würzburg, Germany
Tissue Tek OCT-Medium	Sakura Finetek Europe B.V., Zoeterwoude, Netherlands

3.1.3 Substances

Products	**Manufacturer**
0.9% NaCl isotonic solution	B. Braun Melsungen AG, Melsungen, Germany
2-Methylbutane	Carl Roth GmbH + Co. KG, Karlsruhe, Germany
2x Laemmli Sample Buffer	Bio-Rad, Munich, Germany
4x Laemmli Sample Buffer	Bio-Rad, Munich, Germany
Acetic acid (glacial)	Merck, Darmstadt, Germany
Agarose	AppliChem, Darmstadt, Germany
Ammonium acetate	Sigma, Taufkirchen, Germany
Ammonium persulfate	Sigma, Taufkirchen, Germany
ATP-Na_2 (Adenosine 5′-triphosphate disodium salt)	Sigma, Taufkirchen, Germany
$BaCl_2$	Sigma, Taufkirchen, Germany
Bradford Protein Assay	Bio-Rad, Munich, Germany
BSA (Albumin from bovine serum)	Sigma, Taufkirchen, Germany
$CaCl_2$	Carl Roth GmbH + Co. KG, Karlsruhe, Germany
Ca-Gluconate monohydrate	Carl Roth GmbH + Co. KG, Karlsruhe, D
Chloroform	Sigma, Taufkirchen, Germany
Citric acid monohydrate	Sigma, Taufkirchen, Germany
Creatinine	Sigma, Taufkirchen, Germany
D-Mannitol	Fluka Chemie GmbH, Buchs, CH
D-Potassium gluconate	Sigma, Taufkirchen, Germany
EDTA	Sigma, Taufkirchen, Germany
EGTA	Sigma, Taufkirchen, Germany
Eosin Y	Abcam, Cambridge, UK
Ethanol	J. T. Baker, Deventer, Netherlands
FCS (Fetal Calf Serum)	Gibco Cell Culture Systems - Invitrogen, Karlsruhe, Germany
Fura-2 AM	Invitrogen, ThermoFisher, Darmstadt, Germany
Glucose	Merck, Darmstadt, Germany
Glutaraldehyde solution	Sigma, Taufkirchen, Germany
Glycerol	Sigma, Taufkirchen, Germany
Glycine	Merck, Darmstadt, Germany

HCl	Merck, Darmstadt, Germany
Heparin	Liquemin N 25000, 5 ml, Roche, Mannheim, Germany
HEPES	AppliChem, Darmstadt, Germany
IGEPAL CA-630	Sigma, Taufkirchen, Germany
Isoflurane	Baxter Deutschland GmbH, Unterschleißheim, Germany
Isopropanol	Merck, Darmstadt, Germany
K_2HPO_4	Merck, Darmstadt, Germany
$K_3[Fe(CN)_6]$	Merck, Darmstadt, Germany
$K_4[Fe(CN)_6]$	Sigma, Taufkirchen, Germany
KCl	Merck, Darmstadt, Germany
Ketamine 100mg/mL	Sigma, Taufkirchen, Germany
$KH_2PO_4 \cdot 3H_2O$	Merck, Darmstadt, Germany
L-Glutamine, 200 mM (100x)	Gibco Cell Culture Systems - Invitrogen, Karlsruhe, Germany
Mayer's hemalun solution	Carl Roth GmbH & Co. KG, Karlsruhe, Germany
MEM alpha medium	Gibco Cell Culture Systems - Invitrogen, Karlsruhe, Germany
Methanol	Merck, Darmstadt, Germany
$MgCl_2 \cdot 6H_2O$	Merck, Darmstadt, Germany
$MgSO_4 \cdot 7H_2O$	Merck, Darmstadt, Germany
$Na_2HPO_4 \cdot 2H_2O$	Merck, Darmstadt, Germany
NaCl	Merck, Darmstadt, Germany
NaH_2PO_4	Merck, Darmstadt, Germany
$NaH_2PO_4 \cdot H_2O$	Merck, Darmstadt, Germany
Nonfat-dried milk	AppliChem GmbH, Darmstadt, Germany
Opti-MEM	Gibco Cell Culture Systems - Invitrogen, Karlsruhe, Germany
Opti-MEM™, Reduced Serum Medium	Thermo Fisher Scientific, Dreieich, Germany
Paraffin	Paraplast-Plus Paraffin, Sherwood, St. Louis, USA
Paraformaldehyde	Merck, Darmstadt, Germany
Penicillin-Streptomycin solution	1000 I.E./ml Pen G, 10000 µg/ml Strep.-Sulfat, Gibco Cell Culture Systems - Invitrogen, Karlsruhe, Germany
Periodic acid	Thermo Fisher Scientific, Dreieich, Germany
Picric acid	Sigma, Taufkirchen, Germany
Polyethylene glycol Sorbitan Monolaurate (Tween 20)	Sigma, Taufkirchen, Germany
Precision Plus Protein™ Dual Color Standards	Bio-Rad, Munich, Germany
Protease Inhibitor Cocktail Set III, EDTA-Free	Merck, Darmstadt, Germany
Rotiphorese® Gel 30 (37,5:1) (30% Acrylamide)	Carl Roth GmbH + Co. KG, Karlsruhe, Germany
Schiff's reagent	Sigma, Taufkirchen, Germany
SDS (dodecyl sulfate)	Merck, Darmstadt, Germany
Sodium acetate	Merck, Darmstadt, Germany

Sodium azide	Sigma, Taufkirchen, Germany
Sodium citrate dehydrate	Merck, Darmstadt, Germany
Sodium deoxycholate	Sigma, Taufkirchen, Germany
Sodium Pyruvate, 100 mM solution	Sigma, Taufkirchen, Germany
Sucrose	Merck, Darmstadt, Germany
TEMED 99%, for electrophoresis	Carl Roth GmbH & Co. KG, Karlsruhe, Germany
Tris Hydrochloride	Merck, Darmstadt, Germany
Triton X-100	Sigma, Taufkirchen, Germany
TRIzol™ Reagent	Thermo Fisher Scientific, Dreieich, Germany
Trypsin-EDTA (10x) solution	0,5% Trypsin, 5,3 mM EDTA, Gibco Cell Culture Systems - Invitrogen, Karlsruhe, Germany
Western Blotting Luminol Reagent	Santa Cruz, Heidelberg, Germany
X-Gal (5-Bromo-4-chloro-3-indolyl-β-D-galacto-pyranoside)	Sigma, Taufkirchen, Germany
Xylol	Merck, Darmstadt, Germany
α-Ketoglutarate (α-Ketoglutaric acid)	Sigma, Taufkirchen, D
β-Mercaptoethanol	Merck, Darmstadt, Germany

3.1.4 Enzyme, Kits

Products	**Manufacturer**
Collagenase Typ II (from Clostridium histolyticum)	Sigma, Taufkirchen, D
DNAse I	Roche Diagnostics GmbH, Mannheim, Germany
dNTP-Mix	MBI Fermentas GmbH, St. Leon-Rot, Germany
M-MLV Reverse Transkriptase	Promega, Madison, Wisconsin, USA
M-MLV Reverse Transkriptase Puffer (5x)	Promega, Madison, Wisconsin, USA
Protease (from Streptomyces griseus)	Sigma, Taufkirchen, D
Random Hexamer Primer (100 µM)	MBI Fermentas GmbH, St. Leon-Rot, Germany
REDTaq® ReadyMix™ PCR Reaction Mix	Sigma, Taufkirchen, Germany
RNAse Inhibitor	Peqlab Biotechnologie GMBH, Erlangen, Germany
RNeasy mini kit	Quiagen, Hilden, Germany
SYBR® Green PCR Kit	Quiagen, Hilden, Germany
Quick Ligase	New England Biolabs, Frankfurt, Germany
Trypsin inhibitor	Roche Diagnostics GmbH, Mannheim, Germany
Lipofectamine	Thermo Fisher Scientific, Dreieich, Germany
Gel extraction Kit	QIAGEN GmbH, Hilden, Germany
NucleoSpin Plasmid	Macherey-Nagel GmbH & Co. KG, Düren, Germany
NucleoBond Xtra MIDI	Macherey-Nagel GmbH & Co. KG, Düren, Germany
RNeasy Mini Kit	QIAGEN GmbH, Hilden, Germany

3.1.5 Software

Product	Manufacturer
ImageJ V1.37c	Wayne Rasband, NIH, USA
Labchart® Reader V7.1	ADInstruments, Ltd, Oxford, United Kingdom
IOX v1.8 EMKA Technologies	EMKA Technologies Company, USA
Origin 2017	OriginLab Corporation, Northampton, USA
ZEN Pro V2.3	Zeiss, Jena, Germany
Patch Master V2x65	HEKA Elektronik Dr. Schulze GmbH, Pfalz, Germany
Corel draw X8	Corel corporation, Ottawa, Canada

3.1.6 Oligonucleotide

All oligonucleotides were prepared by Invitrogen, Karlsruhe, Germany.

Gene	Primer	Sequence	Annealing-T.
Kcnj10 (Kir4.1)	sense antisense	AGTCTTGGCCCTGCCTGT TTAGCGACCGACGTCATCT	55 ˚C
Kcnj16 (kir5.1)	sense antisense	TACCGCTGTGTCACCGAAGA GCCAAGGCTGCTCCAATGAT	62 ˚C
Kcnj15 (Kir4.2)	sense antisense	CCCACTGGTGAAGCATACCAA CGATGACGGTTGTCCACAAGT	62 ˚C
Lrp2 (Megalin)	sense antisense	CAGTCAGTGGCCAAGAATG CAGTCTCTGGTCCCATCAC	57 ˚C
Nphs2 (Podocin)	sense antisense	CCATCTGGTTCTGCATAAAGG CCAGGACCTTTGGCTCTTC	57 ˚C
Calb1 (Calbindin-D28K)	sense antisense	CACAGACCTCATGCTGAAAC GGTAGTAACCTGGCCATCTC	57 ˚C
Slc12a3 (NCC)	sense antisense	GCTGACCTGCATTCATTCCT GACCTTGCCGTCCATCAAAG	57 ˚C
Slc12a1 (NKCC2)	sense antisense	TCTGCATCTGCTGCGAAG GGACACCGTCCCTGAAGC	61 ˚C
MCOLN (Mucolipin)	sense antisense	AGATGAGGCGGAAACTCAAGT CCATTCGATCCATGTAGCCCT	61 ˚C
Actb (β-Actin)	sense antisense	CCACCGATCCACACAGAGTACTT GACAGGATGCAGAAGGAGATTACTG	57 ˚C

All primers were prepared for *Mus musculus*, unless otherwise mentioned.

Genotyping of KCNJ16 mice

mKcnj16 wildtype	sense antisense	CCTCCAGAGCATGCCATCGC GATCGCTTAATAGGTCTCCG	63 ˚C
mKcnj16 knockout	sense antisense	GCAGCGCATCGCCTTCTATC TACAAACTCTACTGCCAAAGC	60 ˚C

m = mouse

Site directed mutagenesis of KCNJ6 R35Q

hKcnj16 R35Q	sense antisense	AAGAGCAAGAAGACA**A**TTACTTCAC GTGAAGTAAT**T**GTCTTCTTGCTCTT	55 ˚C

h = human

3.1.7 Antibody

Target	Type	Dilution	Manufacturer
anti-Kir4.1, rabbit polyclonal IgG	Prim. Ab	1:400	Alomone Labs
anti-Kir5.1, rabbit polyclonal IgG	Prim. Ab	1:400	Sigma Prestige Antibody
anti-AQP2, goat polyclonal IgG	Prim. Ab	1:400	Santa Cruz Biotechnologies
Anti-calbindin, mouse monoclonal IgG	Prim. Ab	1:400	Sigma Life Science
Anti-NKCC2, rabbit	Prim. Ab	1:400	Mark Knepper
Anti-cubilin (T-16), goat polyclonal IgG	Prim. Ab	1:200	Santa Cruz Biotechnology
Alexa Fluor® 488 donkey anti-mouse	Sec. Ab	1:400	Invitrogen, Karlsruhe, D.
Alexa Fluor® 488 donkey anti-rabbit	Sec. Ab	1:400	Invitrogen, Karlsruhe, D.
Alexa Fluor® 546 donkey anti-goat	Sec. Ab	1:400	Invitrogen, Karlsruhe, D.
Alexa Fluor® 647 donkey anti-rabbit	Sec. Ab	1:400	Invitrogen, Karlsruhe, D.
Cy5 donkey anti-mouse	Sec. Ab	1:400	Invitrogen, Karlsruhe, D.
HOE33342 (Stock conc.: $5x10^{-4}$ M)	Sec. Ab	1:400	Invitrogen, Karlsruhe, D.

3.1.8 Buffers and solutions

Designation	Substance	Quantity
Fixation solution, pH 7.4	EGTA	1 mM
	K_2HPO_4	15 mM
	$MgCl_2$	2 mM
	NaCl	90 mM
	Paraformaldehyde	3%
	Sucrose	100 mM
	Aqua dest.	
Phosphate buffered saline (PBS), pH 7.4	KH_2PO_4	1.8 mM
	Na_2HPO_4	10.3 mM
	NaCl	137 mM
	in Aqua dest.	

Post fixation solution, pH 7.4	EGTA	1 mM
	K_2HPO_4	15 mM
	$MgCl_2$	2 mM
	NaCl	90 mM
	Paraformaldehyde	1%
	Sucrose	17%
	in Aqua dest.	

PBS-Tween	PBS	99,9%
	Tween 20	0,1%

2% Glutaraldehyde Solution, pH 7,4	Glutaraldehyde	2%
	Sodium cacodylate	0,1 M
	in distilled water	

Citrate buffer, pH 6.0	Sodium citrate dehydrate	2.059 g
	Citric acid monohydrate	0.317 g
	in Aqua dest.	ad 1000 ml

0,1% SDS Solution	SDS	0,1% (v/v)
	in PBS	

Blocking solution, pH 7.4	BSA	5%
	Triton X-100	0.04%
	in PBS buffer	

Solution for Antibody dilution, pH 7.4	BSA	0.5%
	Triton X-100	0.04%
	in PBS buffer	

1% Periodic acid solution	Periodic acid	1% (w/v)
	in distilled water	

X-Gal (5-bromo-4-chloro-3-indolyl-β-D-galactopyranoside) solution I, pH 7.4	Sodium deoxycholate	1 mg/mL
	IGEPAL CA-630	2 mg/mL
	EGTA	5 mM
	$MgCl_2$	2 mM
	K_2HPO_4	100mM
	in distilled water	

X-Gal solution II	X-Gal	0.5 mg/mL
	$K_3[Fe(CN)_6]$	10 mM
	$K_4[Fe(CN)_6]$	10 mM
	in X-Gal solution I	

Sorting solution, pH 7.4	Bovine serum albumin (BSA)	500 mg/L
	In digestion sol.	

Digestion solution I, pH 7.4	NaCl	140 mM
	KH_2PO_4	0.4 mM
	K_2HPO_4 •3 H_2O	1.6 mg/ml
	$MgSO_4$ •7 H_2O	1 mM
	Na-Acetat •3 H_2O	10 mM
	α-ketoglutaric acid	1 mM
	Calcium gluconate monohydrate	1.3 mM
	in Aqua dest.	

Incubation solution, pH 7.4	Glycine	375 mg/L
	Trypsin inhibitor	48 mg/L
	DNAse I	25 mg/L
	in digestion sol.	

Digestion solution II, pH 7.4	Collagenase II	2 mg/mL
	In incubation solution	

Control solution, pH 7.4 (Fura-2-AM Ca^{2+} Measurements)	HEPES	5 mM
	NaCl	130 mM
	Na_2HPO_4 •2H_2O	1.6 mM
	NaH_2PO_4 •H_2O	0.4 mM
	Glucose	5 mM
	$MgCl_2$	1 mM
	$CaCl_2$	1.3 mM
	in Aqua dest.	

Fura-2-AM solution, pH 7.4	Fura-2-AM	5 µM
	BSA	0.1 mg
	in control solution	

HEK cells medium	Fetal Calf Serum (FCS) (heat-inactivated)	10%
	Penicillin-Streptomycin solution	1%
	MEM ALPHA medium	500 mL

CHO cells medium	FCS (heat-inactivated)	10%
	Penicillin-Streptomycin solution	1%
	L-Glutamine	2 mM
	Sodium Pyruvate	1 mM

	MEM ALPHA medium	500 mL

Patch clamp Solution pH 7.4	$CaCl_2$	1.3 mM
	Glucose	5 mM
	HEPES	5 mM
	$K_2HPO_4 \cdot 3H_2O$	1.6 mM
	KH_2PO_4	0.4 mM
	$MgCl_2$	1 mM
	NaCl	145 mM
	in Aqua dest.	

Barium solution, pH 7.4 (Patch-Clamp Measurements)	BaCl	5 mM
	in control solution	

Pipette solution, pH 7.2 (Patch-Clamp Measurements)	Potassium Gluconate	95 mM
	KCl	30 mM
	$Na_2HPO_4 \cdot 2H_2O$	4.8 mM
	$NaH_2PO_4 \cdot H_2O$	1.2 mM
	Glucose	5 mM
	$MgCl_2$	2.38 mM
	$CaCl_2$	0.726 mM
	EGTA	1 mM
	ATP-Na_2	3 mM
	in Aqua dest.	

3.2 Methods

3.2.1 Mice

3.2.1.1 KCNJ16 knockout model

To investigate the importance of Kir5.1 (encoded by the Kcnj16 gene), a knockout mouse ($Kir5.1^{-/-}$) was used as a model organism. The $Kir5.1^{-/-}$ mouse model was generated by Taconic (TF0347) with a genetic background of 129/SvEv-C57BL/6. Mice were backcrossed for at least 5 generations into the C57BL/6J background before experiments were performed. As control animals ($Kir5.1^{+/+}$), mice from the same strain (C57BL6J) were used. All animals were kept according to the current German animal welfare law. The mice had a 12 hour light and dark rhythm and were kept on a standard diet (Sniff V1124) with free access to water. For the experiments, we took animals of both sexes (unless otherwise stated).

3.2.1.2 Isolation of genomic DNA

Tail biopsies (2 mm) of mice were taken to isolate genomic DNA (gDNA). Tails were digested over night at 55 ˚C, in 300 µL Tail Buffer (0.1 M EDTA, 0.5% SDS, 50 mM Tris-

HCl, pH 8) with 1 µL Proteinase K (100 mg/mL). The next day, 100 µL of ammonium acetate (7.5 M) were added to the digested tails, followed by 600 µL of isopropanol, always with proper homogenization of the solution. For the DNA to precipitate, the mixture was incubated for 20 minutes at -20 ˚

Probes were centrifuged for 10 minutes at 13000 rpm in order to obtain the DNA pellet. The pellet was washed with 1 mL of 70% Ethanol, centrifuged once again and supernatant was discarded. Finally, after air drying of the sample for 15 minutes, gDNA was resuspended in 80 µL of TE buffer (10 mM Tris, 1 mM EDTA, pH 7.5) and stored at 4 ˚C.

3.2.1.3 Genotyping of KCNJ16 knockout mice

Genotyping was performed by PCR using the Red Taq Mix. The PCR master mix was prepared using 1 µL of mouse gDNA, 10 µL Red Taq Mix 2x, 7 µL H_2O and 1 µL of sense and antisense primers corresponding to the wildtype and knockout alleles (Section 3.1.6). The conditions used for the run are described in Table 1.

Table 1. PCR program for KCNJ16 genotype.

Temperature	Time	Repetitions
94 °C	4 min	
94 °C	15 sec	10 cycles
65 °C	30 sec	
72 °C	30 sec	
94 °C	15 sec	30 cycles
55 °C	30 sec	
72 °C	30 sec	
72 °C	2 min	
10 °C	∞	

The amplified products of wildtype (wt) and KCNJ16 knockout (ko) alleles were separated in a 2% agarose gel according to the amplicon sizes of 256 bp and 316 bp for wt and ko, respectively.

3.2.1.4 Diet 4% NaCl

Experiments were performed with Kir5.1$^{-/-}$ (n = 10) and control mice (n = 8, 3-4 months old) which were fed a standard salt diet (fortified food with 0.24% sodium, V1124; Ssniff Spezialdiäten GmbH) and water *ad libitum*. Before the experimental diet, animals were weighted; urine samples (spot urine) and blood from the facial vein were collected for basal conditions. Animals were allowed to recover for 7 days. Thereafter, food was switched to high sodium content 4% NaCl (E15431-34; Ssniff Spezialdiäten GmbH) with free access to water. During the time of the diet, the body weight was monitored daily, for 15 consecutive

days and urine samples were collected every two days. At the end of experiment, blood samples were collected from the facial vein and blood electrolytes were analyzed using the blood gas system pHOx plus M.

3.2.1.4.1 Amiloride

Experiments were performed with Kir5.1$^{-/-}$ (n = 9) and control mice (n = 12, 3-5 months old) which were fed a standard diet (fortified food with 0.24% sodium, V1124; Ssniff Spezialdiäten GmbH) and water supplemented with 6% sucrose, 25 mM NaCl and 50 mM KCl, 24 h before experiment. The animals were weighted and the bladder emptied before placed in the metabolic cages. No food was allowed during the experiment time, and urine was collected during 6h. Afterwards, an intraperitoneal injection of amiloride (5 µg/body weight (BW)) was given and the urine collected for 6h. Urine samples were analyzed by ion chromatography according to manufacturer's instructions.

3.2.1.4.2 Collection of blood and urine samples

Blood samples were obtained from the facial vein of the KCNJ16$^{-/-}$ and control mice. Blood samples were collected into 150 µL glass capillaries and analyzed immediately using the blood gas system pHOx plus M (Nova Biomedical). In addition to blood gases (pO_2 and pCO_2), the device measured electrolytes, such as, Na^+, K^+, Ca^{2+}, Mg^{2+} and also the pH of the sample. Additionally, several blood parameters were calculated by the device according to pHOx Plus M Analyzer manual, using the following equations:

Bicarbonate $[HCO_3^-]$:

$$pH = pK + log\frac{[HCO_3^-]}{\alpha(pCO_2)}$$

Rearranging of Henderson-Hasselbalch equation, where pH and pCO_2 are measured and pK = 6.091 and α = 0.03707 (solubility coefficient of CO_2 in plasma at 37 °C), gives equation:

$$log_{10}[HCO_3^-] = pH + log_{10}pCO_2 - 7.604$$

Base excess (BE) of the blood is defined as the concentration of titratable base needed to titrate blood to pH 7.40 at 37 °C while the pCO_2 is held constant at 40 mm Hg and is calculated as:

$$\mathrm{BE} = (1 - 0.014[\mathrm{Hb}])([\mathrm{HC}O_3^-] - 24 + (1.43[Hb] + 7.7)(pH - 7.4),$$

Hb-hemoglobin

Urine samples were collected before and during the diet period. The adult mice emptied their bladder spontaneously after being removed from their cage and urine samples were collected into an Eppendorf and analyzed by Ion Chromatography (IC) Dionex ICS-1600 (Thermo Scientific) for identification and quantification of numerous ions. The samples were prepared and measured by Ines Tegtmeier according to the manufacturer´s instructions.

3.2.2 Cell line

As cell models, two different cell lines were chosen: human embryonic kidney (HEK; single channel experiments) and Chinese hamster ovary (CHO; whole cell experiments) cells. The cells were cultivated at 37 °C, 5% CO_2 in media described in section 3.1.9. For transfection 500.000 cells were seeded into 6-wells on glass cover slips one day prior to transfection with 0.5 µg of cDNA (unless otherwise stated) using the Lipofectamine according to the manufacturer's protocol. For cotransfection experiments, the cells were transfected with wildtype KCNJ10 and wildtype or mutant KCNJ16 ($KCNJ16^{wt}$ or $KCNJ16^{R35Q}$) in pIRES CD8 plasmids. Different stoichiometric ratios were used: a ratio of 1:1 to understand the role of KCNJ16 channels in the overall conductance and a ratio of 1:10 (one part KCNJ10 and nine parts KCNJ16) to avoid contamination with homomeric KCNJ10 channels. Cells were analyzed two days after transfection by immunofluorescence or electrophysiology experiments.

Cells were transfected with bicistronic pIRES CD8 plasmids, which included the transmembrane protein CD8 in addition to the desired protein target KCNJ10, KCNJ16 or mutant $KCNJ16^{R35Q}$. This allowed the use of Dynabeads™ CD8, which are beads coated with a specific monoclonal antibody against human CD8 allowing visual identification of cells that expressed the target proteins.

3.2.3 Histological Methods

3.2.3.1 Tissue fixation by retrograde arterial perfusion

Mice were anesthetized with isoflurane (through inhalation of a gas mixture composed of 2.5% of isoflurane, 50% oxygen and 50% nitrogen at 60 mL/min flow). In deep anesthesia the abdominal cavity was opened and the abdominal aorta was freed from overlaying adipose and connecting tissues and temporarily clamped shortly distal of the renal artery. Then, a small incision was made into the the distal abdominal aorta in order to insert a polyethylene catheter. The catheter was fixed with a second clamp. After incision of the inferior vena cava and removal of the first clamp, the animals were killed by replacing the blood with 0.9% NaCl supplemented with 10 IU/mL of Heparin. After 10 mL of perfusion,

the dead mice were perfused with a fixation solution, at a constant flow rate of 10 mL/min assured by a roller pump.

3.2.3.2 Cryo preparation and sectioning

After perfusion of mice, the tissues were left in a post-fixation solution containing 1.5% paraformaldehyde and high concentration of sucrose, for 1h, at 4 ˚C. The tissues were frozen in 2-methylbutane, at -40 °C and then preserved at -80 ˚C. In a cryostat, sections were made at chamber temperature of -25 ˚C and the object holder was at -20 ˚C. After being applied in polysine™ microscope adhesion slides, the sections were dried for 20 min at room temperature and stored at -20 ˚C.

3.2.3.3 X-Gal stain: detection of β-galactosidase activity

The cryo-sections obtained were incubated with X-Gal (5-bromo-4-chloro-3-indolyl-beta-D-galactopyranoside) solution II (see recipe in 3.1.8) at 37°C. Afterwards, the sections were immersed in PBS and mounted with Dako mounting medium.

X-gal staining is a histochemical method used to detect the presence of the β-galactosidase enzyme, which is encoded by the *LacZ* gene. The enzyme hydrolyzes X-Gal into 5-bromo-4-chloro-3-hydroxyindole that dimerizes and forms an insoluble compound with blue coloration. This allows the use of X-gal for identification of blue staining as an expression marker by placing the *LacZ* gene under the control of the promotor of a gene of interest. Since we had currently no specific antibody available that recognized the protein Kir5.1, localization of KCNJ16 expressing cells was studied by promotor-driven X-gal staining in transgenic Kir5.1$^{-/-}$ mice carrying the *LacZ* gene within the gene locus.

3.2.3.4 Immunofluorescence

Immunohistochemistry is a technique that is used to detect specific biomolecule targets by antibodies. In this method, the labelling was used with two antibodies. A primary antibody that specifically binds to the targeted molecule and a secondary that recognizes and binds the primary antibody and carries a fluorophore. The localization of the antibody was detected by excitation of the fluorophore in the corresponding wavelength. The cryo-sections obtain as mentioned above, were rinsed in PBS for 5 min (two times) before and after incubated in 0.1% SDS solution for epitope unmasking. Afterwards, the sections were incubated with blocking solution (5% BSA solution) for 10 min to mitigate unspecific antibody binding. The antibodies (primary and secondary) were diluted in PBS solution containing 0,5% BSA and 0,04% Triton X-100. The sections were incubated with the primary antibody at 4°C, in a humid chamber, overnight. Afterwards, the tissue was immersed in PBS for 5 min to wash the antibody that did not bind and incubated with the

secondary antibody for 1 h, at room temperature, in the dark. In the end of the process, sections were washed two times with PBS, each time for 5 min, mounted in Dako medium. For immunofluorescence labelling of HEK or CHO, cells were cultivated on glass cover-slips and transfected as described in section 3.2.2. After washing in PBS, the cells were fixed with 3% paraformaldehyde for 10 min and once again thoroughly rinsed with PBS solution. The following procedure was similar to the one performed for cryo-sections.

3.2.4 Molecular Biological Methods

3.2.4.1 Site directed Mutagenesis

To test the cellular effects of the KCNJ16 mutations, the Kir5.1^{R35Q} mutant was generated using site directed mutagenesis. The mutation was introduced into the wildtype human KCNJ16 cDNA and sub cloned into plasmid pIRES CD8 (ampicillin resistance). This allowed the transfection of mammalian cell lines - HEK293T and CHO.

To exchange an individual base (point mutation) in a desired cDNA, specific primers were designed. Primers are complementary to the template DNA around the mutation site allowing the hybridization with a specific DNA sequence. Two fragments carrying the base exchange were obtained and after insertion of the restriction sites for enzyme NotI were ligated into the pIRES CD8 plasmid. The length of both PCR fragments was determined by agarose gel electrophoresis and the desired bands were cut from the gel and purified using QIAquick® gel extraction kit (Quiagen) according to manufacturer's instructions. Ligation, was performed by mixing 1 µL of Quick ligase, 5 µL of appropriated buffer ligase, 3 µL of fragment and 1 µL of vector (both the fragment and the plasmid were cut with the restriction enzyme for 2h at 37 ° prior to the ligation step). The ligated plasmid was transformed into XL1 blue E.Coli cells. Successful mutagenesis was confirmed by sequencing (SeqLab). Plasmid Mini Kit were used to purified the plasmid according to manufacturer's instructions.

Temperature	Time	Repetitions
94 °C	3 min	
94 °C	30 sec	30 cycles
52 °C	30 sec	
72 °C	2min 20 sec	
72 °C	3 min	
10 °C	∞	

3.2.4.2. Isolation of total RNA from Kidneys

Male and female mice tissues were used to isolate RNA. The organs were harvested after euthanasia and tissues were frozen in liquid nitrogen and stored at -80 ˚C. After

homogenization of tissues with a mortar and pestle, the result powder was used on a NucleoSpin RNA kit from Macherey-Nagel according to manufacturer's instructions in order to isolate RNA.

A different method to isolate RNA from mice cochlea was used. According to the protocol of Patil *et al*, 2015, the cochleae were homogenized and the cells lysed in 750 µL Trizol. Afterwards, the mixture was centrifuged at 12000g for 5 min, at 4 ˚C to remove bone debris. Trizol is a monophasic solution that solubilizes biological material and leads to denaturation of protein. After solubilization, the addition of 350 µL of chloroform causes a phase separation by centrifuging the mixture at 12000g for 15 min at 4 ˚C. Protein was extracted to the organic phase (lower layer─chloroform) and the RNA remained in the aqueous phase (upper layer).

In order to precipitate the RNA, 350 µL of 70% ethanol were added to the aqueous phase and the mixture was purified using the NucleoSpin RNA kit from Macherey-Nagel according to the manufacturer's instructions. To confirm the concentration of RNA the samples were measured in a Nanodrop spectrophotometer and stored at -80 ˚C.

3.2.4.3 Reverse Transcription (cDNA-Synthase)

cDNA was synthesized by reverse transcription using an RNA template obtained as described before. RNA was incubated with random primers at 70 ˚C for 5 minutes to linearize the secondary structure of RNA (Table 2). Afterwards, the mixture was placed in ice to allow primers to bind to RNA molecules. To this reaction mixture was added dNTP's, RNAse inhibitor and M-MLV reaction buffer (see Table 3) and the mixture was vortexed and centrifuged. The reverse transcriptase mixture was divided in two reactions: one reaction with the enzyme M-MLV Reverse Transcriptase and to the other only H_2O has a control for genomic DNA contamination in the RNA. The mixes were then incubated according to the protocol (see Table 4) to obtain cDNA.

Table 2. Reaction mixture

1 µg RNA	70 ˚C for 5 min Then in 4 ˚C.
1 µL Random primer	
13 µL Free-nuclease H_2O	

Table 3. Reverse transcription mixture

15 µL of the previous mixture
5 µL M-MLV Reverse Transcriptase Buffer (5X)
1.25 µL dNTP-Mix
1 µL RNAse inhibitor
2.75 µL RNAse-free water

Table 4. PCR Protocol

Temperature	Time
22 °C	10 min
50 °C	50 min
70 °C	15 min
10 °C	∞

3.2.4.4 Quantitative Polymerase chain reaction (Real-time PCR)

The quantitative PCR is determined indirectly by measuring the SYBR® Green fluorescent dye. The dye binds preferentially to the double-strand of DNA and its fluorescence intensity is higher when compared to the free dye.

A SYBR® Green PCR kit and a Light-Cycler System 2.0 from Roche were used to perform real-time PCR. A reaction mixture containing SYBR Green, cDNA obtained from the previous section and sense/antisense primers (see Table below) were incubated for 5 min at 70 °C, before being cooled in ice for 5 min. The amplification procedure is described in the Table below with 40 cycles that allowed for DNA denaturation, hybridization of primers with DNA and elongation phase. To analyze the specificity of the primers the PCR result was run in a 2.5% agarose-gel. The data was normalized to the expression of the housekeeping gene β-actin.

Reaction Mixture
5 µL SYBR Green mix
3 µL RNase free H_2O
0.5 µL sense primer (10 µM)
0.5 µL antisense primer (10 µM)
1 µL of cDNA

Amplification		
95 ˚C	10 min	
95 ˚C	15 sec	40 cycles
55-60 ˚C	20 sec	
72 ˚C	20 sec	
95 ˚C	5 sec	

The sequence and annealing temperature for all used primers can be found in Oligonucleotides (section 3.1.6).

3.2.5 Patch Clamp Experiments of transfected cells

The patch clamp technic allows the study of electrical currents over the membrane of the cell, which mainly results from the activity of ion channels.

The amplifier used was an EPC-10 device coupled to a computer and a Powerlab Data Acquisition system. The software Patchmaster was used for pulse generation and data acquisition along with LabchartPro. All work was acquired at room temperature, with

running solutions (section 3.1.8; Patch clamp Solution). The continuous bath perfusion in the experiments avoided cell damage by discharging K^+ from the reference electrode ("flowing KCl electrode"). The patch pipettes used were obtained from glass capillaries to a resistance of about 7 MΩ.

3.2.5.1 Patch clamp measurements in whole cell mode

Whole cell mode recordings were performed on transiently transfected CHO cells. To achieve the whole cell configuration, a patch pipette (95 mM K-gluconate, 30 mM KCl, 4.8 mM $Na_2HPO_4 \cdot 2H_2O$, 1.2 mM $NaH_2PO_4 \cdot H_2O$, 5 mM Glucose, 2.38 mM $MgCl_2$, 0.726 mM $CaCl_2$, 1 mM EGTA and 3 mM ATP-Na_2) was placed on the cell and the membrane was ruptured by applying suction to the pipette. As a result, the interior of the pipette is now linked to the intracellular space of the cell, which allows controlling intracellular factors.

Using the PatchMaster software (Version V2x65), cells in the whole cell configuration could be measured by switching between voltage and current clamp modus in a frequency of 1.5 Hz. In the current clamp, zero modus (CC0) the current of the whole cell was clamped to zero ampere for 10 seconds and the resting potential of the cell was recorded. In the voltage clamp modus (VC), the whole cell the voltage of the cell was clamped from -120 mV to +30 mV in 30 mV voltage increments lasting for 2 sec and the corresponding current was measured.

The liquid junction potential of the pipette solution and the bath solution (5 mM Hepes, 5 mM glucose, 1.3 mM $CaCl_2$, 1.6 mM $K_2HPO_4 \cdot 3H_2O$, 0.4 mM KH_2PO_4, 1 mM $MgCl_2$, 145 mM NaCl) was 10 mV and corrected by the PatchMaster software. Data was acquired at a frequency of 0.5 kHz.

To control for successful expression of Kir-channels, cells were superfused with bath solution containing 100 µM BaCl, which is a non-selective blocker of K-channels and should effectively reduce the conductance and depolarize the cells.

For analysis of the whole cell recordings, current-voltage relationships were obtained by analyzing one representative trace of one voltage step before and under BaCl per cell using the Labchart Reader software. For each voltage step, averaged currents were calculated. The number of individual cells measured is indicated by the letter n. Experiments were repeated at least three times on different days.

3.2.5.2 Patch clamp measurements in single channel mode

Electrophysiological recordings of single channel currents allows detailed and precise information about the behavior of ion channels. The experiments were performed and carried out, at room temperature, as described before. For these experiments, HEK cells were chosen due to higher probability of obtaining a successful experiment when compared

to CHO cells (used in whole cell) and due to less likely run-down of channels in HEK cells. To record a single channel event a cell-attached or inside-out configuration was obtained. In cell-attached mode, the patch pipette is in contact with the cell membrane and after the seal; different holding potentials were applied to the membrane in order to measure the single channel conductance. Afterwards, to achieve inside-out mode the pipette was retracted to break off a patch of membrane and symmetrical ion concentrations on both sides of the patch were obtained by changing the bath solution to the solution used in the pipette. This made sure that the currents were evoked by voltage, from a holding potential of -10 mV, delivered in -10 mV increments from -120 mV to +50 mV.

Single channel currents were recorded with an EPC-10 amplifier and analyzed with Labchart. The reference electrode in the bath was an Ag/AgCl pellet. The data analysis signals were typically low-pass filtered at 1 kHz by a Bessel filter (Patch Master). In cell-attached experiments, the bath solution was equal to that used by whole cell experiments. In excised inside-out membrane patches, the solution in the bath was the same as in the pipette allowing for a symmetrical environment.

3.2.6 Ca^{2+} Measurements with Fura-2

Fura-2 is a fluorescence Ca^{2+} indicator, which allows measurement of intracellular calcium concentrations. The substance diffuses inside the cell as a nonpolar ester and is cleaved by endogenously expressed esterase regenerating the calcium indicator. The principle of this measurement relies on the fact that Fura-2 changes its fluorescence properties in the presence of Ca^{2+}. When bound to Ca^{2+}, Fura-2 presents an excitation maximum at 340 nm and in the absence of Ca^{2+}; the maximum is at 380 nm. The cells are exposed to the wavelengths and the ratio of the emissions at those wavelengths is directly related to the amount of intracellular calcium. This is the advantage of this ratiometric method, which shows an independence on the dye concentration and the cell thickness.

3.2.6.1 Ca^{2+} measurements in isolated DCTs

The mice were anesthetized with isoflurane, as described before (section 3.2.3.1), and perfused with 10 mL digestion solution II (section 3.1.8) at pH 7.4 and 37˚C.The digestion solution contains collagenase II, which allows the degradation of collagen fibrils present in the connective tissue. The kidneys were quickly removed, sliced and transferred into 2 mL of incubation solution containing 1 mg/mL collagenase and swirled at 850 rpm, at 37 ˚C in the thermomixer. After 10 min, a 1 mL tubule suspension was transferred into 1 mL of ice cold sorting solution containing albumin and kept on ice. One milliliter of incubation buffer was added to the remaining tubule suspension, and the enzymatic reaction continued for 5 min at 850 rpm and 37 ˚C. This procedure was repeated resulting in three tubule fractions.

Isolated and sedimented tubules were resuspended in ice-cold sorting solution and kept on ice until use. Afterwards, the tubules were transferred into the bath of an inverted microscope stage. The bath was thermostat controlled at 37 ˚C and a continuous perfusion at 3-5 mL/min was maintained by a peristaltic perfusion pump. The tubules were monitored and measured by video imaging (Zeiss pro v2.0 and 2.3). The experiments were performed on DCT, a nephron segment immediately adjacent to the glomerulus, and where either superfused on the basolateral side or perfused on the apical side. Superfused isolated tubules were transferred to a cover glass mounted in closed perfusion chamber, and immobilized with two glass pipettes. Perfused tubules were held by a glass pipette and perfused on the apical side by a concentric glass pipette system as described by Greger et al[64]. The DCTs were loaded by incubating for 20 min with fura-2 AM (5 µM) dissolved in control solution and 1% albumin for a better uptake into the cells and to avoid fura crystal, without the toxic effect of pluronic acid. After loading, the tubules were washed to remove non-absorbed fura-2 and measured when the ratio 340/380 was stable. Thereafter, different substances where tested and the response recorded on both wavelengths every 10 seconds. The inclusion criteria depended on the ability of the cells capable of taking up the fura-2 and retain the dye without leak for the duration of the experiments.

Mean fluorescence ratios before and during application of the different substances were calculated for single tubules using the ZEN Pro 2.3 version (Zeiss). n refers to the number of individual DCTs. All experiments were repeated with at least three different mice.

The RNA isolation from the kidney tubules of the nephron was performed after kidney digestion and manually sorting of the tubules. The tubules were dissected based on morphology. The RNA isolation process was has described before (section 3.2.4.2) and the Quick-RNA™ MicroPrep kit (Zymo Research) was used.

3.2.7 Plethysmography

Respiratory function was assessed in awake and unrestrained mice using a whole body plethysmograph (EMKA Technologies). In total, 15 animals were investigated, 8 wildtypes and 7 Kir5.1$^{-/-}$. Mice were placed in separated chambers and allowed to adapt to their new environment for 30 minutes. Baseline and recovery periods were measured at normal atmosphere for at least 30 min. Respiratory parameters of each condition were followed over a period of 30 to 60 minutes with average recordings for every minute. Hypoxia was induced by lowering the oxygen concentration to 10% in the chamber air supply. In these experiments, the oxygen was replaced by nitrogen. The animals were acclimatized for 30 min, left under control conditions for another 30 min (21% O_2) and then hypoxia was induced (10% O2) for 60 min after which the animals were allowed to recover. Hypercapnia was

induced with controlled inflation of 5% CO_2 to the chambers. In these experiments, the CO_2 lead to a decrease of O_2 levels.

3.2.8 Statistics

Data are shown in mean values ± standard error of the mean (SEM). The number of experiments performed for a measurement series was represented by the numbers in the legends of the figures (n). If not stated otherwise, data was compared using a paired or unpaired Student's t-tests using the origin software after a Gaussian distribution was verified. A p-value of 0.05 was accepted to indicate statistical significance, which is indicated by an asterisk (*), a p-value <0.01 was considered to be significant (**) and a p-value <0.001 as highly significant (***) in the respective graph. For multiple testing, the Bonferroni corrections were calculated.

4. Results

4.1 Expression and localization of KCNJ16

4.1.1 KCNJ16 expression in mouse tissues

The first objective of this work was to re-visit in more detail the previously published tissue expression of Kcnj16 (Kir5.1) and its interaction partner Kcnj10 (Kir4.1) in mouse.[65–67] The two channel proteins are known to form heterodimers in some, but not in all, cell types. For this purpose, RNA was isolated from murine tissues and tested for the expression of Kcnj16 and Kncj10 using real-time PCR.

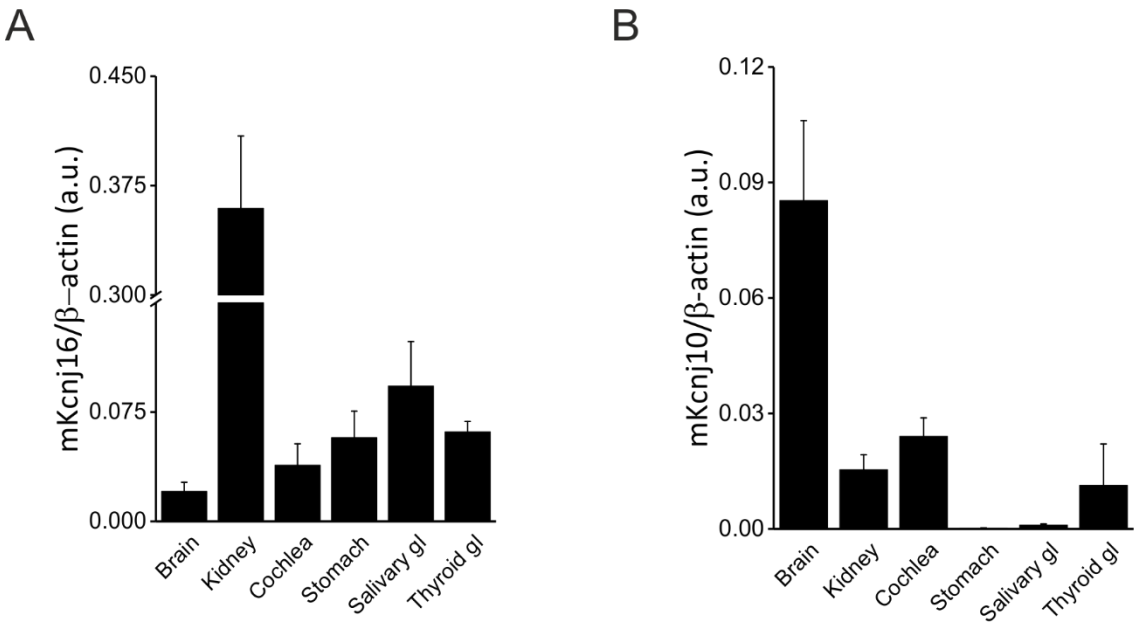

Figure 6. mRNA levels of Kcnj16 and Kcnj10 in several tissues of Kir5.1$^{+/+}$ mice.
mRNA was isolated from various murine tissue and analyzed for expression of (A) Kcnj16 and (B) Kcnj10 (n = 3) and normalized to Actb (β-actin) mRNA levels. KCNJ16 is highly expressed in kidney and salivary gland while KCNJ10 is mainly expressed in brain and cochlea. Data is presented as mean±SEM. Abbreviation: gl=gland.

As shown in Figure 6, Kcnj16 was expressed in several tissues, such as cochlea, stomach and thyroid glands. However, the kidney is the major organ of Kcnj16 expression in the mouse. In contrast, Kcnj10 expression was highest in the brain. Nevertheless, Kcnj16 and Kcnj10 were co-expressed in the kidney, cochlea and thyroid gland.

4.1.2 Kir5.1 (Kcnj16) localization in the kidney

To analyze the expression of Kir5.1 and Kir4.1 within the kidney in more detail, the nephron segments were manually sorted from enzymatically digested mouse kidneys according to distinct morphological criteria (Figure 7).[68] After mRNA isolation, the transcript levels of

Kcnj16 and Kcnj10 (normalized to β-actin mRNA levels) were quantified using real-time PCR.

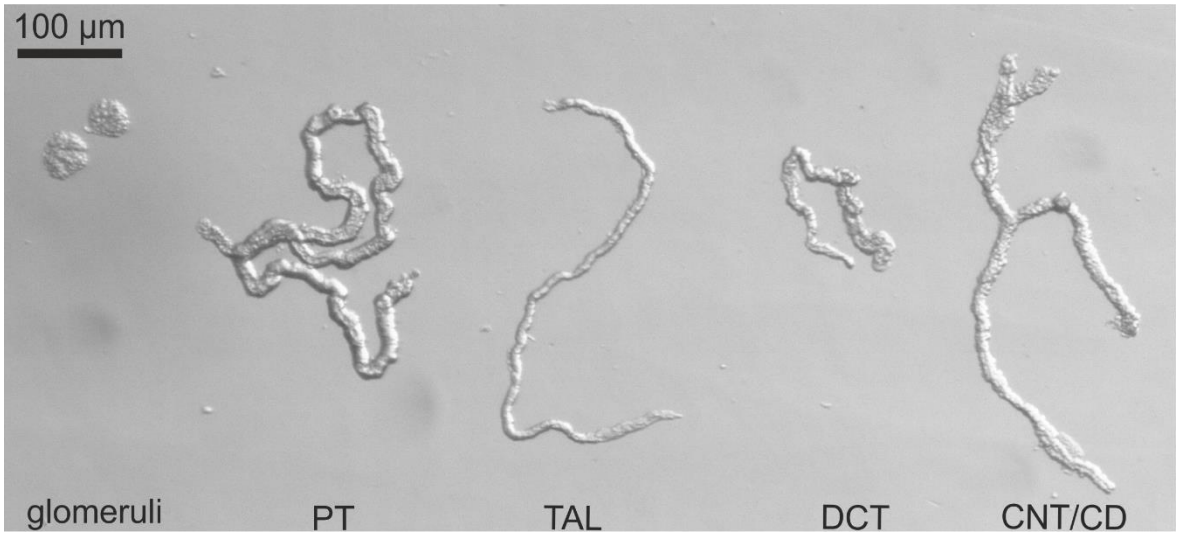

Figure 7. Microdissected tubular segments from the mouse kidney.
Overview of microdissected renal tubule segments sorted according to distinct morphological differences. Proximal tubules (PT) are long and have a smooth surface with no change in diameter. The early S1 segment is convoluted and might still be attached to the glomerulus (glom). The late S3 segment of the PT is long and straight. In contrast, the thick ascending limp (TAL) is also long and straight but has a smaller diameter. The distal convoluted tubule (DCT) shows strong basal infoldings and often a sigmoidal-formed shape. On one end, a TAL and a glomerulus might still be attached at the region of the macula densa (MD). On the other end, the transition into the connecting tubule (CNT) is characterized by the appearance of cobblestone-like principal cells. The collecting duct (CD) can easily be distinguished by their branching and cobblestone-like appearance.

After isolation of tubules, mRNA from all segment was isolated and the correctness of sorting was confirmed by conducting a real-time PCR against several markers for each of the tubular segments. The following markers were used to confirm the sorting of the tubules: megalin, which is expressed in the proximal tubule; podocin, which is expressed in podocytes of the glomeruli; calbindin was used as a DCT/CNT marker; NKCC2 cotransporter as a TAL marker and mucolipin as a collecting duct marker. After the correct sorting of the segments was verified (Supplemental Figure S1), the mRNA levels of Kcnj16 (Figure 8) and Kcnj10 (Figure 9) of the isolated tubules were quantified using real-time PCR. For Kcnj16, the highest transcript levels were found in the DCT followed by the PT. However, Kcnj10 was not expressed in the PT but it was highly expressed in TAL, CD and co-expressed with Kcnj16 in the DCT.

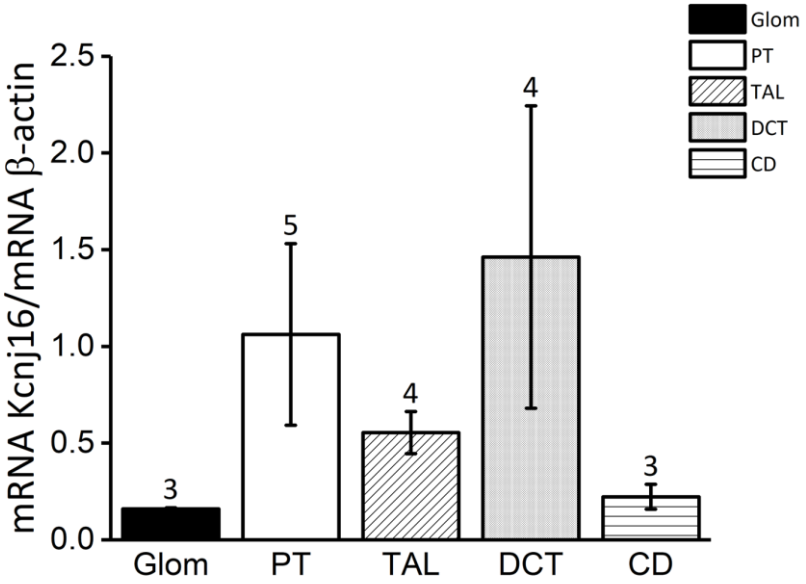

Figure 8. Real-time PCR analysis of Kcnj16 mRNA levels in the nephron segments.
Real-time PCR analysis of manually sorted nephron segments showed mRNA expression of Kcnj16 in the different segments of the kidney. Expression of Kcn16 was predominantly found in the proximal tubule (PT) and distal convoluted tubule (DCT) while lower expression was found glomeruli (Glom), thick ascending limbs (TAL) and collecting ducts (CD). Graphs represent mean mRNA expression levels normalized to β-actin ± SEM; numbers above SEM indicate the number of mice.

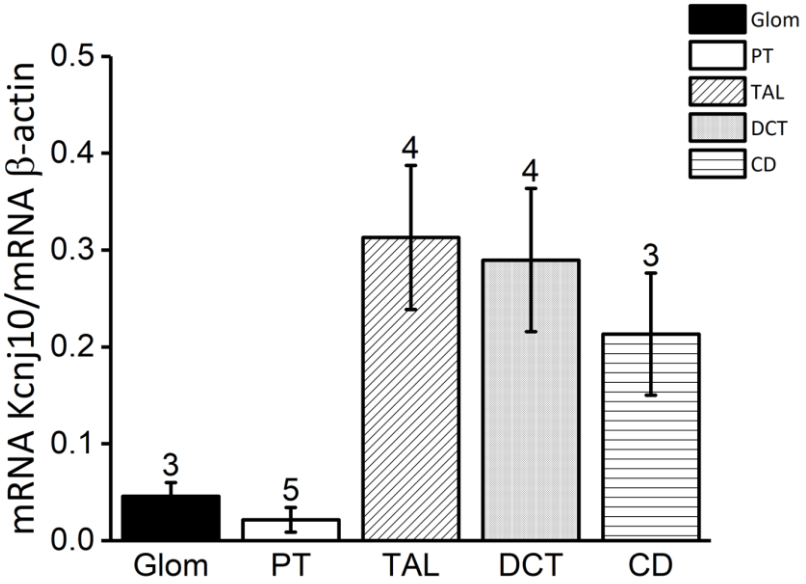

Figure 9. Real-time PCR analysis of KcnJ10 mRNA levels in the nephron segments.
Real-time PCR analysis of manually sorted nephron segments showing mRNA expression of Kcn10 in the different segments of the kidney. Expression of Kcn10 is predominantly found in later nephron segments like thick ascending limbs (TAL), distal convoluted tubules (DCT) and collecting ducts (CD). Low expression was found in glomeruli (Glom) and proximal tubules (PT). Graphs represent mean mRNA expression levels normalized to β-actin ± SEM; numbers above SEM indicate the number of mice.

The expression of Kcnj16 in PTs and DCTs was confirmed using a Kir5.1$^{-/-}$ mouse model, where a *LacZ* gene was placed under the control of the Kcnj16 promotor. This allowed assessing Kcnj16 promotor-driven X-Gal activity. Consecutive cryo-sections of transgenic Kir5.1$^{-/-}$ kidneys were prepared and either stained with X-Gal (see 3.2.3.6) or with specific tubule section markers (calbindin and aquaporin-2). The markers allow identification of the renal tubular segment (Figure 10).

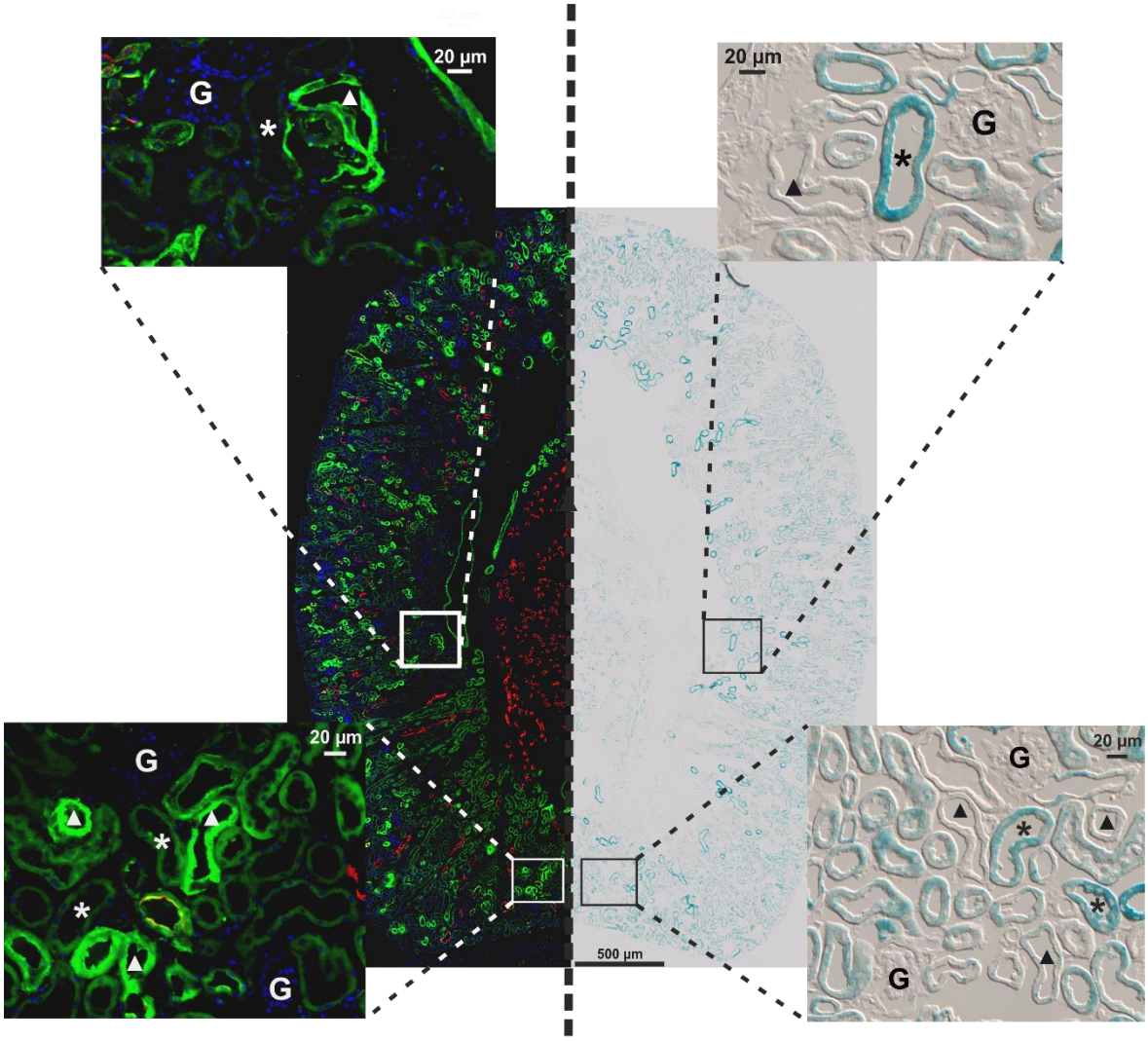

Figure 10. Expression of KCNJ16 in mouse kidney.
Overviews of two consecutive kidneys cryo-sections of Kir5.1$^{-/-}$ mice that were stained either with antibodies against specific tubule markers (left) or with X-Gal (right). The blue X-Gal staining can be found throughout the cortex predominantly in proximal tubules (*) and distal convoluted tubules (▲). This becomes apparent when comparing stained tubules in the mirrored consecutive slide that was stained with antibodies against the distal convoluted tubule marker calbindin (green) or the collecting duct marker aquaporin 2 (red). Nuclei are depicted in blue and can be used to identify glomeruli (G), in which no KCN16 expression could be observed.

Figure 10, illustrates Kcnj16 promotor-driven X-gal staining (blue coloration) in the mouse kidney. Through co-localization analysis, in Kir5.1$^{-/-}$ mouse kidneys, β-galactosidase activity was detected in proximal and distal convoluted tubules (DCT). This became apparent when

consecutive kidney sections were stained with DCT/CNT-marker calbindin. However, not all proximal or distal tubules were positive for KCNJ16 expression. Additionally, no blue coloration of glomeruli or connecting tubule/collecting duct (CNT/CD) stained with aquaporin-2 was observed.

4.1.3 Electrophysiological experiments

A new patient was identified with renal salt wasting with homozygous missense mutation of KCNJ16 gene, the mutation p.Arg35Gln (R35Q), where an arginine (Arg, R) is replaced by a glutamine (Gln, Q). However, a causal link between the mutation and the clinical phenotype could not yet be established because linkage analysis was not possible with only with one patient. Previously, another KCNJ16 p.Arg137Cys (R137C) mutation revealed an effect on membrane localization, as the trafficking of the mutant R137C was affected and the mutant Kir5.1 channels hardly reached the membrane.[69] Therefore, the consequences of the new Kir5.1 mutation on the subcellular localization, membrane targeting and function were studied using immunofluorescence and patch clamp technique (whole cell and single channel experiments).

4.1.3.1 Immunofluorescence of transfected cells

Since Kir5.1 alone does not form a functional homomeric channel, CHO cells were co-transfected with Kir4.1 and Kir5.1 and stained with an anti-Kir5.1 antibody to determine the effect of the mutation R35Q on the trafficking to the membrane and the ability of the proteins to form heteromeric Kir4.1-Kir5.1 channel complexes. Figure 11 shows that both proteins ($Kir5.1^{wt}$, Figure 11 B; and $Kir5.1^{R35Q}$; Figure 11 C) appear to be partially located in the membrane. The mutation R35Q did not seem to affect the trafficking of the protein to the membrane.

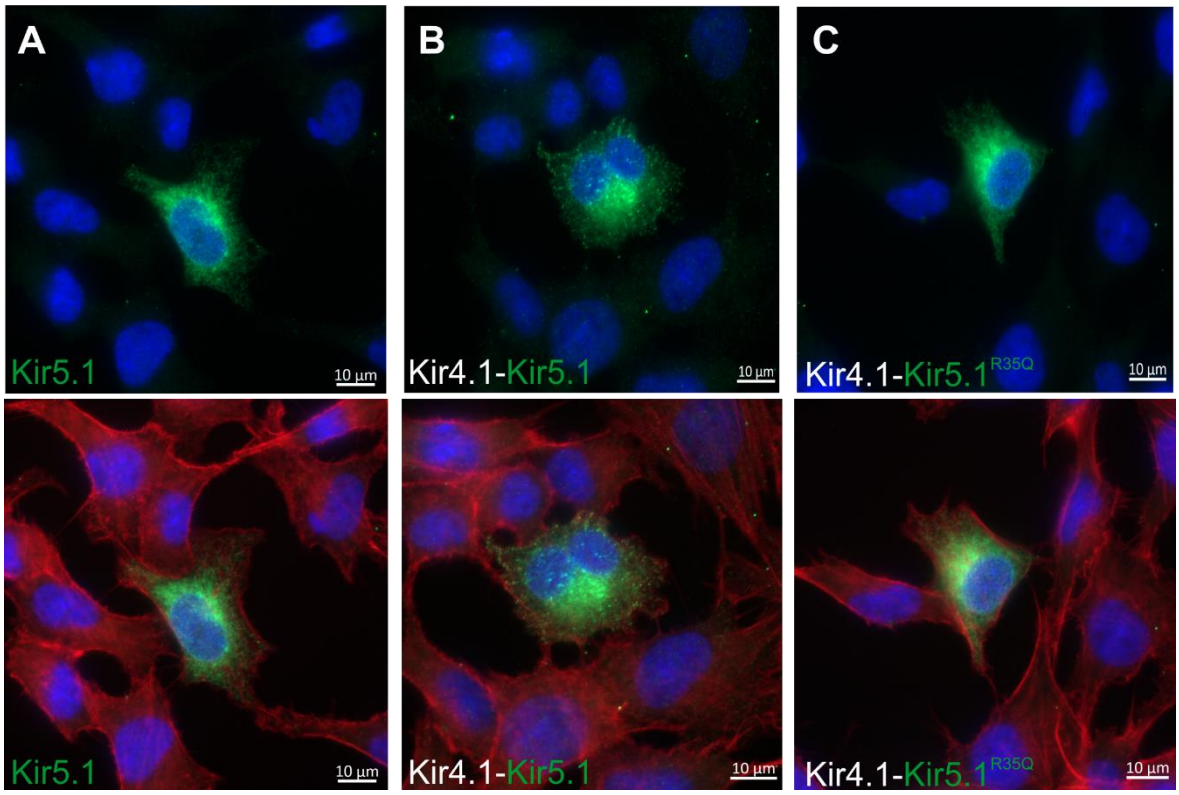

Figure 11. Immunofluorescence of Kir5.1 transfected CHO cells.
CHO cells transfected with Kir4.1 and Kir5.1 were stained with a Kir5.1 antibody (green) and phalloidin (red, distribution of filamentous actin). (A) Kir5.1^{wt}, (B) Kir4.1-Kir5.1^{wt} and (C) Kir4.1-Kir5.1^{R35Q}. Both Kir5.1 forms show a partial membrane localization suggesting that both Kir5.1 variants make heteromeric channel complexes with Kir4.1 and that the traffic of the Kir5.1^{R35Q} mutant was not affected.

4.1.3.2 Whole cell measurements

Immunofluorescence results confirmed that the Kir5.1 mutant R35Q reaches the membrane of the cells and likely forms heteromers with Kir4.1. To investigate the function of the Kir5.1^{R35Q} mutant, patch-clamp measurements were carried out on transfected CHO cells. CHO cells were co-transfected with Kir4.1 and Kir5.1 in two different stoichiometric ratios, a ratio of 1:1 to analyze the effect of Kir5.1 on Kir4.1-mediated currents and a ratio of 1:10, with a 9 fold higher concentration of Kir5.1 to avoid the formation of homomeric Kir4.1 channels.[30]

The membrane potential was measured under control conditions and after applying a Ba^{2+}-containing solution. Ba^{2+} is a divalent cation capable of reversibly blocking a broad variety of K^+ channels.[70,71] It was used to detect the activity of K^+ channels and measure Ba^{2+}-sensitive currents.

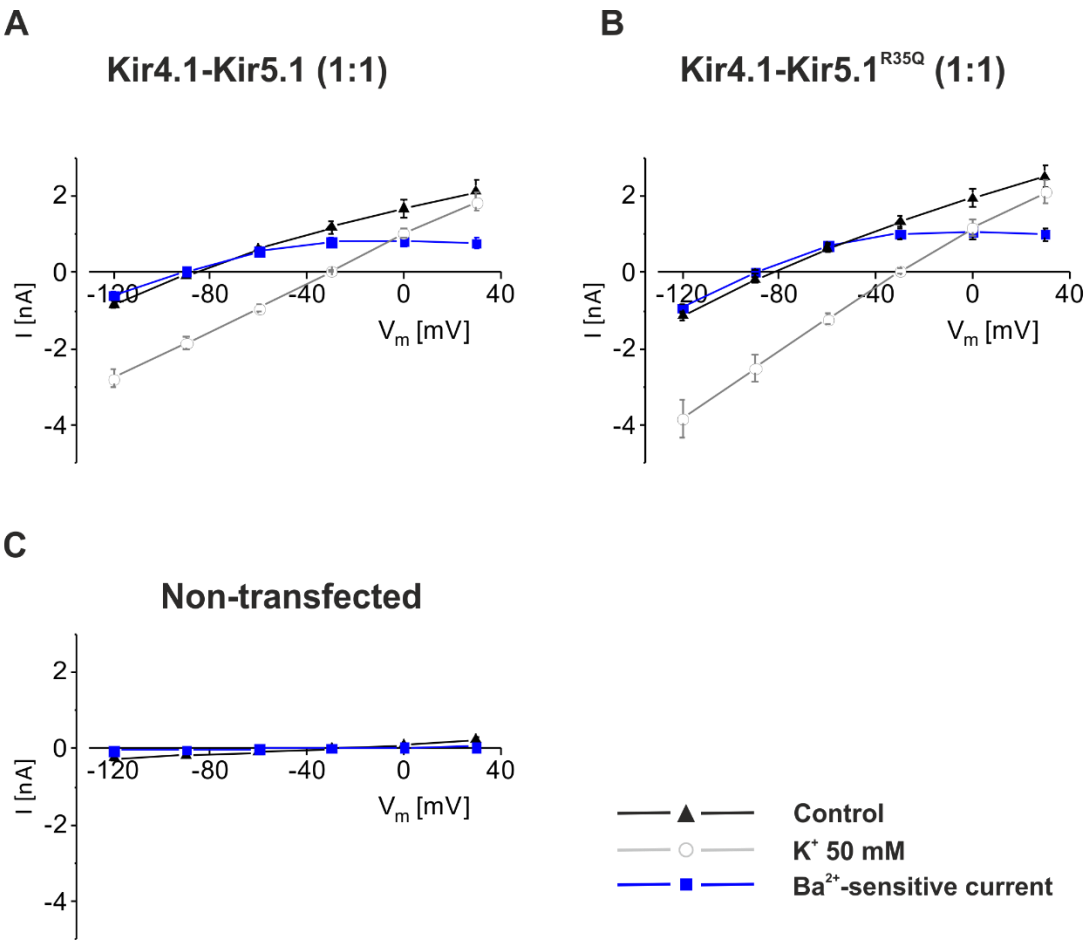

Figure 12. Whole cell currents of heteromeric Kir4.1-Kir5.1 and Kir4.1-Kir5.1^{R35Q} channels. CHO cells were co-transfected with Kir4.1 and (A) Kir5.1^{wt} (n=15) or (B) Kir5.1^{R35Q} (n=16) in a stoichiometric ratio of 1:1. (C) Non-transfected cells served as control cells. Current – voltage (I/V) curves are shown under control (—▲—) and external high K^+ 50 mM (—○—) conditions. Additionally, calculated Ba^{2+}-sensitive I/V curves (—■—) are shown, that were obtained in the presence of 100 µM Ba^{2+} in the bath solution. Values represent mean values ± SEM.

Homomeric Kir5.1 channel complexes, as reported previously, did not induce measurable currents or hyperpolarize the membrane.[39,54,55,72] Instead, Kir5.1 formed heteromers with Kir4.1 resulting in reduced whole-cell conductance when compared to Kir4.1 homomeric channels (Figure 13 A). To study the contribution of Kir5.1 to Kir4.1-mediated currents, cells were co-transfected with Kir4.1. The membrane voltage of cells expressing homomeric Kir4.1 or Kir4.1-Kir5.1 (wt or R35Q) heteromers were hyperpolarized close to equilibrium potential of K^+ (Figure 12 and 13) when compared to non-transfected cells (-29±5 mV; Figure 12 C). Cells co-expressing Kir4.1-Kir5.1, in a ratio 1:1 exhibited large K^+ currents and were strongly hyperpolarized (Figure 12 A). Similar results were obtained for the Kir4.1-Kir5.1^{R35Q} (Figure 12 B) channel that was undistinguishable from the K^+ currents elicited Kir4.1 alone (Figure 13 A). These effects may be due to homomeric Kir4.1 channels that have a tendency to assemble. To reduce the formation of Kir4.1 homomers, cells were co-

transfected with Kir4.1-Kir5.1 (wt or R35Q) in a ratio of 1:10 (Figure 13). As shown in Figure 13 C and E, both heteromeric channel complexes containing Kir5.1 have smaller whole-cell currents when compared to homomeric Kir4.1-mediated currents (Figure 13 A).

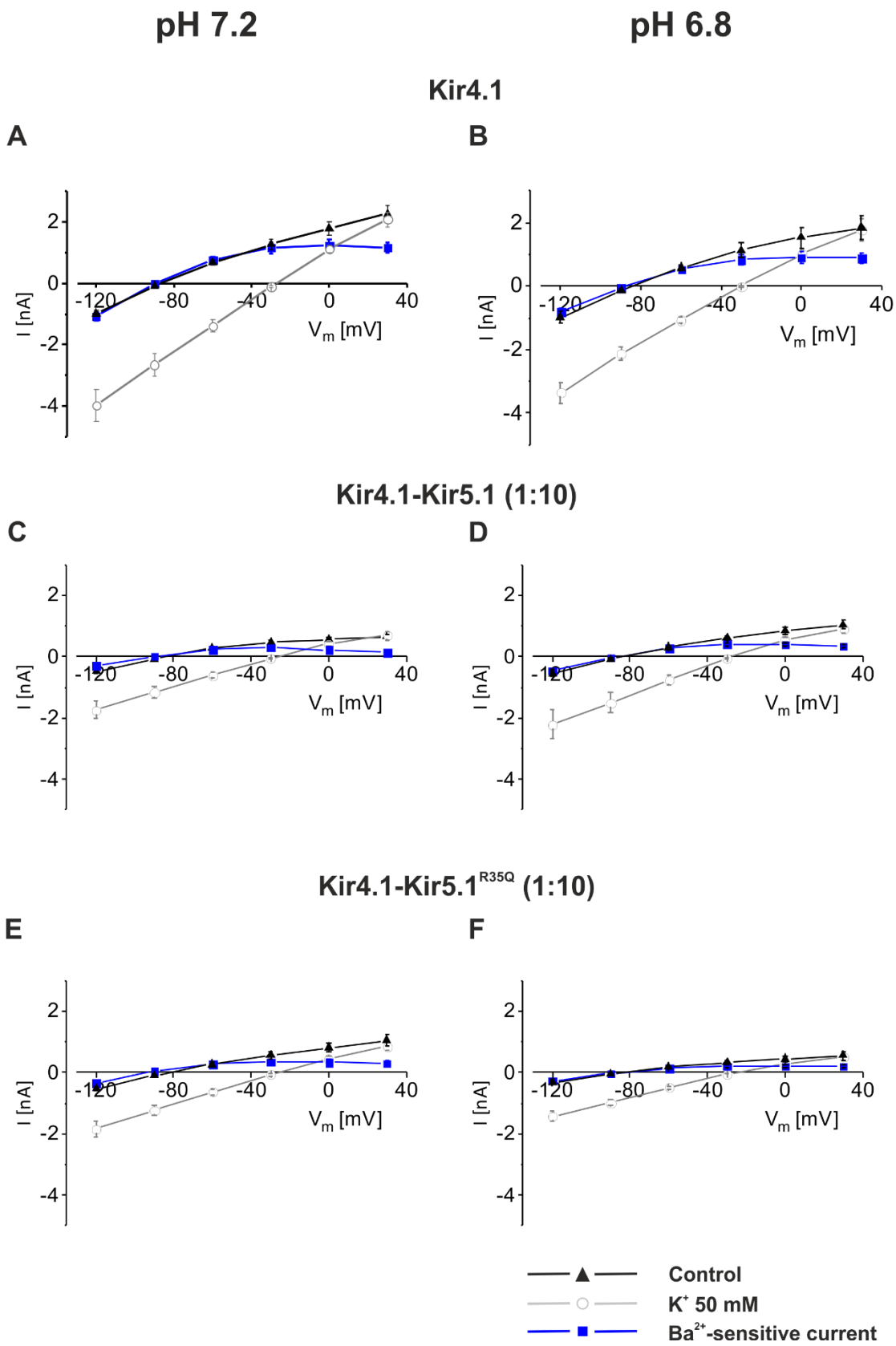

Figure 13. Effect of intracellular pH on Kir4.1-Kir5.1-mediated whole cell currents.
Whole cell currents of CHO cells co-transfected with Kir4.1 and Kir5.1 under two different pH pipette solutions, pH=7.2 and 6.8. Current–voltage (I/V) relationship of (A-B) Kir4.1, (C-D) heteromers Kir4.1-Kir5.1^{wt} and (E-F) Kir4.1-Kir5.1^{R35Q} (1:10) under control (—▲—) and K^+ 50 mM (—○—) solutions. Mean values ± SEM of whole cell conductance are shown before applying K^+; after applying 50 mM of K^+ and calculated Ba^{2+}-sensitive currents (—■—).

Application of Ba^{2+} (100 µM) led to depolarization of the cells due to inhibition of Kir channels by Ba^{2+} ions. As a measure of the Kir K^+ currents, the Ba^{2+}-sensitive currents were calculated (blue squares in charts). Expression of Kir4.1 homomeric or heteromeric channels induced large Ba^{2+}-sensitive currents. However, heteromeric Kir4.1-Kir5.1^{R35Q} channels displayed similar currents that were not different from the wildtype Kir4.1-Kir5.1 heteromers suggesting that surprisingly the missense mutation did not affect the channel function. The conductance of the heteromeric Kir4.1-Kir5.1 channel was reported to be sensitive to intracellular pH, while extracellular acidification in oocyte experiments showed no effect on whole cell currents. To test whether intracellular pH was able to regulate Kir4.1-Kir5.1 channels in CHO cells, the pipette solution was changed from pH 7.2 to more acidic pH 6.8 (Figure 13 B, D and F). Surprisingly, the heteromeric Kir4.1-Kir5.1 channels, either Kir5.1^{wt} or Kir5.1^{R35Q}, exhibited currents similar to those under control conditions. This is in contrast to previous reports showing an inhibition of heteromeric channel activity at acidified intracellular pH.[55,58,73]

The apparent lack of sensitivity towards intracellular pH change could be explained by i) lack of heteromeric channel assembly or ii) insufficient diffusion of the pipette solution into the cells allowing pH-regulating mechanism of the cell to keep intracellular pH rather constant. To test the first hypothesis, single channel experiments were performed allowing to assess the presence or absence of heteromers according to their specific single channel properties.

4.1.3.3 Effects of Kir5.1 mutation at single channel level

The mutant Kir4.1-Kir5.1^{R35Q} channels showed K^+ currents in whole cell experiments similar to wildtype Kir4.1-Kir5.1. To assess whether transfection of both Kir4.1 and Kir5.1 resulted in heteromeric channels assembly, single channel recordings were made of transfected HEK cells. Heteromerization between Kir4.1 and Kir5.1 is known to produce channels with characteristic single channel properties. In the cell-attached configuration with a bath-like pipette solution, Kir4.1-expressing cells (Figure 14 A) showed large inwardly rectifying currents with clear single channel levels and no sub-states. In line with previous reports, the conductance at 0 mV was ~30 pS. Additionally, homomeric Kir4.1 exhibited a high open probability (70-80%).[30]

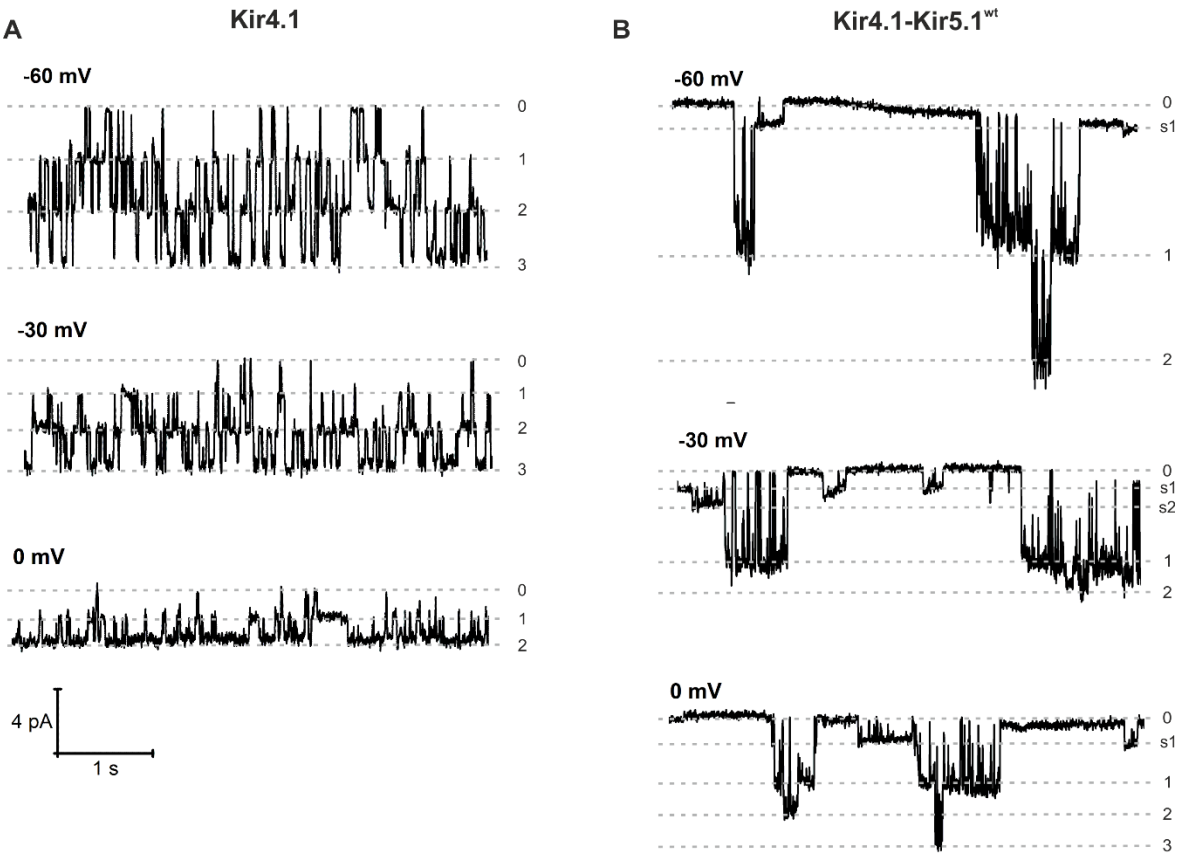

Figure 14. Representative single channel trace of HEK cells transfected with Kir4.1 and Kir4.1-Kir5.1^{wt}.
Single channel recordings of transfected HEK cells in the cell-attached configuration at voltage clamps of 0, -30 and -60 mV. (A) Homomeric Kir4.1 channels showed clear single channel levels and high open probability while (B) Kir4.1-Kir5.1^{wt} heteromeric channels showed larger channel conductance and additional sub-states (s1-s2). Additionally, open probability of Kir4.1-Kir5.1^{wt} was lower compared to Kir4.1 homomeric channels.

In contrast, Kir4.1-Kir5.1^{wt} heteromers produced higher single channel current amplitudes when compared to Kir4.1 homomers. In single channel recordings of Kir4.1-Kir5.1 (Figure 14 B) and Kir4.1-Kir5.1^{R35Q} (Figure 15 A) heteromers regularly displayed sub-states of smaller sizes, as reported previously.[56] The amplitude of Kir4.1-Kir5.1^{R35Q} did not differ from the ones of Kir4.1-Kir5.1 channels, which exhibited large current amplitudes and sub-states activity. During the time of the recording heteromeric Kir5.1^{wt} or Kir5.1^{R35Q} were not as active when compared to homomeric Kir4.1 channels.

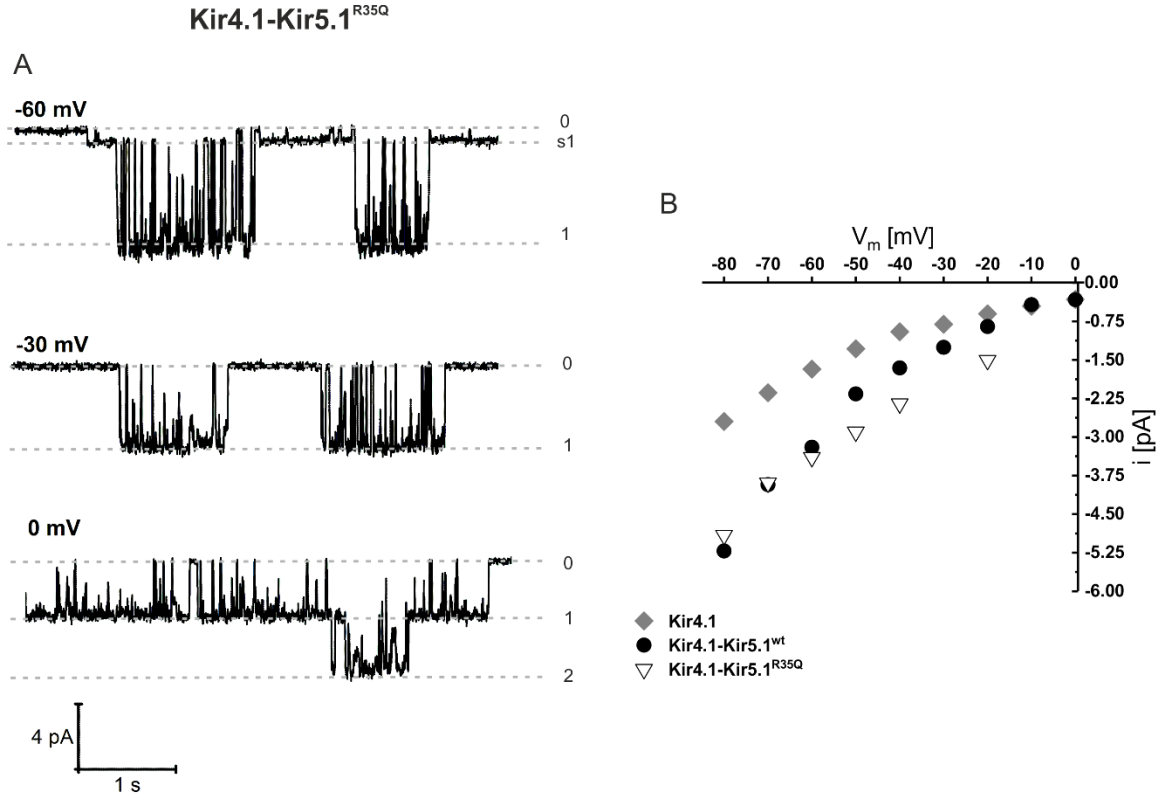

Figure 15. Electrophysiological single channel analysis of heteromeric Kir4.1-Kir5.1^{R35Q} channels.
Single channel recording of transfected HEK cells in cell-attached configuration at voltage clamps of 0, -30 and -60 mV. (A) Kir4.1-Kir5.1^{R35Q} channels showed higher conductance with characteristic sub-states but reduced open probability. (B) Single channel current-voltage relationship of measurements in inside-out patch configuration with symmetrical solutions presented a 32 pS conductance for Kir4.1, 56.6 pS for Kir4.1-Kir5.1^{wt} and 56.7 pS for Kir4.1-Kir5.1^{R35Q}.

Figure 15 B shows single channel recordings of homomeric Kir4.1, heteromeric Kir4.1-Kir5.1^{wt} and Kir4.1-Kir5.1^{R35Q} in the inside-out configuration. The solution used in the bath and the pipette were the same in order to have symmetrical conditions to circumvent concentration differences as a driving force for K^+ ions. Single channel conductance was calculated between membrane voltage of -10 and -80 mV, and heteromeric Kir4.1-Kir5.1 and Kir4.1-Kir5.1^{R35Q} presented similar conductance (~60 pS), which was higher than that obtained for homomeric Kir4.1 of ~30 pS.

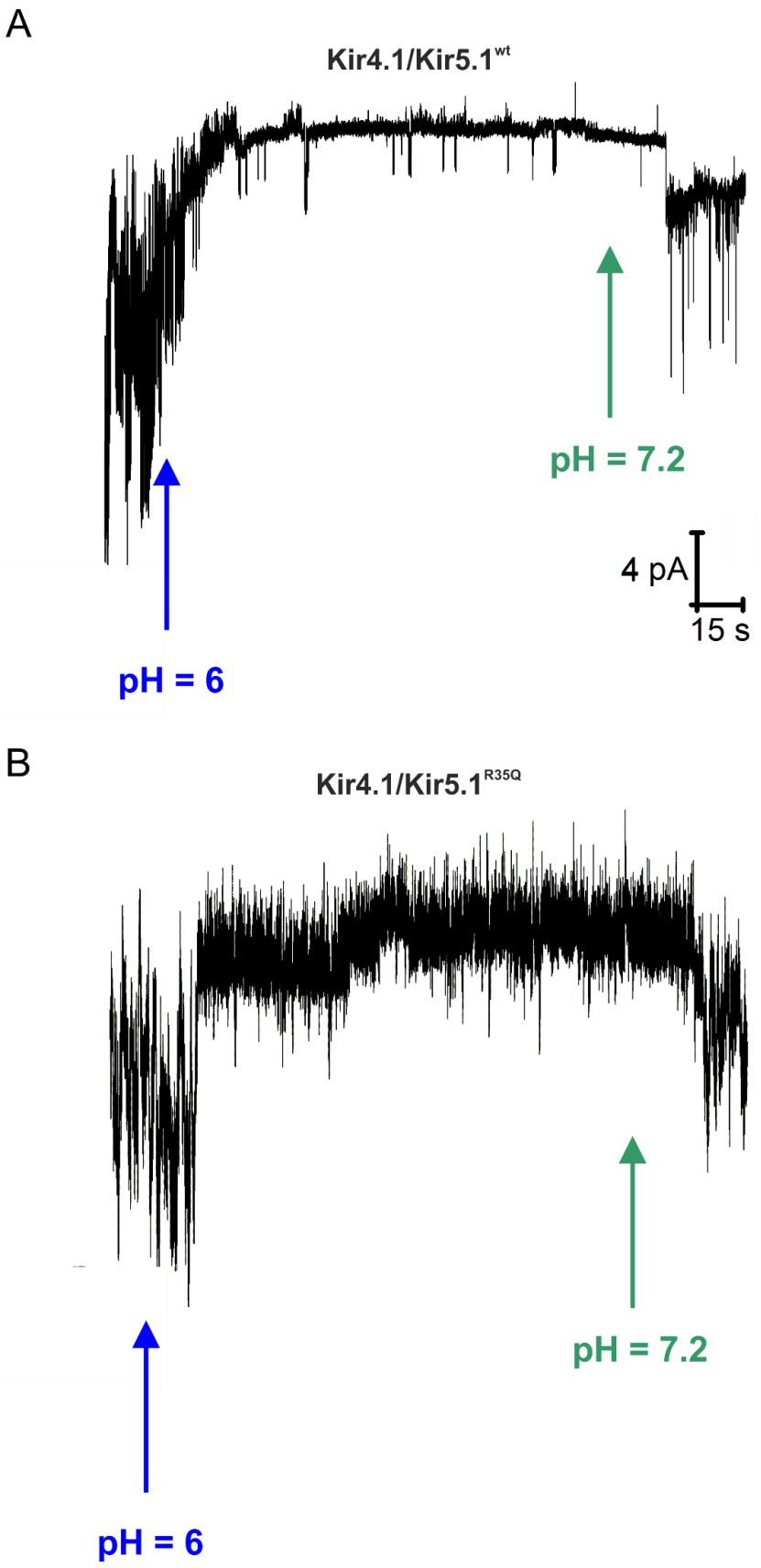

Figure 16. Sensitivity of Kir4.1-Kir5.1 channels to intracellular pH.
Representative inside-out patch recordings of transfected HEK cells. Channel activity was evoked by voltage command to -70 mV during patch perfusion with control solution with pH7.2. Blue arrows indicate a change to pH 6.0 and consequent channel inhibition of (**A**) Kir4.1-Kir5.1^{wt} and (**B**) Kir4.1-Kir5.1^{R35Q} and recovery after adding the solution with pH 7.2 (green arrow).

To confirm the effect of intracellular acidification on the heteromeric channels activity from excised membrane patches were recorded. Figure 16 shows that exposure of the intracellular surface of the patch to a solution of pH 6.0 (blue arrow) rapidly reduced the activity of these channels. This effect was reversible after adding the solution with pH 7.2 (green arrow) with recovery of the channels activity. These results clearly demonstrate that intracellular acidification inhibits both the Kir4.1-Kir5.1^{R35Q} and the Kir4.1-Kir5.1^{wt} heteromeric channels.

4.2 Kir5.1$^{-/-}$ Mouse Model

The electrophysiological analysis of the Kir5.1^{R35Q} mutation did not reveal a loss-of- or gain-of-function, which still might be explained by the lack of physiological conditions in heterologous expression systems. Nevertheless, expression and localization of Kir5.1 in the kidney as well as the tubulopathy of the patient with the Kir5.1^{R35Q} mutation still suggested a role of Kir5.1 in tubular transport. More specifically, the hypokalemic acidosis in combination with hypercalciuria and hypermagnesuria observed in this patient suggested an impairment of the distal tubules. A renal tubular acidosis resulting from severe proximal tubular dysfunction would likely present with phosphaturia, glycosuria, aminoaciduria, uricosuria, and tubular proteinuria as well. Additionally, previous publications of a Kir5.1$^{-/-}$ mouse model from Paulais et al. already showed that Kir5.1$^{-/-}$ mice developed hypokalemic acidosis although no hypocalcaemia or hypomagnesemia was observed.[54] The functional importance of Kir channels in ion transport in the DCT has also been recognized by mutations in Kir4.1 which cause EAST/SeSAME syndrome and are known to have electrolyte imbalance with hypokalemia, metabolic alkalosis, hypomagnesemia and hypocalciuria.[16,25,30,33,52]

Besides a role in renal electrolyte balance, Kir5.1 was also suggested to be involved in the development of hypertension. According to Palygin et al.[74] expression of Kir5.1 was upregulated after a high salt diet (4% NaCl) which correlated between the development of salt-sensitive hypertension and basolateral K^+ channel function in Dahl salt-sensitive rats. Based on those previous studies, we analyzed the electrolyte excretion as well as blood parameters in our own Kir5.1$^{-/-}$ mice as well as the effects of a high salt diet (4% NaCl) in this model.

4.2.1 Basal electrolyte excretion of adult mice

To investigate the importance of Kcnj16 deletion on electrolyte balance and K^+ homeostasis in the body and taking into account the results from Palygin et al. we examined electrolyte excretion in adult (3-4 months) control (n = 20) and Kir5.1$^{-/-}$ mice (n = 19) of both genders.[74]

Basal electrolyte excretion was determined by collecting spot urine at least four times under control diet and measuring the electrolytes by ion chromatography. Since the concentration of the ions in the urine depends strongly on urine concentration (i.e. water reabsorption), electrolytes were normalized to creatinine. Creatinine is a breakdown product of creatine phosphate in muscles, freely filtered in the glomerulus and hardly reabsorbed or secreted along the nephron and is therefore usually excreted into the urine at a constant rate and used to normalize the values. Creatinine levels had a tendency to be lower in the Kir5.1$^{-/-}$ mice, but Kir5.1$^{-/-}$ mice were significantly smaller (21.69±1.24 g) when compared to the wildtype (26.30±0.90 g). Thus, when we normalized the absolute creatinine excretion (corresponding to creatinine production) to the body weight similar levels of absolute creatinine excretion were observed between the groups. Henceforth, all urinary electrolytes were normalized to creatinine concentrations.

A

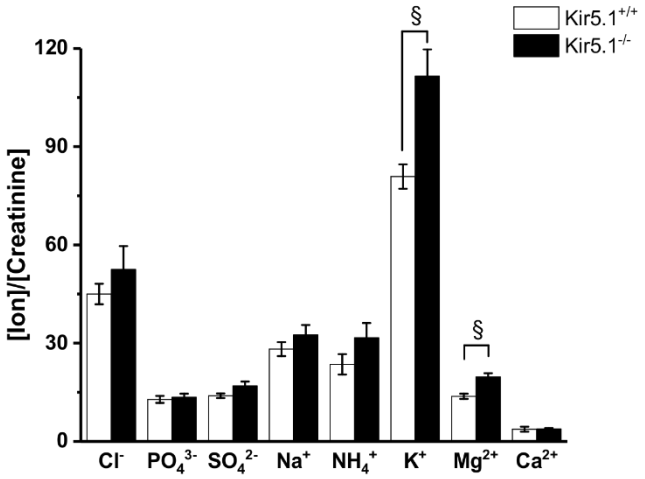

B

	Kir5.1$^{+/+}$		Kir5.1$^{-/-}$		
	Mean	SEM	Mean	SEM	p-value
Cl^-	45.0	3.1	52.5	7.1	0.340
PO_4^{3-}	12.8	1.1	13.5	1.1	0.670
SO_4^{2-}	13.9	0.7	17.0	1.3	0.046
Na^+	28.2	2.1	32.6	3.0	0.246
NH_4^+	23.5	3.1	31.7	4.5	0.152
K^+	80.9	3.7	111.5	8.2	0.002
Mg^{2+}	13.8	0.8	19.7	1.1	0.0001
Ca^{2+}	3.7	0.8	3.8	0.3	0.920

Figure 17. Normalized electrolyte excretion of mice during standard food.
(A) Electrolyte excretion of Kir5.1$^{-/-}$ (n = 19) and control Kir5.1$^{+/+}$ (n=20) mice under standard diet. All ions concentrations were normalized to creatinine concentration in urine and presented as [mM ion/mM Creatinine]. (B) Table displaying electrolyte excretion values presented in graph. Kir5.1$^{-/-}$ mice excreted higher amounts of measured ions like SO_4^{2-}, K^+ and Mg^{2+}. Statistical analysis was performed with an unpaired Student's t-test and the level of significance is provided in the table (B). After Bonferroni corrections, p-values ≤ 0.006 were accepted as significantly different (§).

Under control conditions, the normalized electrolyte excretion of mice showed similar results for both groups of animals in Cl^-, PO_4^{3-} and Na^+, NH_4^+ and Ca^{2+} excretion. However, for Mg^{2+} and K^+ there were significant differences between the two groups with Kir5.1$^{-/-}$ animals showing a higher excretion of those electrolytes in the urine. In Figure 17, the same values are presented in the table. K^+ and Mg^{2+} ions were excreted at higher levels into the urine by the knockout animals suggesting hypokalemia and hypermagnesuria, which is in agreement with the phenotype displayed by the human patient.

4.2.2 Effect of amiloride on electrolyte excretion levels

Considering the hypokalemia displayed by the human patient and the mice, we investigated the effect of the K^+-sparing diuretic amiloride. Amiloride is a blocker of the epithelium sodium channel ENaC, which mediates sodium reabsorption in the late DCT (DCT2), CNT and CD and therefore promotes the loss of Na^+ and reduces K^+ secretion into the urine. Urine samples from animals (Kir5.1$^{+/+}$, n = 12 and Kir5.1$^{-/-}$, n = 9) kept in metabolic cages were collected for 6h at control conditions and 6h after amiloride injection.

As depicted in Figure 18, the mice showed increased urinary Na^+ and decreased K^+ excretion 6h after amiloride injection (5 µg/g BW i.p). The response was similar in both groups (Figure S2) indicating that ENaC-mediated Na^+ absorption was not altered by deletion of Kir5.1. The small effect of amiloride could also be due to the salt supplementation of the water (see Method section for details), 24h before the experiment, given to the mice. Nevertheless, the results display a tendency of Kir5.1$^{-/-}$ to have a higher amiloride-sensitive K^+ excretion. In light of these results, amiloride could be used to normalize plasma K^+ in hypokalemic human patients suffering from a Kir5.1 defect.

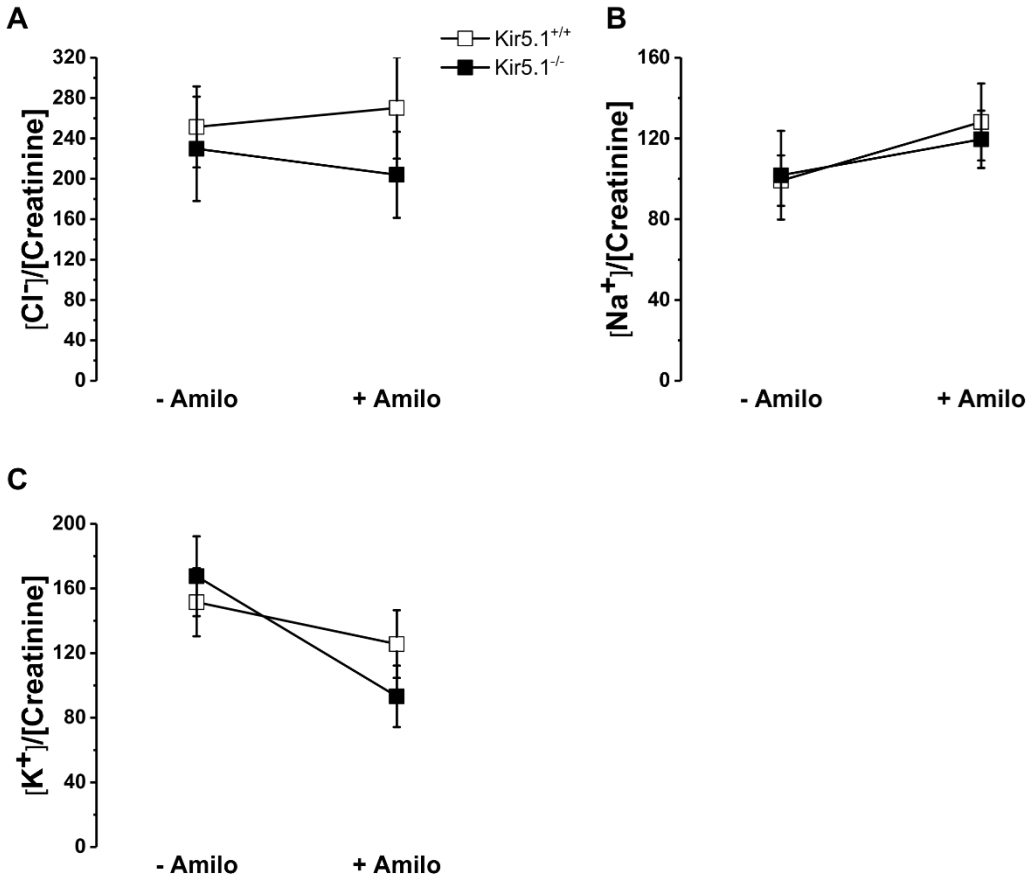

Figure 18. Effect of amiloride on normalized electrolyte excretion of mice.

Electrolyte excretion of Kir5.1$^{-/-}$ (n = 19, ■) and control Kir5.1$^{+/+}$ (n=20, □) mice under standard diet. All ions concentration were normalized to creatinine concentration in the urine are presented as [mM ion/mM Creatinine]. (A) Cl^-, (B) Na^+, (C) K^+. Statistical analysis was performed with an unpaired Student's t-test.

4.2.3 Effect of high Na^+ diet on electrolyte excretion levels

The role of Kir5.1 in the development of hypertension was investigated by Palygin and co-workers. They created a Dahl salt-sensitive Kir5.1 deficient rat model that exhibited a renal phenotype reminiscent of SeSAME/EAST and Kir4.1 deletion: salt wasting, hypomagnesemia, and hypokalemia.[74] Interestingly, the absence of Kir5.1 resulted in prominent retention of Kir4.1 in the cytosol of DCTs suggesting improper translocation of Kir4.1 in the absence of Kir5.1 in rats. This is the opposite of the marked upregulation of plasma membrane Kir4.1 in normotensive mice lacking Kir5.1.[54] To determine whether improper Kir4.1 translocation is a common feature in hypertension or whether it is a feature only found in rat models, we induced a high salt stress in adult (3-4months) control Kir5.1$^{+/+}$ (n = 8) and Kir5.1$^{-/-}$ mice (n = 10). The mice were feed a high Na^+ (HNa) diet for 15 days, which is commonly used to induce hypertension in C57BL6/J mice.[75,76] Blood was taken seven days before the start of the diet to allow the mice to recover.

After the control period, Kir5.1$^{+/+}$ and Kir5.1$^{-/-}$ mice were fed a high salt diet (4% NaCl). During the diet, urine samples were collected. At the end of the diet, blood was collected again. Figure 19, shows the time course of the normalized electrolyte excretion under high salt diet. Day 0 represents the mean excretion before the experimental diet.

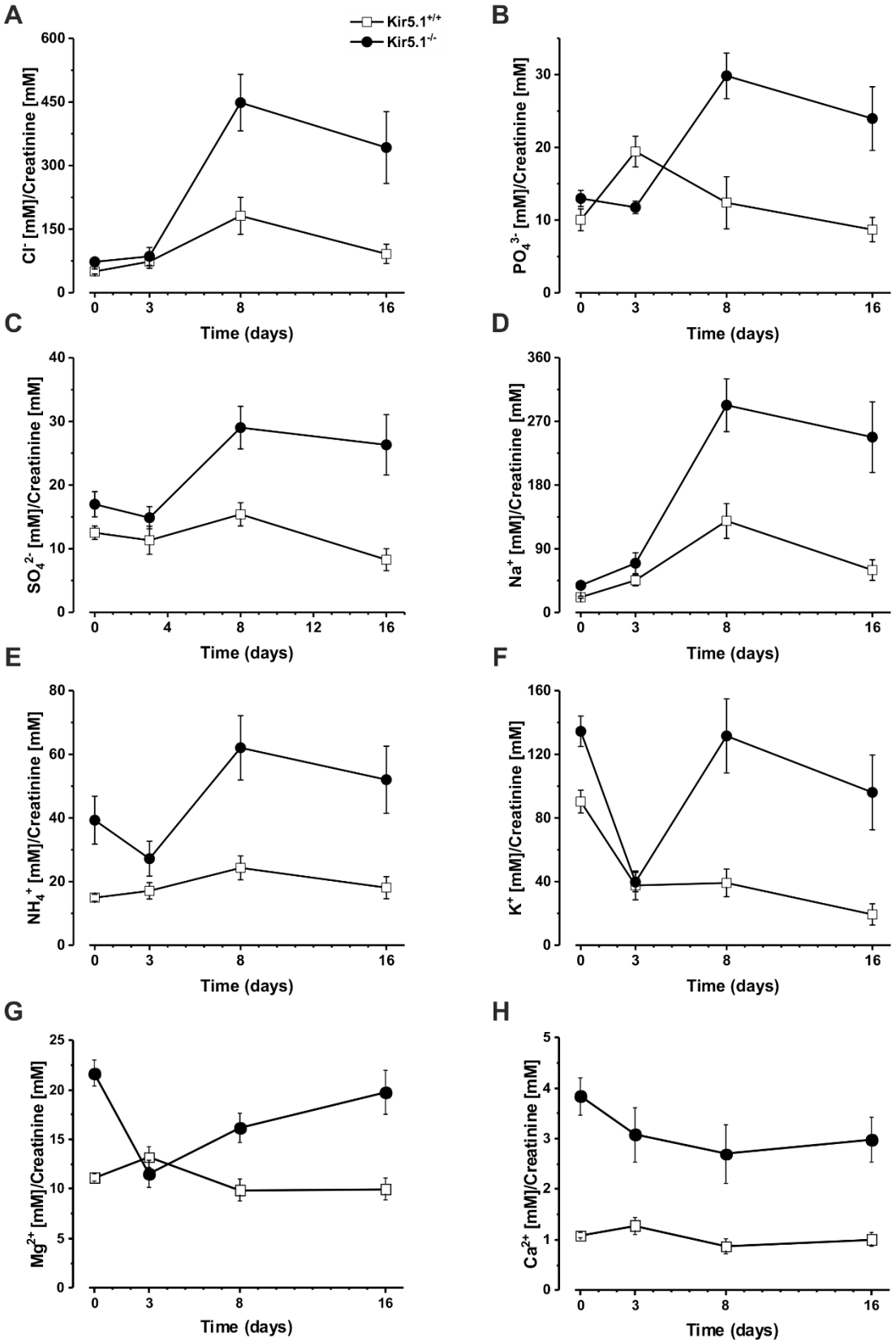

Figure 19. Normalized excretion of various electrolytes from Kir5.1$^{-/-}$ and control mice under high salt (4%) diet.

Excretion of (A) Cl^-, (B) PO_4^{3-}, (C) SO_4^{2-}, (D) Na^+, (E) NH_4^+, (F) K^+, (G) Mg^{2+} and (H) Ca^{2+} in the urine were investigated during the high Na^+ diet. All values were normalized to creatinine. The day 0 corresponds to the mean excretion before the start of the diet. During the course of the diet, electrolyte loss in Kir5.1$^{-/-}$ mice become more pronounced which suggests an impaired adaptation

mechanism in the Kir5.1$^{-/-}$ mice. Data represents mean values ± SEM. Statistical analysis was performed with an unpaired Student's t-test between the groups.

Kir5.1$^{-/-}$ mice display a higher excretion of ions in the urine during the diet when compared to Kir5.1$^{+/+}$ mice. As expected, control animals also display an increased excretion of Na^+ and Cl^- in response to the high Na^+ diet. It is noticeable, that from day 8 to the end of the diet Kir5.1$^{-/-}$ mice excreted statistically significant higher amounts of ions to the urine (Table S1). At the end of HNa diet, urinary excretion of all analyzed electrolytes was significantly elevated in Kir5.1$^{-/-}$ animals when compared to wildtype (Figure 20) suggesting an impaired adaptation capacity in the Kir5.1$^{-/-}$ mice.

A

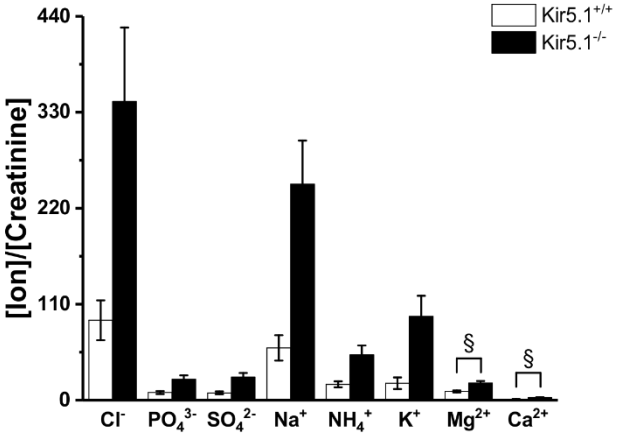

B

	Kir5.1$^{+/+}$		Kir5.1$^{-/-}$		
	Mean	SEM	Mean	SEM	p-value
Cl^-	91.5	22.9	342.4	84.7	0.027
PO_4^{3-}	8.7	1.7	23.9	4.4	0.012
SO_4^{2-}	8.3	1.7	26.3	4.7	0.007
Na^+	59.9	14.5	247.6	49.8	0.007
NH_4^+	18.1	3.5	52.0	10.6	0.018
K^+	19.3	6.7	96.1	23.5	0.016
Mg^{2+}	10.0	1.1	19.7	2.2	0.003
Ca^{2+}	1.0	0.1	3.0	0.4	0.002

Figure 20. Normalized excretion of various electrolytes from Kir5.1$^{-/-}$ and control mice after high salt (4%) diet.
(A) Electrolyte excretion of Kir5.1$^{-/-}$ (n = 10) and Kir5.1$^{+/+}$ (n=8) mice subjected to HNa diet (16 day). All ions concentration were normalized to creatinine concentration in urine and presented as [mM ion/mM creatinine]. (B) Table with electrolyte excretion values presented in graph. Kir5.1$^{-/-}$ mice excrete higher amounts of all measured ions suggesting a tubular disorder. Data represents mean values ± SEM. Statistical analysis was performed with an unpaired Student's t-test and the level of significance is provided in the table (B). After Bonferroni corrections, p-values ≤ 0.006 were accepted as significantly different (§).

Analysis of urine excretion at the end of HNa diet revealed a salt-wasting phenotype in Kir5.1$^{-/-}$ mice with a higher excretion of electrolytes in the urine. However, K^+, Na^+ and Cl^- were the major electrolytes excreted (Figure 20).

Even though Kir5.1$^{-/-}$ animals displayed a higher loss of ions into the urine no significant alteration was observed in mice weight (Figure 21 B). Both groups displayed similar weight with small fluctuations throughout the 16 days subjected to HNa diet. Creatinine concentration values, even though not significantly different revealed a similar pattern since at day 8 there seemed to be a dilution of the urine in both groups (Figure 21 A).

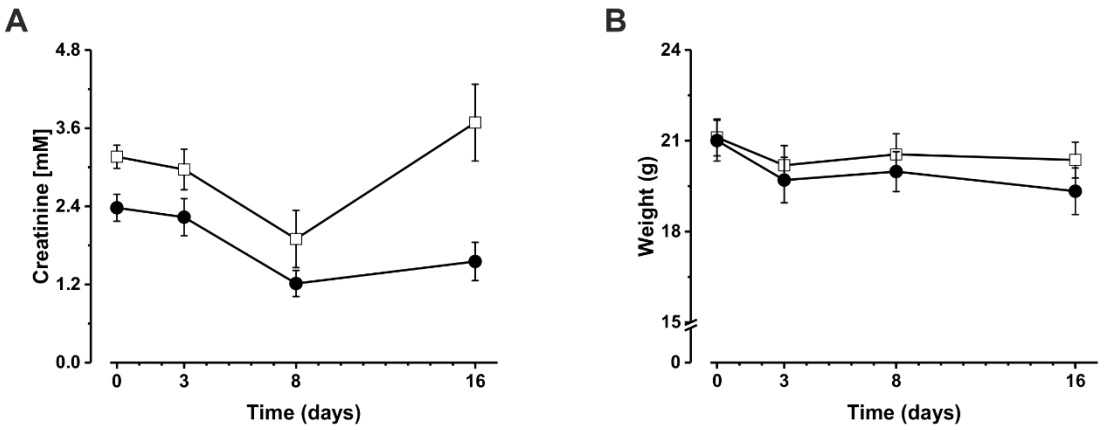

Figure 21. Creatinine values and weight of Kir5.1$^{+/+}$ and Kir5.1$^{-/-}$ mice during high salt (4%) diet.
(A) Creatinine concentration values and (B) body weight of Kir5.1$^{+/+}$ (—□—) and Kir5.1$^{-/-}$ (—●—) animals throughout the HNa diet. The day 0 corresponds to the time before the diet (control). Data represents mean values ± SEM. Statistical analysis was performed with an unpaired Student's t-test between the groups.

4.2.4 Measurement of electrolytes in blood samples

To analyze the phenotype of Kir5.1$^{-/-}$ animals and taking into account the results obtained in electrolytes excretion, blood samples before and after high Na^+ diet were measured. Venous blood from the facial vein of conscious Kir5.1$^{+/+}$ and Kir5.1$^{-/-}$ mice was analyzed for pH, hematocrit, gas contents and concentrations of ions Na^+, K^+, HCO_3^-, Ca^{2+} and Mg^{2+} by a blood gas analyzer. Some parameters were calculated from measured values, i.e. HCO_3^- and base excess (BE). Blood was collected before and after the HNa diet and results are presented in Figure 22.

Before the HNa diet, most blood parameters were similar in both genotypes. However, blood [K^+], [Na^+] and partial pressure of carbon dioxide (pCO_2) were significantly lower in Kir5.1$^{-/-}$ mice. These results are largely in agreement with observations of Paulais and coworkers who observed a hypokalemic acidosis. The lack of overt acidosis in our model could be explained by the reduced pCO_2 levels compensating the acidosis.

After the HNa diet, Kir5.1$^{-/-}$ animals were still hypokalemic with higher [HCO_3^-] and pCO2 levels and a slight increase in BE (more positive values) and no change in pH. In Kir5.1$^{+/+}$, Na^+, K^+, HCO_3^- did not change with high Na^+ diet. BE significantly increased (more positive), pCO_2 values lowered with an increase of pH. Hematocrit, [Ca^{2+}] and [Mg^{2+}] concentrations in both group of animal were not altered before and after the diet (Figure S3).

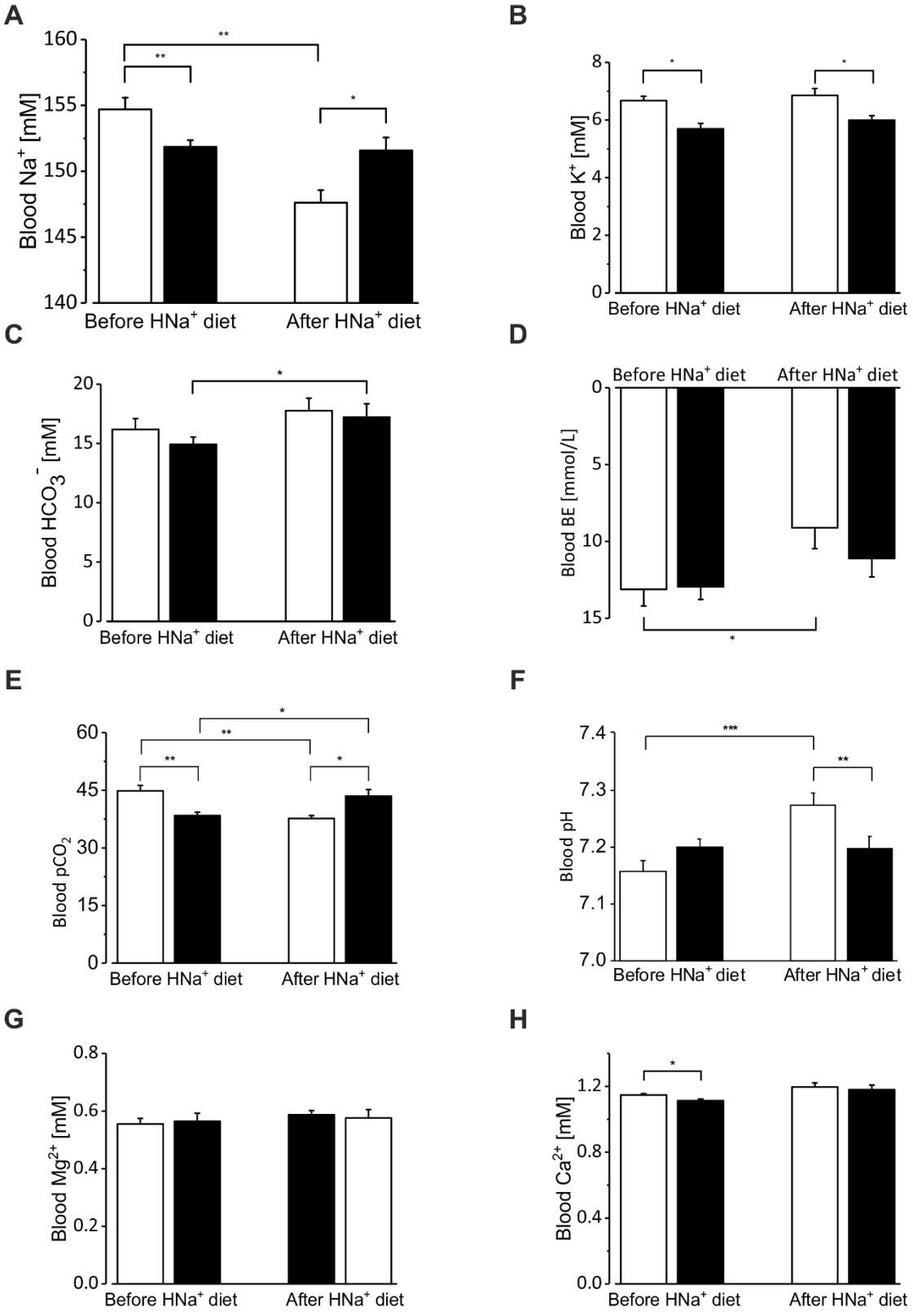

Figure 22. Effects of high salt diet on blood parameters of Kir5.1$^{+/+}$ and Kir5.1$^{-/-}$.
(A) Na^+, (B) K^+, (C) HCO_3^-, (D) BE (presented as negative values), (E) pCO_2, (F) pH, (G) Mg^{2+} and (H) Ca^{2+} were analyzed by blood-gas analyzer of blood samples obtained from facial vein of conscious Kir5.1$^{+/+}$ (□; n = 8) and Kir5.1$^{-/-}$ (■; n=10) mice. Kir5.1$^{-/-}$ mice presented hypokalemia, high [HCO_3^-] and pCO_2 levels with no change in pH and a slight increase in BE. Data represents mean values ± SEM. Statistical analysis was performed with a paired Student's t-test between before and

after the diet for Kir5.1$^{-/-}$ and for Kir5.1$^{+/+}$. In addition, an unpaired Student's t-test between Kir5.1$^{-/-}$ and Kir5.1$^{+/+}$ (*, p≤0.05; **, p≤0.01; *** p≤0.001) was calculated.

4.2.5 Respiratory response of Kir5.1$^{-/-}$

In the previous section, analysis of blood parameters suggested that Kir5.1$^{-/-}$ mice might have compensated a metabolic acidosis by increasing respiration. According to previous publications, Kir5.1 was proposed as being involved in respiratory response. To examine ventilatory responses upon hypoxia and hypercapnia in conscious freely moving Kir5.1$^{+/+}$ (n = 8) and Kir5.1$^{-/-}$ (n = 7) mice were assessed by whole body plethysmograph. Kir5.1$^{-/-}$ mice were expected to have a decreased ventilatory response to hypoxia and hypercapnia due to the possible role of Kir5.1 in mediating respiratory responses. The animals were placed in recording chambers, which were flushed continuously with a mixture of 79% nitrogen and 21% oxygen at room temperature. Levels of O_2 in the chamber were monitored using O_2 sensor (Oxydig). The mice were allowed to acclimatize for at least 30 min to the chamber at control conditions (21% O_2, 79% N_2) before measurements of baseline respiration were recorded.[61]

Under control conditions, main breathing parameters were similar in the two genotypes. When exposed to hypoxic conditions (10% O_2 in the inspired gas mixture; Figure 23) both Kir5.1$^{+/+}$ and Kir5.1$^{-/-}$ mice increased their breathing frequency (f_R) and minute volume (MV), the total volume breathed in one minute. The overall ventilatory response of the Kir5.1$^{-/-}$ animals were similar to that of the Kir5.1$^{+/+}$. The Kir5.1$^{-/-}$ displayed only a slightly lower response in peak expiratory flow (PEF, Figure 23) as a result of lower O_2 presence in the air, though the differences were not significant.

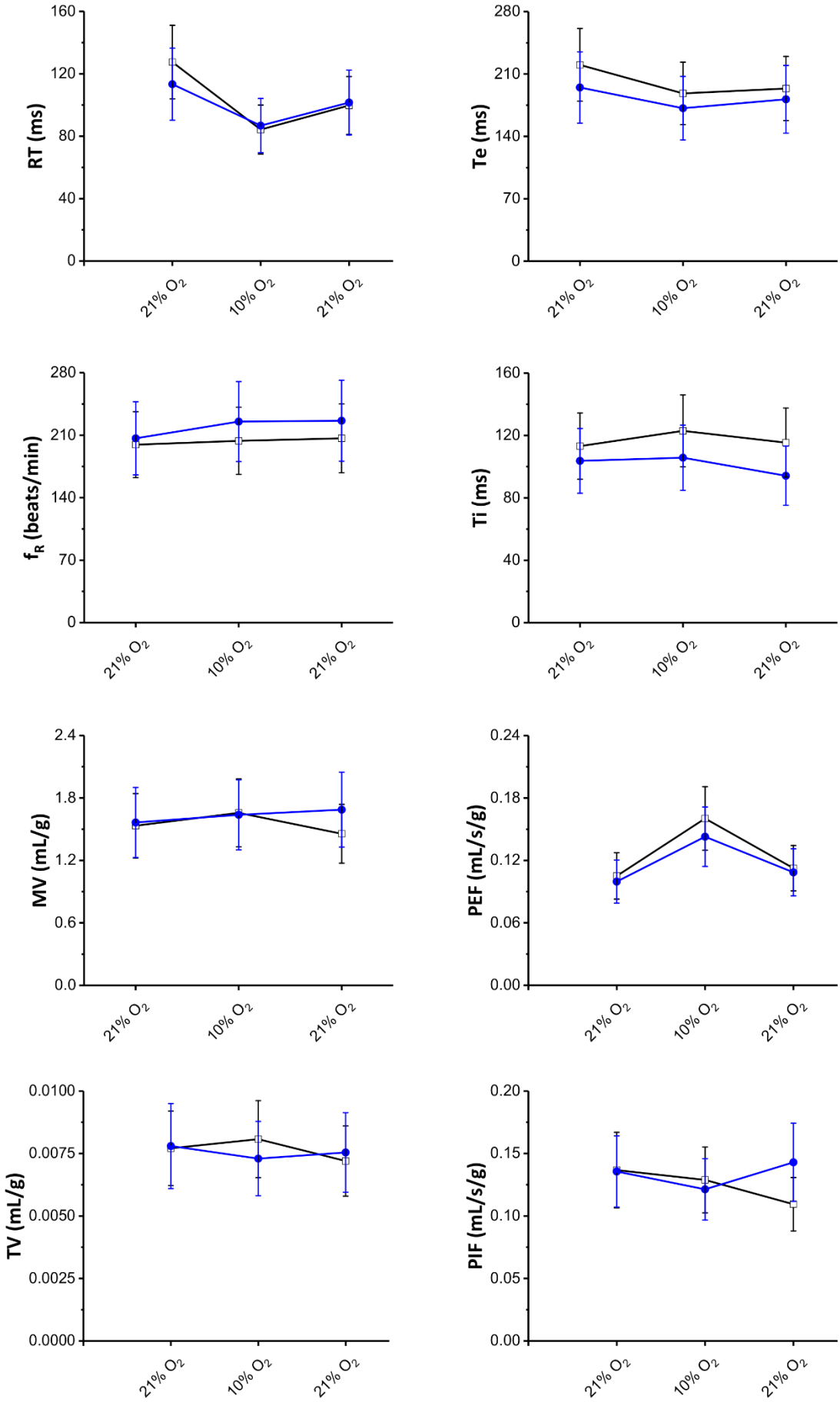
RT (ms)
160
120
80
40
0
Te (ms)
280
210
140
70
0
f_R (beats/min)
Ti (ms)
MV (mL/g)
2.4
1.8
1.2
0.6
0.0
PEF (mL/s/g)
0.24
0.18
0.12
0.06
0.00
TV (mL/g)
0.0100
0.0075
0.0050
0.0025
0.0000
PIF (mL/s/g)
0.20
0.15
0.10
0.05
0.00
21% O_2
10% O_2
21% O_2

Figure 23. Ventilatory responses to hypoxia in Kir5.1$^{+/+}$ and Kir5.1$^{-/-}$ mice.
Ventilatory responses to hypoxia (10% O_2 in the inspired air) in conscious Kir5.1$^{+/+}$ (□; n=8) and Kir5.1$^{-/-}$ (●; n=7) mice. Kir5.1$^{-/-}$ and Kir5.1$^{+/+}$ mice increased their breathing frequency in response to hypoxia. However, the overall responses were similar in both groups. Data is presented as means ± SEM. Unpaired Student's t-test was used to compare respiratory parameters between both genotypes at hypoxia. Abbreviations: RT, relaxation time; f_R, respiratory rate; MV, minute volume; TV, tidal volume; PIF, peak inspiratory flow; PEF, peal expiratory flow; T_i, inspiratory flow and Te, expiratory time.

Animals exposed to hypercapnia (5% CO_2) were also exposed to hyperoxic conditions. In this series of experiments, mice were left in the chamber to acclimatize, then they were exposed to 30 min of normoxia (21% O_2) and 30 min in hyperoxic conditions (100% O_2) to obtain baseline respiratory values. Afterwards, 5% CO_2 was added to the chambers (in 95% O_2). The respiratory responses evoked by hypercapnia in Kir5.1$^{-/-}$ (high levels of inspired CO_2) increased respiratory frequency (f_R) as well as tidal volume (TV). The increase in minute volume was mainly caused by an increase of TV. Again, the overall response to hyperoxic hypercapnia was similar in Kir5.1$^{-/-}$ (n = 8) and their wildtype counterparts (n = 7; Figure 24).

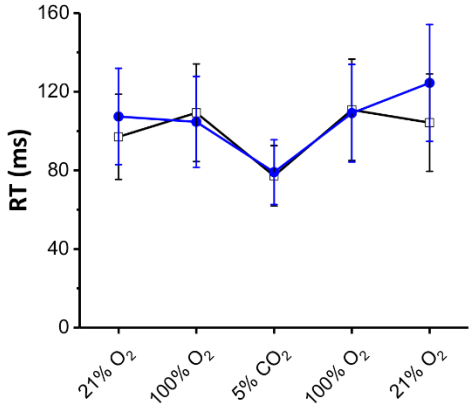
RT (ms)
160
120
80
40
0
21% O2
100% O2
5% CO2
100% O2
21% O2

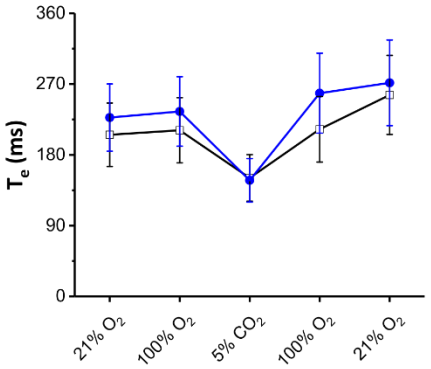
Te (ms)
360
270
180
90
0
21% O2
100% O2
5% CO2
100% O2
21% O2

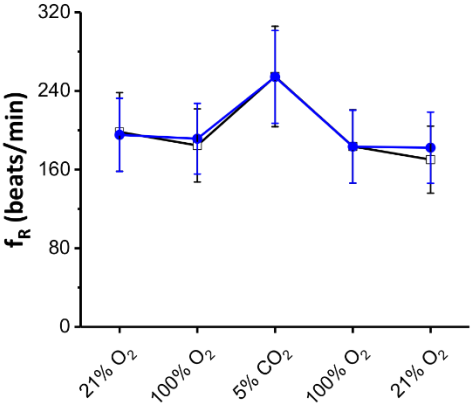
fR (beats/min)
320
240
160
80
0
21% O2
100% O2
5% CO2
100% O2
21% O2

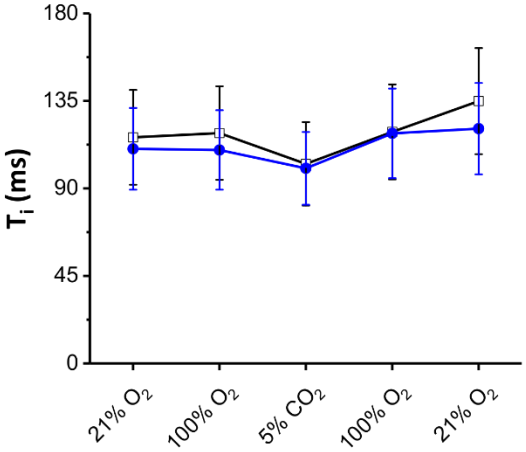
Ti (ms)
180
135
90
45
0
21% O2
100% O2
5% CO2
100% O2
21% O2

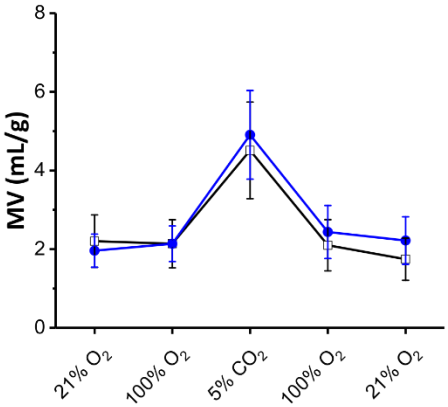
MV (mL/g)
8
6
4
2
0
21% O2
100% O2
5% CO2
100% O2
21% O2

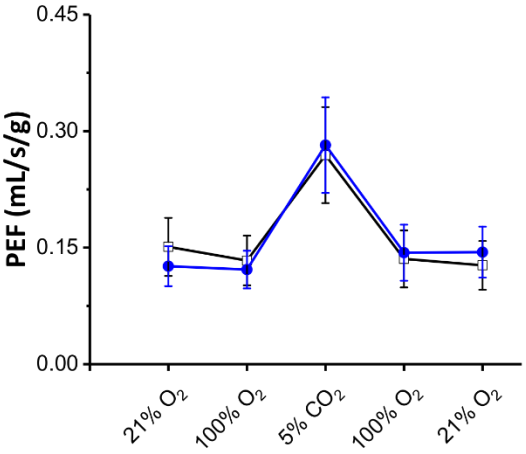
PEF (mL/s/g)
0.45
0.30
0.15
0.00
21% O2
100% O2
5% CO2
100% O2
21% O2

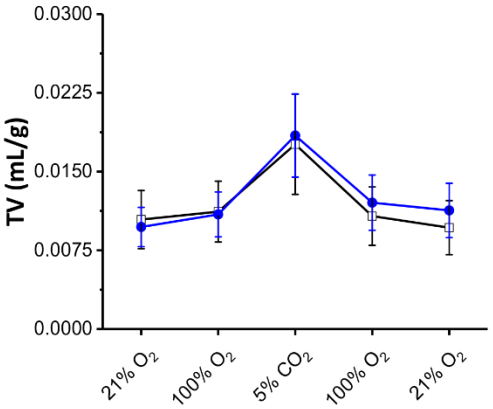
TV (mL/g)
0.0300
0.0225
0.0150
0.0075
0.0000
21% O2
100% O2
5% CO2
100% O2
21% O2

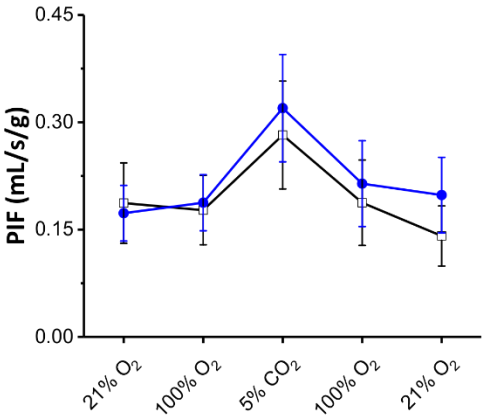
PIF (mL/s/g)
0.45
0.30
0.15
0.00
21% O2
100% O2
5% CO2
100% O2
21% O2

Figure 24. Ventilatory responses to hyperoxic hypercapnia in Kir5.1$^{+/+}$ and Kir5.1$^{-/-}$ mice. Ventilatory responses to levels of hyperoxic hypercapnia (100% O_2 in the inspired air and 5% CO_2) in conscious Kir5.1$^{+/+}$ (□; n=8) and Kir5.1$^{-/-}$ (●; n=7) mice. Kir5.1$^{-/-}$ and Kir5.1$^{+/+}$ mice increased their breathing frequency and minute volume in response to hyperoxic hypercapnia. However, the overall responses were similar in both groups. Data are presented as means ± SEM. Unpaired Student's t-test (corrected for multiple testing) was used to compare respiratory parameters between both genotypes at hypercapnia. RT, relaxation time; f_R, respiratory rate; MV, minute volume; TV, tidal volume; PIF, peak inspiratory flow; PEF, peal expiratory flow; T_i, inspiratory flow and Te, expiratory time.

4.2.6 Ca^{2+} measurements on isolated tubules

Terker and coworkers already proposed that the DCT is able to sense varying plasma K^+ concentrations and to translate it into inhibition of Na^+ uptake via the NCC. Consequently, the Na^+ load to downstream segments of the nephron, i.e. connecting tubule and collecting duct, increases. High Na^+ load in those segments allows K^+ secretion to run at maximal rates in order to normalize plasma K^+ (Figure 3).[26] In their model, the "messenger" controlling NCC activity is intracellular Cl^-, which controls the Cl^--sensitive kinases of the WNK1/SPAK/OSR family which in turn control NCC activity and membrane localization of NCC through phosphorylation. In addition to the WNK–SPAK pathway, several other proteins were identified to control NCC, including parvalbumin, serum and glucocorticoid-inducible kinase Sgk1, ubiquitin ligase Nedd4–2, and protein phosphatase 4 among others.[13,77] We hypothesized, based on these data, that besides the intracellular Cl^- other "second messengers" might be activated in response to alterations of plasma K^+ levels. Here, we tested whether Ca^{2+} signals might also be implicated in basolateral K^+ sensing. Since Kir5.1 is expressed together with Kir4.1 in the DCT and was shown to be important for the maintenance of DCT's basolateral membrane potential, the main goal in this chapter was to test if Kir5.1 deletion influences the ability of DCTs to sense K^+ concentrations variations and to translate it into variations of intracellular Ca^{2+} as a second messenger.

4.2.5.1 Superfused DCT tubules

To measure Ca^{2+} signals in isolated tubules, the tubule suspension was transferred to a closed perfusion chamber and one DCT was selected based on distinct morphological criteria like strong basal infoldings and often an S-formed shape with varying diameter.

4.2.5.1.1 Calibration of fura-2 fluorescence ratios on isolated DCTs

As depicted in Figure 25 C and D, in tubules from Kir5.1$^{+/+}$ and Kir5.1$^{-/-}$ animals an increase in Ca^{2+} levels in response to ionomycin (Ion) and a slight decrease after adding a Ca^{2+}-free solution was observed. Ionomycin was used in order to calibrate the fura-2 fluorescence signals. As an ionophore, ionomycin, permeabilized the cell membrane and increased the levels of $[Ca^{2+}]_i$ due to Ca^{2+} influx across the plasma membrane and its ability to induce the release of cytosolic Ca^{2+} from cytosolic stores. However, the response of tubules to

ionomycin was highly variable and – due to this large scattering – not statistically significant. The use of a Ca^{2+}-free solution, with the aim of strongly lowering intracellular Ca^{2+}, was also not satisfactory and it was hardly possible to lower the fura-2 ratio bellow basal values (Figure 25). Due to these technical difficulties, the use of the Grynkiewicz equation for calculating absolute Ca^{2+} was considered not appropriate. Therefore, raw data (fura-2 ratios) are presented in the following experiments.

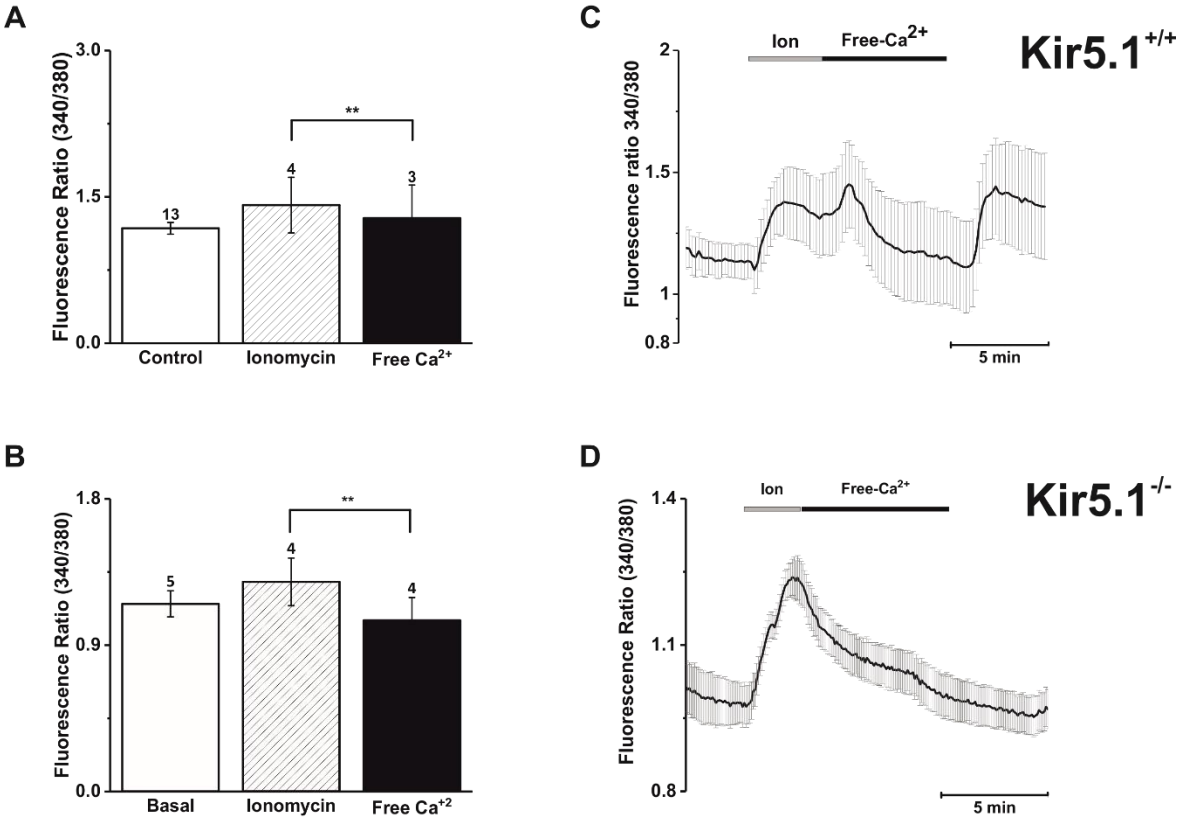

Figure 25. Effect of ionomycin on calcium signals in isolated murine DCTs.
Mean values of maximal fura-2 ratios during superfusion with ionomycin (Ion, 10 µM) in (A) Kir5.1$^{+/+}$ and (B) Kir5.1$^{-/-}$ distal convoluted tubules (n=4; tubules). Superfusion of DCTs with ionomycin induced a Ca^{2+} influx and store release of Ca^{2+}, as evidenced by increase of the ratio 340/380. Representative traces of isolated murine DCTs of (C) Kir5.1$^{+/+}$ and (D) Kir5.1$^{-/-}$ mice. Traces represent mean of ROIs ± SEM. Paired Student's t-test was used to analyze between basal and ionomycin and ionomycin and Free Ca^{2+} solution of each group of animals(*, p≤0.05; **, p≤0.01; *** p≤0.001). Numbers above bars represent the number of individual DCTs.

4.2.5.1.2 Effects of extracellular K^+ on intracellular Ca^{2+}

The ability of the DCTs to react to extracellular K^+ concentrations was accessed by superfusion of the DCTs with solutions with low K^+ concentration (LK; 1 mM) compared to control solution (3.6 mM K^+). The change between physiological K^+ concentrations (control) to LK caused a reversible increase in $[Ca^{2+}]_i$. As it can be observed in Figure 26, lowering K^+ concentration in both Kir5.1$^{+/+}$ (A) and Kir5.1$^{-/-}$ (B) DCTs increased Ca^{2+} compared to basal conditions. However, we did not observe a difference between wildtype or Kir5.1$^{-/-}$

mean response (unpaired student's t-test; p-value 0.409) suggesting that Kir5.1 is not essential for sensing of K^+.

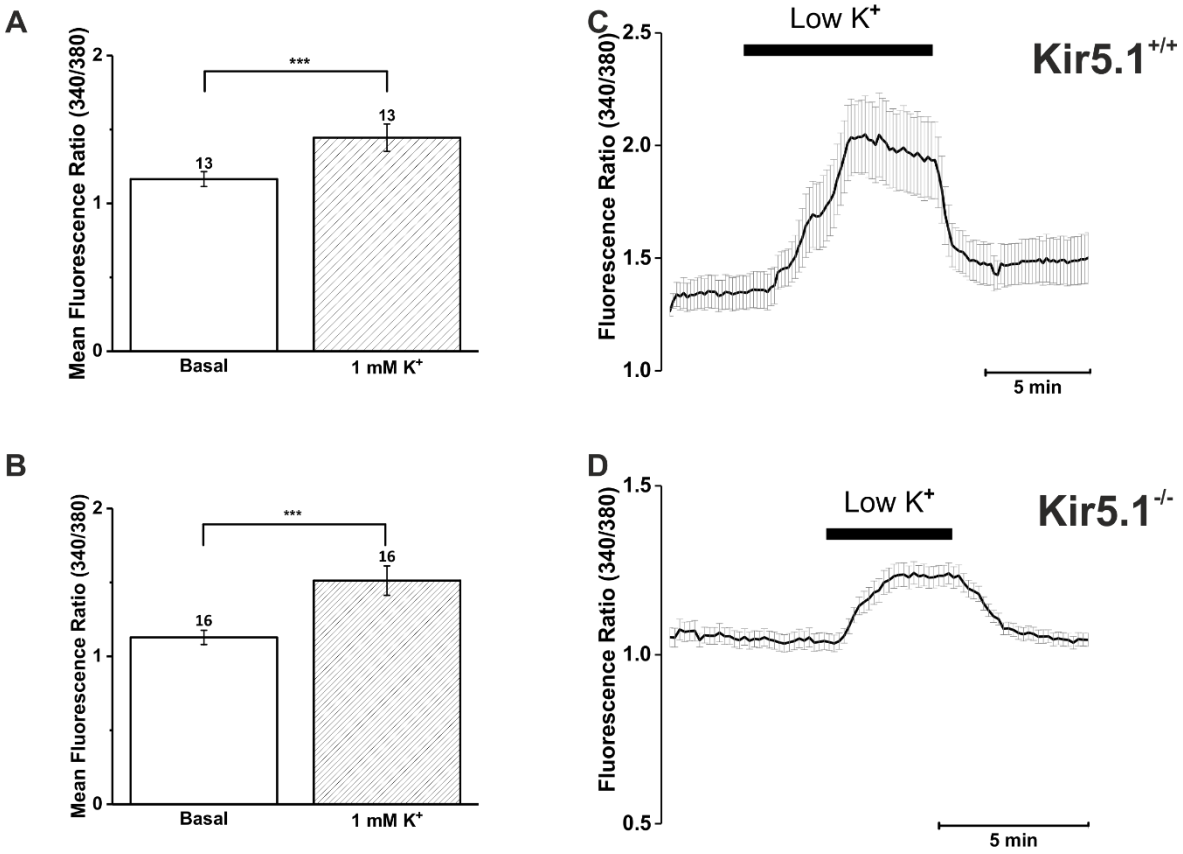

Figure 26. Effect of low K^+ on Ca^{2+} signals of isolated murine DCTs.
Mean values of maximal fura-2 ratios 340/380 during superfusion with low K^+ (1 mM) in (A) Kir5.1$^{+/+}$ (n=13; tubules) and (B) Kir5.1$^{-/-}$ (n=16; tubules) murine DCTs. Superfusion of DCT with low K^+ induced increase of intracellular Ca^{2+} indicating that DCTs are able to sense changes in basolateral K^+ and to translate it into a Ca^{2+} signal. Representative traces from isolated murine DCTs of (C) Kir5.1$^{+/+}$ and (D) Kir5.1$^{-/-}$ mice superfused with LK solution. Paired Student's t-test was used to test for the statistical difference between basal and LK of each group of animals. Traces represent mean of at least 3 ROIs ± SEM.

DCTs superfused with high K^+ (HK; 10 mM) showed the opposite effect, leading to a decrease in $[Ca^{2+}]_i$, however the magnitude of the effect was small and not significantly different (Figure 27).The results obtained suggested that DCTs are indeed capable of sensing changes in K^+ concentration and translate those changes into variations of the second messenger Ca^{2+}.

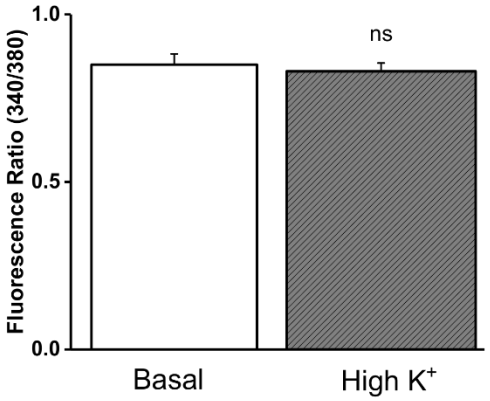

Figure 27. Effect of High K^+ (10 mM) on Ca^{2+} signals of isolated murine DCTs.
Mean values of maximal fura-2 ratios 340/380 during superfusion with high K^+ (10 mM) in Kir5.1$^{+/+}$ murine DCTs. Superfusion of DCT with high K^+ did not induce decrease of intracellular Ca^{2+} and the change was not statistically different. Paired Student's t-test was used to analyze between basal and HK Kir5.1$^{+/+}$ animals (n = 20).

4.2.5.1.3 Effects of extracellular Ba^{2+} on intracellular Ca^{2+}

The previous set of experiments revealed that intracellular Ca^{2+} activities of DCTs are influenced by varying extracellular K^+. However, Kir5.1 deficient tubules showed the same mean increase in Ca^{2+} when K^+ concentrations were lowered indicating that Kir5.1 is not an indispensable component of the K^+ sensor in DCTs. However, the effects might be mediated by the close homologue Kir4.1. To study whether the effect of extracellular K^+ in the DCT was dependent of Kir channels, Ba^{2+}, a reversible blocker of K^+ channels was used. As can be shown in Figure 28, a strong increase in the ratio occurred when Ba^{2+} was applied. This change in fluorescence ratio may either be the result of Ba^{2+} binding to fura-2 (mimicking Ca^{2+}) and/or the result of a rise of $[Ca^{2+}]_i$, induced by Ba^{2+}-induced depolarization of the membrane.[78] The effect of Ba^{2+} resulted in a similar rise of the fluorescence in Kir5.1$^{+/+}$ and Kir5.1$^{-/-}$ isolated DCTs.

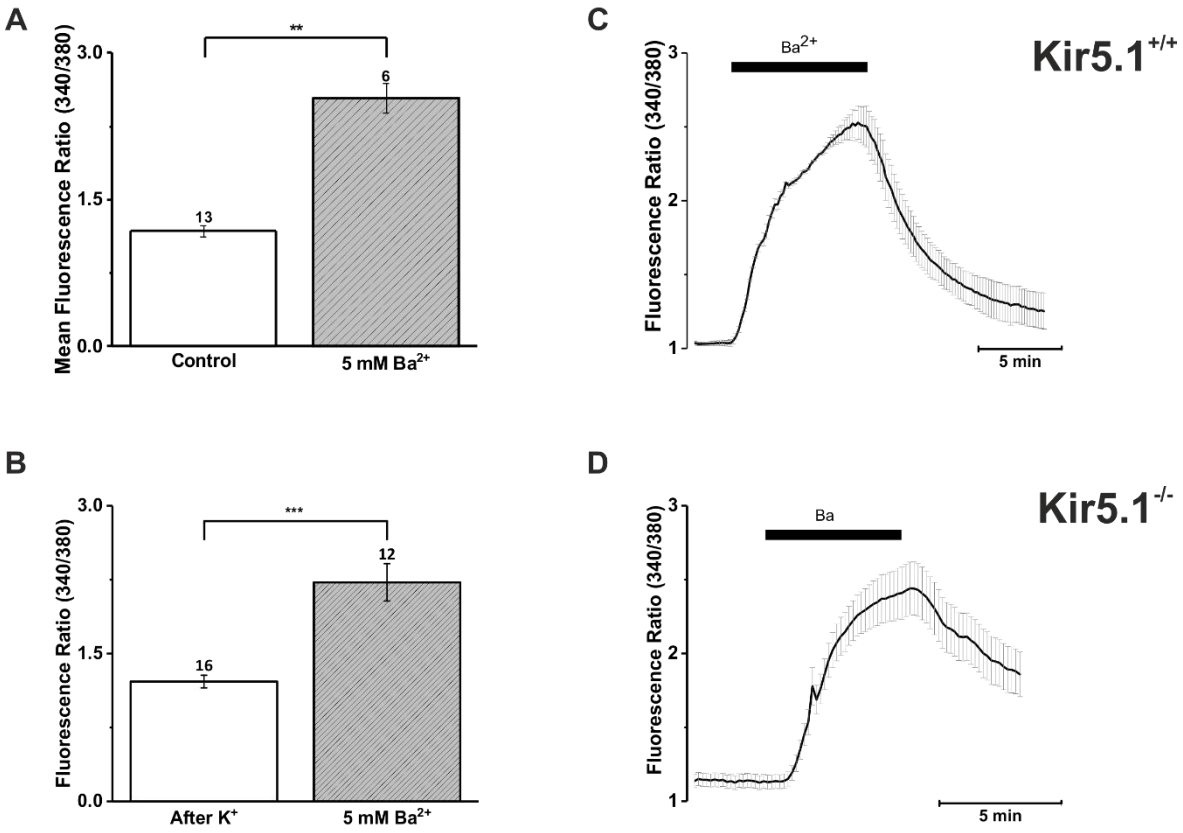

Figure 28. Effect of Ba^{2+} (5 mM) on Ca^{2+} signals of isolated murine DCTs.
Mean values of maximal fura-2 ratios during superfusion with Ba^{2+} (1 mM) in (A) Kir5.1$^{+/+}$ (n=13; tubules) and (B) Kir5.1$^{-/-}$ mice (n=16; tubules). Superfusion of DCTs with Ca^{2+} lead to an increase of intracellular Ca^{2+} as can be seen by the increased 340/380 ratio. Representative tracing of isolated murine DCTs of (C) Kir5.1$^{+/+}$ and (D) Kir5.1$^{-/-}$ mice superfused with Ba^{2+}. Traces represent mean of at least three ROIs ± SEM. Paired Student's t-test was used to test for statistical difference between basal and Ba^{2+} of each group of animals.

Even though Ba^{2+} itself led to an increase in fura-2 ratio, the effect of low extracellular K^+ (LK) under Ba^{2+} conditions was studied. In the presence of Ba^{2+}, no LK-induced rise of $[Ca^{2+}]_i$ was observed (Figure 29). However, the LK solution did result in a rise of $[Ca^{2+}]_i$ after Ba^{2+} was washed out suggesting that Kir channels might be involved in sensing altered basolateral K^+ conditions in the DCT.

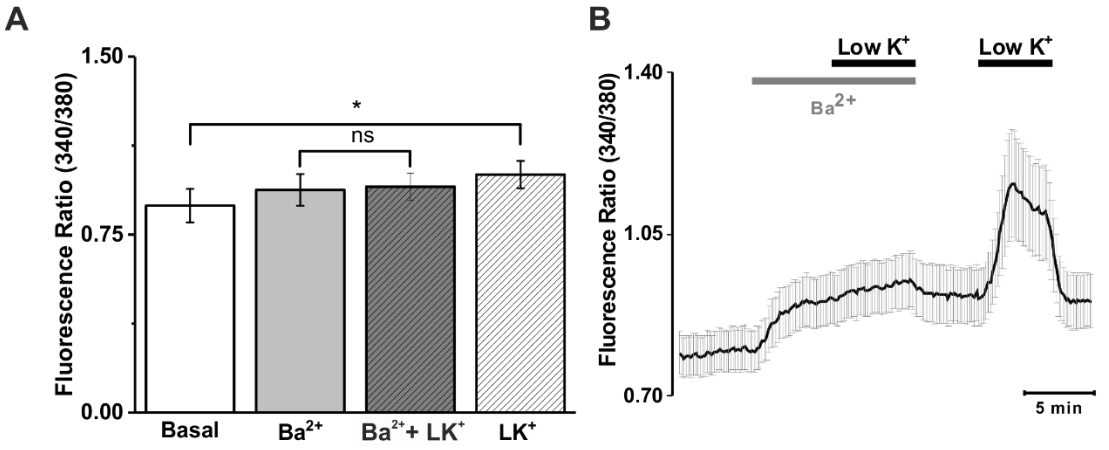

Figure 29. Effect of LK in the presence of Ba^{2+} inhibitory conditions on Ca^{2+} signals of isolated murine DCTs.
(A) Mean values of maximal fura-2 ratios 340/380 during superfusion with LK in the presence of Ba^{2+} in Kir5.1$^{+/+}$ murine DCTs (n= 12; tubules). (B) Representative tracing of isolated murine DCTs superfused with Ba^{2+} + Low K^+. Superfusion of DCT with low K^+ in the presence of Ba^{2+} did not induced an increase of intracellular Ca^{2+} suggesting that the increase of $[Ca^{2+}]_i$ when LK is applied was mediated by K^+ channels. Trace represents mean of at least three ROIs ± SEM. This experiment was done by Dr. Anna-Lena Forst and bachelor student Alexander Fischer.

4.2.5.2 Perfused DCT tubules

Previous experiments suggested that extracellular K^+ concentrations affect cytosolic Ca^{2+} activity of DCTs and that this Ca^{2+} might contribute to the K^+-sensing mechanisms of these cells. However, the superfusion of the tubules might also affect luminal K^+ concentrations and the change in intracellular Ca^{2+} might reflect a mixed response to variations in basolateral and apical K^+ concentrations. To test whether the basolateral and/or apical membrane of DCTs responds to changes in extracellular K^+ concentrations tubules were transferred to the bath on a heated (37 °C) microscope stage and DCTs were perfused using a concentric glass pipette system.

To be able to control successful apical perfusion of the tubules with LK solution, the fluorescence dye Cy5 was added to the LK solution and Cy5 fluorescence was measured through the experiment.

Figure 30 shows the effect of K^+ concentration on $[Ca^{2+}]_i$ levels. A rise in intracellular Ca^{2+} was only observed when basolateral, but not apical, K^+ was reduced from 3.6 to 1.0 mM. A successful perfusion of the LK-solution on the apical side was confirmed by the presence of a clear peak in Cy5 fluorescent (Figure 30 B).

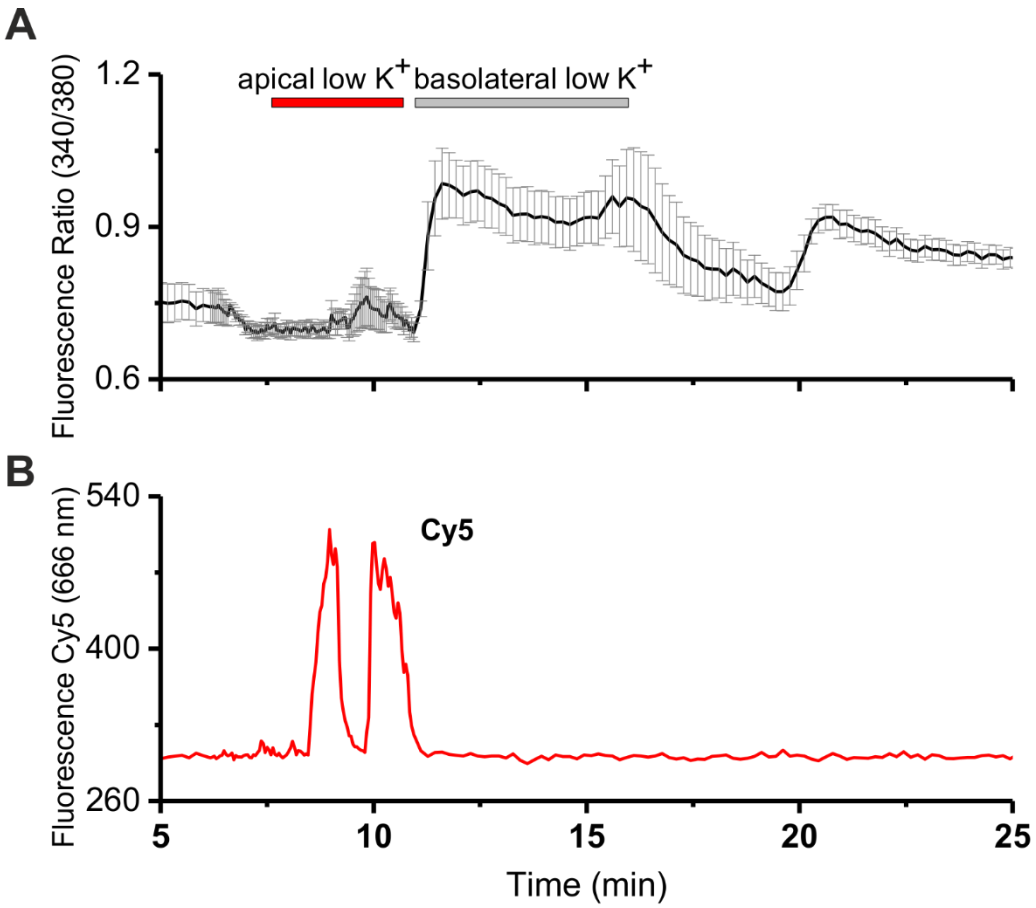

Figure 30. Effect of low K^+ concentrations on the apical and basolateral side on Ca^{2+} activity of isolated murine DCTs.
(A) Representative trace of isolated perfused DCT (n=7; DCT tubules) of a Kir5.1$^{+/+}$ mice with low K^+ solution present either on the apical or the basolateral side. A rise in intracellular Ca^{2+} (fura-2 ratios) was only observed when basolateral K^+, but not apical K^+, was reduced from 3.6 to 1.0 mM. Traces represent mean of at least 3 ROIs. (B) Corresponding trace of Cy5 fluorescence present in the apical low K^+ solution indicated successful apical perfused with low K^+ solution.

Figure 31 A summarizes the findings of changing apical and basolateral K^+. The data results from seven tubules (n=7) and revealed that apical low K^+ solution did not affect intracellular Ca^{2+} activity. However, altering basolateral K^+ in the same experiments resulted in a significant increase in $[Ca^{2+}]_i$. These results clearly suggest that only varying basolateral, but not apical, K^+ concentrations affects $[Ca^{2+}]_i$ signals in the DCT.

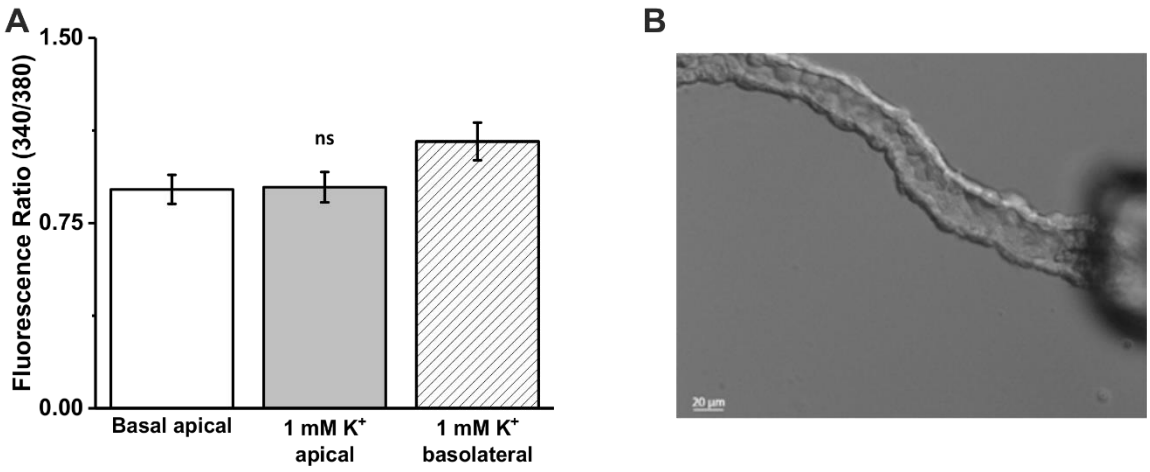

Figure 31. Mean values of maximal fura-2 ratios during perfusion and superfusion with low K^+ in isolated murine Kir5.1$^{+/+}$ DCTs.
(A) Mean values (n=7 tubules) during apical and basolateral application of K^+ (1 mM) in Kir5.1$^{+/+}$ DCT. (B) Morphological aspect of a DCT perfused by a concentric glass pipette. Paired Student's t-test was used to analyze between 3.6 and 1.0 mM K^+ in the apical or basolateral sides.

5. Discussion

5.1 Kcnj16 expression

Kir4.1 (KCNJ10) and Kir5.1 (KCNJ16) channels belong to the inwardly rectifying potassium channels family and mediate important K^+ conductances in brain, kidney and other tissues. In contrast to Kir4.1, Kir5.1 is unable to form functional homomeric channels.[39] Kir5.1 channels were first cloned from brain and high expression was reported in kidney, stomach, brain, pancreas and thyroid gland.[10,54,65,79] In the distal nephron, especially in the distal convoluted tubule, Kir5.1 associates with Kir4.1 to form functionally important basolateral K^+ channels whose activity to salt transport in this segment is depending on.

The expression patterns of Kcnj10 and Kcnj16 were assessed by real-time PCR on wildtype mouse tissues. Besides high expression in kidney, brain, stomach and thyroid gland, we also found expression of Kcnj16 in the cochlea. The expression pattern of Kcnj10 showed some overlap but also differences, e.g. Kcnj10 is weakly expressed in the stomach but at higher levels in the brain. This clearly suggest that Kir5.1 and Kir4.1 form heterodimers only in some tissues (e.g. in the distal convoluted tubules (DCT) of the kidney), but not (or less) in others (e.g. stomach and brain; Figure 6). Using Kcnj16 promotor driven X-Gal staining of Kir5.1$^{-/-}$ mice (Figure 10) and manual sorting of enzymatically digested tubules, we found KCNJ16 expression in the proximal tubule (PT) and DCT while KNCJ10 was only found in the distal parts of the nephron but not the PT (Figure 8 and 9). These findings are in agreement with the above mentioned studies showing colocalization of Kir4.1 and Kir5.1 in the basolateral membrane of DCT.[50,55] These results strongly suggest that Kir5.1 may cooperate with other channels in the proximal tubule in order to form functional channels. A likely candidate would be the close homolog Kir4.2 (KCNJ15), which was found to interact with Kir5.1 in renal epithelia.[57]

5.2 Role of KCNJ16 in the kidney

Mutations in the *KCNJ10* gene are causative for the autosomal recessive EAST/SeSAME syndrome, a complex disorder with a tubulopathy as renal manifestation. Unlike *KCNJ10*, no published report is yet available linking a renal pathology to mutations in the *KCNJ16* gene. However, Prof. Dr. Martin Konrad in University Münster, has identified in a single patient, suffering from renal salt wasting, hypokalemia and acidosis a homozygous c.104G>A mutation (NCBI Reference Sequence: NM_001291625.1) within the *KCNJ16* gene (unpublished data).

This mutation leads to the missense mutation p.Arg35Gln (R35Q) in Kir5.1 (UniProt: Q9NPI9), replacing the charged aliphatic arginine (R) by the neutral and polar amino acid glutamine (Q). This mutation is located in the N-terminal region of the protein (Figure 5).

Since computer predictions (PolyPhen2; http://genetics.bwh.harvard.edu/pph2/index.shtml) suggested a devastation effect of the mutation on channel function we hypothesized that Kir5.1^{R35Q} might be causative for the patient's symptoms and might lead to impaired functionality of the DCT.[16,30,33]

5.2.1 Electrophysiological characterization of the Kir5.1^{R35Q} mutation

In our Chinese hamster ovary (CHO) cell heterologous expression system, the mutation R35Q did not seem to change the subcellular localization of the protein. However, also in the case of the wildtype Kir5.1 protein the vast majority of the protein was found in the endoplasmic reticulum of CHO cells, even when coexpressed with Kir4.1. Therefore, immunofluorescence was not sensitive enough to assess a possible impairment of membrane trafficking (Figure 11). To understand the nature of the Kir5.1^{R35Q} mutation, patch clamp recordings of HEK and CHO cells were performed. Since Kir5.1 alone does not produce functional homomeric channels in most expression systems, cells were always co-transfected with Kir4.1. Whole cell measurements of CHO cells transfected with Kir4.1-Kir5.1^{wt} or Kir4.1-Kir5.1^{R35Q} exhibited similar membrane potentials close to the equilibrium potential of K^+ suggesting normal K^+-conductance of the Kir5.1^{R35Q} mutant (Figure 12 A, B and 13 C and E). Application of Ba^{2+} led to a strong depolarization attributed to inhibition of Ba^{2+}-sensitive K^+ channels. This Ba^{2+} effect was not observed in non-transfected cells indicating that K^+ channels were successfully formed in cells transfected with Kir channels (Figure 12 C). However, no differences in Ba^{2+}-sensitive currents were observed in Kir4.1-Kir5.1^{wt} and Kir4.1-Kir5.1^{R35Q} expressing cells. Additionally, the observed inwardly rectifying single channel conductance of ~56 pS for Kir4.1-Kir5.1^{wt} and for Kir4.1-Kir5.1^{R35Q} were in line with previously reported conductances for heteromeric Kir4.1-Kir5.1 channels arguing against a loss-of-function of the Kir5.1^{R35Q} mutant.[50,51,56,80]

To confirm that the currents obtained were in fact the result of heteromeric channel formation and not contamination of homomeric Kir4.1 channels, single channel measurements in the cell-attached mode were performed using HEK cells. Cells transfected with homomeric Kir4.1 displayed a conductance of only ~30 pS (Figure 14 A). In contrast, Kir4.1-Kir5.1^{wt} heteromers showed a conductance of ~56 pS, almost double of that obtained for homomeric Kir4.1. Additionally, Kir4.1-Kir5.1^{wt} recordings displayed the characteristic Kir4.1-Kir5.1 channel sub-states, which is in agreement with the formation of Kir4.1-Kir5.1 heteromeric channels even when the Kir5.1 is mutated (Figure 14 B and 15 A).[51,56] Analysis

of the open probability also revealed no difference between the Kir4.1-Kir5.1^{wt} or Kir4.1-Kir5.1^{R35Q} expressing cells.

In addition to the recordings in the cell-attached configuration, inside-out measurements were performed to investigate a potential different pH sensitivity of Kir4.1-Kir5.1^{R35Q} heteromers (Figure 16). However, both heteromers were similarly inhibited by intracellular pH arguing against a grossly altered pH sensitivity of the Kir4.1-Kir5.1^{R35Q} heteromer.
In summary, the performed electrophysiological characterization of Kir5.1^{R35Q} revealed 1. No abnormal channel assembly with Kir4.1, 2. Unaltered conductance of the Kir4.1-Kir5.1^{R35Q} heteromers, 3. Unchanged open probabilities of the Kir4.1-Kir5.1^{R35Q} heteromers, and 4. Preserved intracellular pH sensitivity of the Kir4.1-Kir5.1^{R35Q} heteromers when compared to Kir4.1-Kir5.1^{wt}. These data argue against a loss-of-function effect of the Kir5.1^{R35Q} mutant and further studies are needed to understand if and how the mutation affects the functional properties of the Kir5.1 protein. Apparently, the Kir5.1^{R35Q} variant is still able to interact with Kir4.1 in a normal way and to form heteromeric channels similar to wildtype Kir5.1. It is, however, still possible that the Kir5.1 ^{R35Q} variant differs from the wildtype with regard to the efficiency of this interaction (reduced efficiency due to overexpression) or other aspects, e.g. interaction with Kir4.2. In the distal convoluted tubules, however, Kir4.1-Kir5.1 are considered the most relevant basolateral K^+ conductance.

5.2.2 Kir5.1-mediated K^+ sensing in DCT

The distal convoluted tubule is a metabolically highly active nephron segment and plays a key role in Na^+, K^+ and divalent cations homeostasis. The symptoms of the Kir5.1 knockout mouse and our own expression analysis suggested that Kir5.1 might control DCT function in combination with Kir4.1. Studies with mutated Kir4.1 showed that EAST-causing mutations are loss-of-function mutations that impair the function of the Kir4.1-Kir5.1 channel and, thereby, the basolateral recycling of K^+ that is needed for high activity of the Na^+/K^+-ATPase.[16]

Unexpectedly, the genetic inactivation of Kir5.1 had the opposite effect: loss of Kir5.1 in mice resulted in an enhanced basolateral K^+ conductance carried by homomeric Kir4.1 channels.[54] Apparently, a major function of Kir5.1 is to exert an inhibitory effect on Kir4.1 and to allow precise regulation of the heteromeric channels, e.g. by internal pH.[54] In addition, recent studies proposed that the DCT, besides fine-tuning of the salt reabsorption, might also be involved in sensing plasma K^+ and indirectly regulating plasma K^+ balance.[18,26,48] Terker et al. suggested a molecular mechanism where the DCT senses and responds to changes in K^+ balance via altering the membrane voltage thereby affecting

intracellular [Cl^-] which in turn regulates the activity of the NCC via Cl^--sensitive WNK and SPAK kinases (Figure 3).[17] The identity of the molecular K^+ sensor is thought to be Kir4.1, although it seems likely that Kir5.1 is also involved.

Our electrophysiological analysis of the Kir5.1^{R35Q} mutant suggested a normal interaction with Kir4.1. Given the absence of a pathological phenotype in our experiments with the Kir5.1^{R35Q} variant, it appears likely that the variant is not causative of the renal phenotype of Prof. Konrad's patient. The patient's symptoms are probably caused by mutations in other genes, but we cannot fully exclude that some functional impairment of the Kir5.1^{R35Q} was missed in our studies. Although the Kir5.1^{R35Q} variant appeared normal, the physiological relevance of Kir5.1 for K^+ sensing in the DCT cells was still largely unknown. To address the question of Kir5.1 function in DCT cells and its ability to act as a K^+ sensor, we isolated murine DCT tubules from control and Kir5.1$^{-/-}$ mice.

The ability of DCT to sense varying basolateral K^+ conditions were tested by superfusion with solution containing 1 mM K^+ instead of 3.6 mM (Figure 26). Superfusion of isolated DCTs with 1 mM K^+ resulted in an increase in intracellular [Ca^{2+}], even though the magnitude of the effect was small compared to superfusion with Ba^{2+} (Figure 28). The relative small effect size may be due to expression of calbindin in the DCT that binds and diffuses the Ca^{2+} ions to the basolateral membrane.[12] The increased $[Ca^{2+}]_i$ observed in isolated DCTs upon perfusion with 1 mM K^+ might be due to a hyperpolarization of the basolateral membrane potential as hypothesized by Weinstein and co-workers.[26,81] This hyperpolarization of the basolateral membrane would increase transepithelial membrane potential and therefore the driving force for an influx of Ca^{2+}. However, the change in transepithelial membrane potential seems independent of Kir5.1 because even in the absence of Kir5.1, similar increases in intracellular Ca^{2+} signals were observed in response to low K^+ suggesting that the absence of Kir5.1 did not alter the ability of the DCT to sense low K^+ conditions (Figure 26 B and D).

To further test if basolateral K^+ channels are indeed K^+ sensors, the reversible K^+ channel inhibitor Ba^{2+} was used. After superfusing Ba^{2+}, there was an increase in fura-2 signals (Figure 28). This result was unexpected and may result from Ba^{2+} entering the cells and mimicking intracellular Ca^{2+} consequently elevating fura-2 signals. As reported previously, Ba^{2+} and Ca^{2+} may enter the cytosol through the same pathway.[26,70,78] Nonetheless, Ba^{2+} prevented the low K^+-induced rise in intracellular Ca^{2+} (Figure 29) suggesting that Ba^{2+}-sensitive K^+ channels are indeed K^+ sensors in the DCT that help to translate varying external K^+ levels into intracellular Ca^{2+} signals.

Since basolateral superfusion of tubules with 1 mM K^+ might also affect apical K^+ levels, we tested the specificity of K^+ sensing by apical perfusion of the tubule with low K^+ solution (LK) while keeping the basolateral solution constant. Interestingly, apical perfusion of DCTs with LK solution did not affect the Ca^{2+} levels (Figure 30). This response was unexpected since low K^+ on the apical side probably leads to hyperpolarization of the apical membrane which would increase the driving force for Ca^{2+} reabsorption via apical TRPV5 mediating Ca^{2+} transport. Unfortunately, we could not measure the apical membrane voltage directly. It is conceivable that i) the apical membrane did not sufficiently hyperpolarized at low K^+ solution (e.g. due to rather low K^+ conductance compared to the basolateral channels or due to strong inward rectification of the apical K^+ conductance); or ii) that the Ca^{2+} increase observed at low basolateral K^+ concentrations is caused by store release or basolateral net Ca^{2+} influx.[2,13,82]

In summary, our results disclosed that only decreasing K^+ on the basolateral side leads to increased Ca^{2+} levels. Additionally, Kir5.1 seems to have no effect on the K^+ sensing properties of the DCT, at least with regard to its Ca^{2+} increasing effect. In its role as a second messenger, changes of cytosolic Ca^{2+} in DCT cells may be consistent with the suggested theory of Terker et al. assuming that variations of extracellular K^+ are sensed by DCT through changes of the membrane voltage.[26] To further study this theory, electrophysiological measurements of membrane potential in DCT tubules are required. Additionally, our studies do not reveal as to whether the source of Ca^{2+} is intra- or extracellular, a question that needs to be addressed in future studies.

5.3 Phenotype of Kir5.1$^{-/-}$ mice

The symptoms of hypokalemia and hypermagnesuria present in the patient carrying the homozygous Kir5.1^{R35Q} mutation suggested a renal involvement of Kir5.1 - although we were unable to find a functional deficit of this channel mutant in *in vitro* studies. In order to rule out limitations of our cellular model systems as cause of a missing phenotype and to gain further insights into the possible role of Kir5.1 in the kidney, we investigated the renal phenotype of a Kir5.1$^{-/-}$ mouse model.

5.3.1 Electrolyte balance in Kir5.1$^{-/-}$ mice

Paulais and co-workers published a Kir5.1$^{-/-}$ mouse model in a C57Bl/6 background.[54] They found a Kir5.1$^{-/-}$ phenotype that besides hypokalemia was the opposite of the symptoms in EAST syndrome: hyperchloremic metabolic acidosis, hypercalciuria and hypermagnesuria (for comparison of biological parameters refer to Table 5).[16,25,30,33,52,54] We analyzed our own Kir5.1$^{-/-}$ mice (also in C57Bl/6 background) to compare our findings with those observed by

Paulais and co-workers. In accordance with previous studies, Kir5.1$^{-/-}$ mice displayed hypokalemia and hypermagnesuria (Figure 17). Strikingly, we did not observe an acidosis as presented by Paulais, which might be due to the significantly reduced pCO_2 levels (Figure 22 E) that suggests respiratory compensation of the acidosis.

Table 5. Comparison of biological parameters of patients with mutated Kir4.1 (resulting in EAST/SeSAME syndrome), the patient with mutated Kir5.1^{R35Q}, Kir4.1$^{-/-}$ and Kir5.1$^{-/-}$ mice models compared to their respective controls.
Parameters are indicated as normal, elevated (↑) or reduced (↓) compared to their respective controls. Abbreviations: n. a., not available, n. d., not determined.

	Patients with EAST (mutated Kir4.1$^{-/-}$)[33]	Kir4.1$^{-/-}$ mice[83]	Patient with Kir5.1^{R35Q} (unpublished data)	Kir5.1$^{-/-}$ mice (Paulais et al)[54]	Kir5.1$^{-/-}$ mice (own data)
Plasma					
Na^+	normal	normal	n. a.	normal	↓
Cl^-	↓	n. a.	n. a.	↑	n. d.
K^+	↓	↓	↓	↓	↓
Ca^{2+}	normal	normal	↓	normal	↓
Mg^{2+}	↓	(↓)	↓	normal	normal
Renin system	renin ↑	normal aldosterone	n. a.	normal aldosterone	normal aldosterone[69]
Blood					
pH	alkalosis	(alkalosis)	acidosis	acidosis	normal
HCO_3^-	↑	↑	n. a.	↓	normal
pCO_2	normal	normal	n. a.	normal	↓
Urine					
Osmolality	normal	↓	n. a.	↓	normal
Na^+	(↓)	↓	n. a.	normal	normal
Cl^-	n. a.	↓	n. a.	normal	normal
K^+	↑	↓	n. a.	↑	↑
Ca^{2+}	↓	normal	n. a.	↑	normal
Mg^{2+}	↑	normal	n. a.	↑	↑
NH_4^+	n a.	↑	n. a.	normal	normal

Paulais and co-workers suggested that the Kir5.1$^{-/-}$ phenotype was due to enhanced function of the DCT as short-term treatment of the mice with the NCC inhibitor hydrochlorothiazide resulted in rectified hypercalciuria but increased Na^+ excretion of the Kir5.1$^{-/-}$ mice.

In summary, our Kir5.1$^{-/-}$ mice display hypokalemia and hypermagnesuria but no overt acidosis. The absence of acidosis in our mice might be the result of reduced pCO_2 levels that compensate the acidosis. In agreement with the data obtained from Paulais, in Kir5.1$^{-/-}$ we (published in the thesis of Evelyn Humberg) did not observe an activation of the renin–angiotensin–aldosterone system (RAAS) suggesting that the renal phenotype is mild and compensation mechanisms do not require activation of the RAAS.[54,69] The ENaC-mediated Na^+ absorption in the amiloride-sensitive distal nephron appears to be normal in Kir5.1$^{-/-}$ mice; however, there might be a slight (not significant) increase in amiloride-sensitive K^+ excretion (Figure 18). Paulais et al.[54] concluded from their results that NaCl reabsorption is increased in Kir5.1$^{-/-}$ mice. Under such conditions, distal Na^+ delivery would be reduced and, as a consequence, K^+ secretion would be rather decreased but not increased. Our results indicate that amiloride-sensitive K^+ secretion is not impaired but rather increased suggesting that K^+ secretion in the distal nephron likely contributes to the hypokalemia phenotype. It is, however, conceivable that also more proximal parts of the nephron contribute to the renal K^+ loss, e.g. the proximal tubule, which is known to express Kir5.1. Future studies will be needed to address the function of Kir5.1 in proximal tubules.

5.3.2 Effect of high Na^+ diet in Kir5.1$^{-/-}$ mice

Besides the physiological role of Kir5.1$^{-/-}$ in electrolyte homeostasis, other studies by Palygin et al. suggested an essential role of Kir5.1 in the pathophysiology of hypertension. It is well recognized that higher levels of Na^+ intake are associated with elevated blood pressure.[74,84,85] Importantly, the effect of dietary Na^+ on blood pressure is dependent on other components of the diet and, specifically, its K^+ content.[86] Since both Kir4.1 and Kir5.1 seem to regulate K^+ homeostasis, the role of Kir5.1 in the development of hypertension was investigated by Palygin and co-workers. They created a Dahl salt-sensitive Kir5.1 deficient rat model that exhibited a renal phenotype reminiscent of SeSAME/EAST and Kir4.1 deletion: salt wasting, hypomagnesemia, and hypokalemia.[74]

Interestingly, the absence of Kir5.1 resulted in prominent retention of Kir4.1 in the cytosol of DCTs suggesting improper translocation of Kir4.1 in the absence of Kir5.1 in rats. This is the opposite of the marked upregulation of plasma membrane Kir4.1 in normotensive mice lacking Kir5.1.[54] To determine whether improper Kir4.1 translocation is a common feature in hypertension or whether it is a feature only found in rat models, we induced hypertension in Kir5.1$^{-/-}$ mice by feeding a high Na^+ (HNa) diet, which was commonly used to induce hypertension in C57BL6/J mice.[75,76] The HNa diet was fed for two weeks and blood and urine samples were taken in regular intervals.

As expected, the HNa diet resulted in massively increased excretion of Na^+ and Cl^- in control and Kir5.1$^{-/-}$ mice (Figure 20 and 21). All other electrolytes were also significantly elevated, which is likely due to the different composition of the standard diet and the HNa diet. However, Kir5.1$^{-/-}$ mice did always wasted significantly more electrolytes when compared to control animals, an effect that was only partially seen before the start of the diet. Beside the loss of Na^+, K^+, Mg^{2+}, Ca^{2+} and NH_4^+, the HNa diet also unmasked an impaired handling of Cl^-, phosphate and sulfate in Kir5.1$^{-/-}$ mice (Figure 32). Since the main site for phosphate and sulfate reabsorption is the proximal tubule these data suggests that Kir5.1 is involved in proximal tubular function.

Interestingly, control animals developed a respiratory alkalosis with reduced pCO_2 but unaltered HCO_3^- levels after feeding of HNa diet. This effect was not seen in Kir5.1$^{-/-}$ animals. Contrary, the blood pH remained unaltered but pCO_2 levels and HCO_3^- levels significantly increased after HNa diet (Figure 22). The animals also presented a more positive base excess, low pCO_2 levels and higher pH which suggests that Kir5.1$^{+/+}$ mice develop respiratory alkalosis in response to the high Na^+ diet. At present, we have no conclusive explanation for the pronounced salt-wasting during the high Na^+ diet. It appears as if the inactivation of Kir5.1 led to an impaired ability to adapt properly to high salt intake. Future studies will be necessary to corroborate these findings and to measure blood pressure under high salt diet (which we have not yet done to avoid interference of blood pressure measurements with renal salt excretion due to increased stress levels). The high salt diet experiments also suggest that the clinical symptoms of patients might be substantially influenced by dietary salt intake.

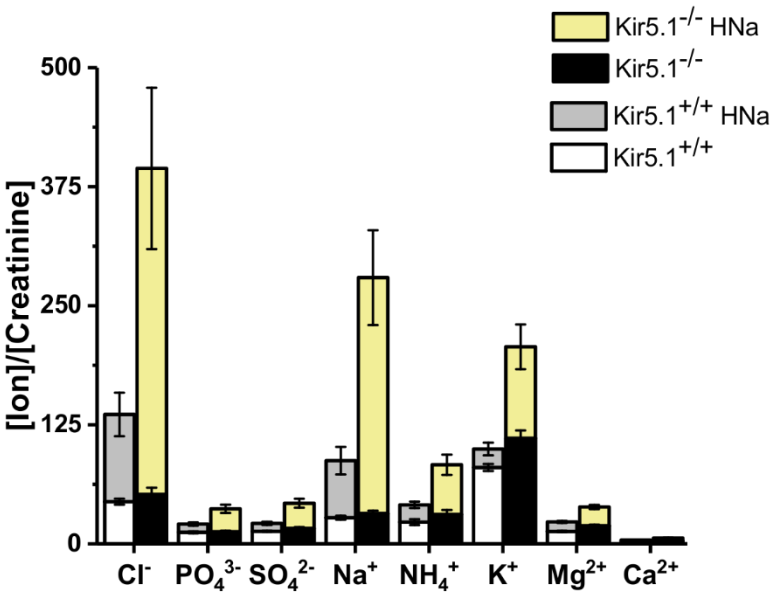

Figure 32. Comparison of urinary excretion of control (white and grey) and Kir5.1$^{-/-}$ (black and yellow) mice under standard diet and high Na$^+$ diet.
A high Na$^+$ diet (HNa) did result in elevation of Cl$^-$, Na$^+$ and K$^+$ excretion in both control and Kir5.1$^{-/-}$ mice.

5.3.2 Role of KCNJ16 in respiration

To comprehend the nature of the mechanisms of compensation exhibited by Kir5.1$^{-/-}$ mice plethysmography studies were performed. Kir5.1 and Kir4.1 are expressed in some of the areas involved in chemoreception such as the brainstem and peripheral chemoreceptors.[39,62,87] It was suggested that Kir5.1 contributes to the chemosensory control of breathing.[60,61,88] Besides, heteromeric Kir4.1-Kir5.1 channels have characteristics that potentially allow some sort of chemosensitivity, in particular the inhibition by intracellular acidification.[53,55,57]

Contribution of Kir5.1 to the control of breathing was assessed by plethysmography studies under hypoxia and hypercapnia conditions. Ventilatory responses under normal conditions were similar in both groups of animals. In response to hypoxia, the Kir5.1$^{-/-}$ mice increased their depth of breathing and minute ventilation in a similar way like Kir5.1$^{+/+}$ animals (Figure 23). And also under hypercapnia conditions, the stimulation of respiration was similar in both genotypes (Figure 24).

Thus, the physiological regulation of respiration was preserved in our Kir5.1$^{-/-}$ mice suggesting that Kir5.1 does not have an indispensable role for chemoreception. Since several other K$^+$ channels are expressed in central and peripheral chemoreceptors, it is likely that those conductances compensate for the loss of Kir5.1.[60]

Taken together, the data presented here suggest that Kir5.1 is required for the fine-tuning of renal salt excretion and pH homeostasis. Genetic inactivation of Kir5.1 causes hypokalemia and results in the propensity to develop metabolic acidosis, hypomagnesemia and hypocalcemia. The phenotypes of Kir5.1 knockout mouse models mimic at least to some extent the clinical symptoms of a patient homozygous for R35Q, a rare missense variation of Kir5.1. However, in heterologous expression system, the R35Q mutant of Kir5.1 produced normal channel currents indicating that this variant is at least not a complete loss-of-function mutant. Further studies and the data from additional patients are required to decipher the precise role of Kir5.1 in the kidney and its possible role for human diseases.

6. Summary

In the kidney, inwardly rectifying K^+ channels of the Kir (KCNJ) family are essential for the control of salt transport. In the basolateral membrane of distal convoluted tubules (DCT), Kir4.1 (KCNJ10) together with Kir5.1 (KCNJ16) appears to be relevant for salt transport and adaptation of DCT to plasma K^+ levels, so called K^+ sensing. Loss-of-function mutations in KCNJ10 are known to result in EAST/SeSAME syndrome, a complex disorder with a renal salt wasting tubulopathy and alkalosis. Also for Kir5.1 a role in renal transport is likely: Paulais et al. observed hypokalemia, acidosis and hypercalciuria in a Kir5.1$^{-/-}$ mouse model and our collaborator Prof. Konrad identified in a patient with hypokalemia and acidosis a homozygous mutation of Kir5.1 (R35Q).

We hypothesized that the mutation R35Q leads to impaired channel function and disturbed salt transport in the kidney, especially in the DCT. To address this question, I characterized the mutant Kir5.1 channel and studied the phenotype of Kir5.1$^{-/-}$ mice.

The effect of the Kir5.1^{R35Q} mutant on protein function was analyzed using immunofluorescence and patch-clamp experiments. Although computer algorithms had predicted a functional deficit, I found the conductance of cells transfected with Kir4.1-Kir5.1^{R35Q} heteromers unaltered compared to Kir4.1-Kir5.1^{wt}. Also on the single channel level, the properties of the Kir5.1^{R35Q} mutant were normal and the subcellular localization appeared unaltered. Taken together, the function of the Kir5.1^{R35Q} mutant seems at least largely preserved or normal. However, smaller functional deficits or modified channel regulation might still have escaped our notice.

To gain further insights into the role of Kir5.1 in the kidney, I investigated the renal phenotype of another Kir5.1$^{-/-}$ mouse model (not identical to the one of Paulais et al.). Using sorted tubules, I observed high Kir5.1 mRNA expression in DCT and in proximal tubules. Analysis of the Kir5.1$^{-/-}$ mice corroborated the hypokalemia phenotype, but the acidosis appeared compensated. Kir5.1$^{-/-}$ mice displayed a pathologically increased renal salt loss when fed a high NaCl diet pointing to a reduced capacity to adapt to dietary salt intake. To elucidate the role of Kir5.1 for K^+ sensing in the DCT, isolated DCTs were exposed to changes of basolateral and apical K^+. Fura-2 measurements revealed that only basolateral, but not apical, application of low K^+* solution increased intracellular Ca^{2+} levels. However, deletion of Kir5.1 did not alter the Ca^{2+} signals suggesting that Kir5.1 channels are not essential for this component of the K^+ sensing mechanism.

Taken together, this study provided evidence that the rare Kir5.1 variant R35Q is probably not (or not alone) causative for acidosis and hypokalemia observed in a single patient

carrying this mutation. Nevertheless, our Kir5.1 knockout showed similar symptoms. Clearly, the role of Kir5.1 in the kidney is very complex and still incompletely understood. Further studies and the data from additional patients are required to decipher the precise role of Kir5.1 in the kidney and its possible role for human diseases.

7. Zusammenfassung

In der Niere spielen die einwärtsgleichrichtenden K^+-Kanäle Kir4.1 (KCNJ10) und Kir5.1 (KCNJ16) eine wichtige Rolle. In der basolateralen Membran des distalen Konvoluts (DCT) sind Kir4.1/Kir5.1-Kanäle entscheidend für den Salztransport und die Anpassung des Transports an das Plasma-K+, das so genannte "K^+ Sensing". Mutationen von KCNJ10 führen zum EAST/SeSAME-Syndrom, einem komplexen Krankheitsbild mit renalem Salzverlust und Alkalose. Auch Kir5.1 soll eine Rolle in der Niere haben: Paulais et al. beobachteten Hypokaliämie, Azidose und Hyperkalziurie in einer Kir5.1$^{-/-}$-Maus und unser Kooperationspartner Prof. Konrad identifizierte in einem Patienten mit Hypokaliämie und Azidose eine homozygote Mutation von Kir5.1 (R35Q).

Wir hypothetisierten daher, dass die R35Q-Mutation krankheitsverursachend sein könnte und insbesondere den Transport im DCT beeinträchtigt. Um diese Frage zu klären, habe ich daher die R35Q-Mutante charakterisiert und den Phänotyp der Kir5.1$^{-/-}$-Maus untersucht.

Die Auswirkungen der Mutation habe ich mittels Immunfluoreszenz und Patch-Clamp untersucht. Obwohl Computeralgorithmen einen Funktionsdefekt vorhersagten, war die Leitfähigkeit von Zellen, die mit Kir4.1/Kir5.1^{R35Q} transfiziert waren, ähnlich denen von Zellen mit Wildtypkanälen. Auch auf der Einzelkanalebene war kein Funktionsdefekt nachweisbar und die subzelluläre Lokalisation erschien unverändert. Zusammengefasst war die Funktion der R35Q-Mutante scheinbar normal oder zumindest weitgehend erhalten. Jedoch ist es denkbar, dass uns kleinere Funktionsdefekte oder eine veränderte Regulation entgangen sind.

Um weitere Einblicke in die Rolle von Kir5.1 in der Niere zu erhalten, habe ich den Phänotyp eines von Paulais et al. unabhängigen Kir5.1-Knockoutmausmodells untersucht. Mittels sortierter Tubulussegmente beobachtete ich eine starke Kir5.1 mRNA-Expression im DCT und im proximalen Tubulus. Untersuchungen an der Knockoutmaus bestätigten die Hypokaliämie, die Azidose erschien jedoch kompensiert. Kir5.1$^{-/-}$-Mäuse zeigten einen pathologisch verstärkten renalen Salzverlust unter einer hoch-NaCl-Diät, was für eine beeinträchtige Fähigkeit zur Anpassung an die diätetische Salzaufnahme spricht. Um die Rolle von Kir5.1 für das „K^+ Sensing" im DCT zu untersuchen, wurden isolierte DCTs veränderten K^+ Konzentrationen auf der basolateralen oder apikalen Seite ausgesetzt. Fura-2-Messungen zeigten, dass nur die basolaterale, nicht aber apikale Erniedrigung des K^+ zu einem intrazellulären Ca^{2+}-Anstieg führte. Jedoch war dieses Ca^{2+}-Signal unabhängig von der Anwesenheit von Kir5.1, was darauf hinweist, dass Kir5.1 bei dieser Komponente des „K^+ Sensings" keine Rolle spielt.

Zusammengefasst liefert diese Studie Hinweise, dass die seltene Kir5.1-Variante R35Q vermutlich nicht (oder nicht alleine) für die Azidose und die Hypokaliämie des einzelnen Patienten verantwortlich ist. Nichtsdestotrotz zeigten unsere Kir5.1-Knockoutmäuse einen ähnlichen Phänotyp. Ganz offensichtlich ist die Rolle von Kir5.1 in der Niere sehr komplex und noch immer nur unvollständig verstanden. Weitere Studien und zusätzliche Patientendaten werden nötig sein, um die genaue Funktion von Kir5.1 in der Niere und seine Bedeutung für menschliche Erkrankungen zu klären.

8. References

1. Zhuo, J. L. & Li, X. C. Proximal nephron. *Compr. Physiol.* **3,** 1079–123 (2013).

2. Subramanya, A. R. & Ellison, D. H. Distal convoluted tubule. *Clin. J. Am. Soc. Nephrol.* **9,** 2147–63 (2014).

3. Eladari, D., Chambrey, R. & Peti-Peterdi, J. A new look at electrolyte transport in the distal tubule. *Annu. Rev. Physiol.* **74,** 325–49 (2012).

4. Zacchia, M., Abategiovanni, M. L., Stratigis, S. & Capasso, G. Potassium: From Physiology to Clinical Implications. *Kidney Dis. (Basel, Switzerland)* **2,** 72–9 (2016).

5. Welling, P. A. Roles and Regulation of Renal K Channels. *Annu Rev Physiol* **78,** 415–435 (2016).

6. Ellison, D. H., Terker, A. S. & Gamba, G. Potassium and Its Discontents: New Insight, New Treatments. *J. Am. Soc. Nephrol.* **27,** 981–9 (2016).

7. Xi, Q., Hoenderop, J. G. J. & Bindels, R. J. M. Regulation of magnesium reabsorption in DCT. *Pflugers Arch.* **458,** 89–98 (2009).

8. McCormick, J. A. & Ellison, D. H. in *Comprehensive Physiology* 45–98 (John Wiley & Sons, Inc., 2014). doi:10.1002/cphy.c140002

9. Hoenderop, J. G. J., Nilius, B. & Bindels, R. J. M. Calcium absorption across epithelia. *Physiol. Rev.* **85,** 373–422 (2005).

10. Hamilton, K. L. & Devor, D. C. Basolateral membrane K+ channels in renal epithelial cells. *Am. J. Physiol. Renal Physiol.* **302,** F1069-81 (2012).

11. Faroqui, S., Sheriff, S. & Amlal, H. Metabolic acidosis has dual effects on sodium handling by rat kidney. *Am. J. Physiol. Renal Physiol.* **291,** F322-31 (2006).

12. Lee, C.-T., Ng, H., Lee, Y., Lai, L. & Lien, Y.-H. H. The role of calbindin-D28k on renal calcium and magnesium handling during treatment with loop and thiazide diuretics. *Am. J. Physiol. Renal Physiol.* **310,** F230-6 (2016).

13. Alexander, R. T. & Dimke, H. Effect of diuretics on renal tubular transport of calcium and magnesium. *Am. J. Physiol. Renal Physiol.* **312,** F998–F1015 (2017).

14. Hoenderop, J. G. J. *et al.* Renal Ca2+ wasting, hyperabsorption, and reduced bone thickness in mice lacking TRPV5. *J. Clin. Invest.* **112,** 1906–14 (2003).

15. Reilly, R. F. & Ellison, D. H. Mammalian distal tubule: physiology, pathophysiology, and molecular anatomy. *Physiol. Rev.* **80,** 277–313 (2000).

16. Bandulik, S. *et al.* The salt-wasting phenotype of EAST syndrome, a disease with multifaceted symptoms linked to the KCNJ10 K+ channel. *Pflugers Arch.* **461,** 423–35 (2011).

17. Terker, A. S. *et al.* Unique chloride-sensing properties of WNK4 permit the distal nephron to modulate potassium homeostasis. *Kidney Int.* **89,** 127–34 (2016).

18. Penton, D. *et al.* Extracellular K(+) rapidly controls NaCl cotransporter phosphorylation in the native distal convoluted tubule by Cl(-) -dependent and independent mechanisms. *J. Physiol.* **594,** 6319–6331 (2016).

19. Dong, K. *et al.* Romk1 Knockout Mice Do Not Produce Bartter Phenotype but Exhibit Impaired K Excretion. *J. Biol. Chem.* **291,** 5259–69 (2016).

20. van der Hagen, E. A. E. *et al.* The Na+/Ca2+ Exchanger 1 (NCX1) Variant 3 as the Major Extrusion System in Renal Distal Tubular Transcellular Ca2+-Transport. *Nephron* **131,** 145–52 (2015).

21. Lambers, T. T., Bindels, R. J. M. & Hoenderop, J. G. J. Coordinated control of renal Ca2+ handling. *Kidney Int.* **69,** 650–4 (2006).

22. Hoover, R. S., Tomilin, V., Hanson, L., Pochynyuk, O. & Ko, B. PTH modulation of NCC activity regulates TRPV5 Ca2+ reabsorption. *Am. J. Physiol. Renal Physiol.* **310,** F144-51 (2016).

23. Jeon, U. S. Kidney and calcium homeostasis. *Electrolyte Blood Press.* **6,** 68–76 (2008).

24. Blaine, J., Chonchol, M. & Levi, M. Renal control of calcium, phosphate, and magnesium homeostasis. *Clin. J. Am. Soc. Nephrol.* **10,** 1257–72 (2015).

25. Scholl, U. I. *et al.* SeSAME/EAST syndrome--phenotypic variability and delayed activity of the distal convoluted tubule. *Pediatr. Nephrol.* **27,** 2081–2090 (2012).

26. Terker, A. S. *et al.* Potassium modulates electrolyte balance and blood pressure through effects on distal cell voltage and chloride. *Cell Metab.* **21,** 39–50 (2015).

27. Cheng, C.-J., Shiang, J.-C., Hsu, Y.-J., Yang, S.-S. & Lin, S.-H. Hypocalciuria in patients with Gitelman syndrome: role of blood volume. *Am. J. Kidney Dis.* **49,** 693–700 (2007).

28. McCormick, J. A. *et al.* Hyperkalemic hypertension-associated cullin 3 promotes WNK signaling by degrading KLHL3. *J. Clin. Invest.* **124,** 4723–36 (2014).

29. Vidal-Petiot, E. *et al.* WNK1-related Familial Hyperkalemic Hypertension results from an

increased expression of L-WNK1 specifically in the distal nephron. *Proc. Natl. Acad. Sci. U. S. A.* **110,** 14366–71 (2013).

30. Reichold, M. *et al.* KCNJ10 gene mutations causing EAST syndrome (epilepsy, ataxia, sensorineural deafness, and tubulopathy) disrupt channel function. *Proc. Natl. Acad. Sci. U. S. A.* **107,** 14490–5 (2010).

31. Méndez-González, M. P. *et al.* Novel KCNJ10 Gene Variations Compromise Function of Inwardly Rectifying Potassium Channel 4.1. *J. Biol. Chem.* **291,** 7716–26 (2016).

32. Williams, D. M. *et al.* Molecular basis of decreased Kir4.1 function in SeSAME/EAST syndrome. *J. Am. Soc. Nephrol.* **21,** 2117–29 (2010).

33. Bockenhauer, D. *et al.* Epilepsy, ataxia, sensorineural deafness, tubulopathy, and KCNJ10 mutations. *N. Engl. J. Med.* **360,** 1960–70 (2009).

34. Scholl, U. I. *et al.* Seizures, sensorineural deafness, ataxia, mental retardation, and electrolyte imbalance (SeSAME syndrome) caused by mutations in KCNJ10. *Proc. Natl. Acad. Sci. U. S. A.* **106,** 5842–7 (2009).

35. Freudenthal, B. *et al.* KCNJ10 mutations disrupt function in patients with EAST syndrome. *Nephron. Physiol.* **119,** p40-8 (2011).

36. Cheng, C.-J., Sung, C.-C., Huang, C.-L. & Lin, S.-H. Inward-rectifying potassium channelopathies: new insights into disorders of sodium and potassium homeostasis. *Pediatr. Nephrol.* **30,** 373–83 (2015).

37. Su, X.-T. *et al.* Disruption of KCNJ10 (Kir4.1) stimulates the expression of ENaC in the collecting duct. *Am. J. Physiol. Renal Physiol.* **310,** F985-93 (2016).

38. Kuang, Q., Purhonen, P. & Hebert, H. Structure of potassium channels. *Cell. Mol. Life Sci.* **72,** 3677–93 (2015).

39. Sepúlveda, F. V, Pablo Cid, L., Teulon, J. & Niemeyer, M. I. Molecular aspects of structure, gating, and physiology of pH-sensitive background K2P and Kir K+-transport channels. *Physiol. Rev.* **95,** 179–217 (2015).

40. Hibino, H. *et al.* Inwardly rectifying potassium channels: their structure, function, and physiological roles. *Physiol. Rev.* **90,** 291–366 (2010).

41. Pessia, M., Tucker, S. J., Lee, K., Bond, C. T. & Adelman, J. P. Subunit positional effects revealed by novel heteromeric inwardly rectifying K+ channels. *EMBO J.* **15,** 2980–7 (1996).

42. Sansom, M. S. P. *et al.* Potassium channels: structures, models, simulations. *Biochim.*

Biophys. Acta **1565,** 294–307 (2002).

43. Abraham, M. R., Jahangir, A., Alekseev, a E. & Terzic, A. Channelopathies of inwardly rectifying potassium channels. *FASEB J.* **13,** 1901–10 (1999).

44. Pattnaik, B. R., Asuma, M. P., Spott, R. & Pillers, D.-A. M. A. M. Genetic defects in the hotspot of inwardly rectifying K(+) (Kir) channels and their metabolic consequences: a review. *Mol. Genet. Metab.* **105,** 64–72 (2012).

45. Ishii, M. *et al.* Differential expression and distribution of Kir5.1 and Kir4.1 inwardly rectifying K+ channels in retina. *Am. J. Physiol. Cell Physiol.* **285,** C260-7 (2003).

46. Pan, C. *et al.* Downregulation of inwardly rectifying potassium channel 5.1 expression in C57BL/6J cochlear lateral wall. *J. Huazhong Univ. Sci. Technolog. Med. Sci.* **36,** 406–9 (2016).

47. Hibino, H. *et al.* Expression of an inwardly rectifying K+ channel, Kir5.1, in specific types of fibrocytes in the cochlear lateral wall suggests its functional importance in the establishment of endocochlear potential. *Eur. J. Neurosci.* **19,** 76–84 (2004).

48. Cuevas, C. A. *et al.* Potassium Sensing by Renal Distal Tubules Requires Kir4.1. *J. Am. Soc. Nephrol.* **28,** 1814–1825 (2017).

49. Su, X.-T. & Wang, W.-H. The expression, regulation, and function of Kir4.1 (Kcnj10) in the mammalian kidney. *Am. J. Physiol. Renal Physiol.* **311,** F12-5 (2016).

50. Lachheb, S. *et al.* Kir4.1/Kir5.1 channel forms the major K+ channel in the basolateral membrane of mouse renal collecting duct principal cells. *Am. J. Physiol. Renal Physiol.* **294,** F1398-407 (2008).

51. Tanemoto, M., Kittaka, N., Inanobe, A. & Kurachi, Y. In vivo formation of a proton-sensitive K+ channel by heteromeric subunit assembly of Kir5.1 with Kir4.1. *J. Physiol.* **525 Pt 3,** 587–92 (2000).

52. Zaika, O. L. *et al.* Direct inhibition of basolateral Kir4.1/5.1 and Kir4.1 channels in the cortical collecting duct by dopamine. *Am. J. Physiol. Renal Physiol.* **305,** F1277-87 (2013).

53. Rapedius, M. *et al.* Control of pH and PIP2 gating in heteromeric Kir4.1/Kir5.1 channels by H-Bonding at the helix-bundle crossing. *Channels (Austin).* **1,** 327–30 (2007).

54. Paulais, M. *et al.* Renal phenotype in mice lacking the Kir5.1 (Kcnj16) K+ channel subunit contrasts with that observed in SeSAME/EAST syndrome. *Proc. Natl. Acad. Sci. U. S. A.* **108,** 10361–6 (2011).

55. Tucker, S. J., Imbrici, P., Salvatore, L., D'Adamo, M. C. & Pessia, M. pH dependence of the inwardly rectifying potassium channel, Kir5.1, and localization in renal tubular epithelia. *J. Biol. Chem.* **275,** 16404–7 (2000).

56. Shang, L., Ranson, S. V. & Tucker, S. J. Kir5.1 underlies long-lived subconductance levels in heteromeric Kir4.1/Kir5.1 channels from Xenopus tropicalis. *Biochem. Biophys. Res. Commun.* **388,** 501–5 (2009).

57. Pessia, M., Imbrici, P., D'Adamo, M. C., Salvatore, L. & Tucker, S. J. Differential pH sensitivity of Kir4.1 and Kir4.2 potassium channels and their modulation by heteropolymerisation with Kir5.1. *J. Physiol.* **532,** 359–67 (2001).

58. Lam, H. D., Lemay, A.-M., Briggs, M. M., Yung, M. & Hill, C. E. Modulation of Kir4.2 rectification properties and pHi-sensitive run-down by association with Kir5.1. *Biochim. Biophys. Acta* **1758,** 1837–45 (2006).

59. Ramos, H. E. *et al.* Molecular insights into the possible role of Kir4.1 and Kir5.1 in thyroid hormone biosynthesis. *Horm. Res. Paediatr.* **83,** 141–7 (2015).

60. D'Adamo, M. C. *et al.* Genetic inactivation of Kcnj16 identifies Kir5.1 as an important determinant of neuronal PCO2/pH sensitivity. *J. Biol. Chem.* **286,** 192–8 (2011).

61. Trapp, S., Tucker, S. J. & Gourine, A. V. Respiratory responses to hypercapnia and hypoxia in mice with genetic ablation of Kir5.1 (Kcnj16). *Exp. Physiol.* **96,** 451–9 (2011).

62. Xu, H., Cui, N., Yang, Z., Qu, Z. & Jiang, C. Modulation of kir4.1 and kir5.1 by hypercapnia and intracellular acidosis. *J. Physiol.* **524 Pt 3,** 725–35 (2000).

63. Cui, N. *et al.* Modulation of the heteromeric Kir4.1-Kir5.1 channels by P(CO(2)) at physiological levels. *J. Cell. Physiol.* **189,** 229–36 (2001).

64. Greger, R. & Hampel, W. A modified system for in vitro perfusion of isolated renal tubules. *Pflugers Arch.* **389,** 175–6 (1981).

65. Liu, Y. *et al.* The human inward rectifier K(+) channel subunit kir5.1 (KCNJ16) maps to chromosome 17q25 and is expressed in kidney and pancreas. *Cytogenet. Cell Genet.* **90,** 60–3 (2000).

66. https://www.ncbi.nlm.nih.gov/UniGene/ESTProfileViewer.cgi?uglist=Hs.463985.

67. https://www.ncbi.nlm.nih.gov/UniGene/ESTProfileViewer.cgi?uglist=Mm.30176.

68. Gong, Y. *et al.* Claudin-14 regulates renal Ca^{++} transport in response to CaSR signalling via a novel microRNA pathway. *EMBO J.* **31,** 1999–2012 (2012).

69. Humberg, E. Die physiologische und pathophysiologische Bedeutung von KCNJ16. (PhD Thesis, Universität Regensburg, 2014).

70. Yamaguchi, D. T., Green, J., Kleeman, C. R. & Muallem, S. Properties of the depolarization-activated calcium and barium entry in osteoblast-like cells. *J. Biol. Chem.* **264,** 197–204 (1989).

71. Sohma, Y., Harris, A., Wardle, C. J., Argent, B. E. & Gray, M. A. Two barium binding sites on a maxi K+ channel from human vas deferens epithelial cells. *Biophys. J.* **70,** 1316–25 (1996).

72. Hibino, H., Fujita, A., Iwai, K., Yamada, M. & Kurachi, Y. Differential assembly of inwardly rectifying K+ channel subunits, Kir4.1 and Kir5.1, in brain astrocytes. *J. Biol. Chem.* **279,** 44065–73 (2004).

73. Casamassima, M., D'Adamo, M. C., Pessia, M. & Tucker, S. J. Identification of a heteromeric interaction that influences the rectification, gating, and pH sensitivity of Kir4.1/Kir5.1 potassium channels. *J. Biol. Chem.* **278,** 43533–40 (2003).

74. Palygin, O. *et al.* Essential role of Kir5.1 channels in renal salt handling and blood pressure control. *JCI Insight* **2,** 1–16 (2017).

75. Combe, R. *et al.* How Does Circadian Rhythm Impact Salt Sensitivity of Blood Pressure in Mice? A Study in Two Close C57Bl/6 Substrains. *PLoS One* **11,** e0153472 (2016).

76. Walkowska, A., Pawlak, M., Jane, S. M., Kompanowska-Jezierska, E. & Wilanowski, T. Effects of high and low sodium diet on blood pressure and heart rate in mice lacking the functional grainyhead-like 1 gene. *Physiol. Res.* **66,** 163–165 (2017).

77. Picard, N. *et al.* Protein phosphatase 1 inhibitor-1 deficiency reduces phosphorylation of renal NaCl cotransporter and causes arterial hypotension. *J. Am. Soc. Nephrol.* **25,** 511–22 (2014).

78. Przywara, D. A., Chowdhury, P. S., Bhave, S. V, Wakade, T. D. & Wakade, A. R. Barium-induced exocytosis is due to internal calcium release and block of calcium efflux. *Proc. Natl. Acad. Sci. U. S. A.* **90,** 557–61 (1993).

79. Mouri, T. *et al.* Assignment of mouse inwardly rectifying potassium channel Kcnj16 to the distal region of mouse chromosome 11. *Genomics* **54,** 181–2 (1998).

80. Shang, L. & Tucker, S. J. Non-equivalent role of TM2 gating hinges in heteromeric Kir4.1/Kir5.1 potassium channels. *Eur. Biophys. J.* **37,** 165–71 (2008).

81. Weinstein, A. M. A mathematical model of rat distal convoluted tubule. I. Cotransporter function in early DCT. *Am. J. Physiol. Renal Physiol.* **289,** F699-720 (2005).

82. Cha, S.-K., Kim, J.-H. & Huang, C.-L. Flow-induced activation of TRPV5 and TRPV6 channels stimulates Ca(2+)-activated K(+) channel causing membrane hyperpolarization. *Biochim. Biophys. Acta* **1833,** 3046–3053 (2013).

83. Ripper, M. Die Bedeutung des basolateralen Kalium-Kanals KCNJ10 für die Transportfunktion in der Niere. (PhD Thesis, Universität Regensburg, 2016).

84. Kotchen, T. A., Cowley, A. W. & Frohlich, E. D. Salt in health and disease--a delicate balance. *N. Engl. J. Med.* **368,** 1229–37 (2013).

85. O'Donnell, M. *et al.* Urinary sodium and potassium excretion, mortality, and cardiovascular events. *N. Engl. J. Med.* **371,** 612–23 (2014).

86. Mente, A. *et al.* Association of urinary sodium and potassium excretion with blood pressure. *N. Engl. J. Med.* **371,** 601–11 (2014).

87. Zhang, X. *et al.* The disruption of central CO2 chemosensitivity in a mouse model of Rett syndrome. *Am. J. Physiol. Cell Physiol.* **301,** C729-38 (2011).

88. Yamamoto, Y., Ishikawa, R., Omoe, K. & Taniguchi, K. Expression of inwardly rectifying K+ channels in the carotid body of rat. *Histol. Histopathol.* **23,** 799–806 (2008).

9. Supplements

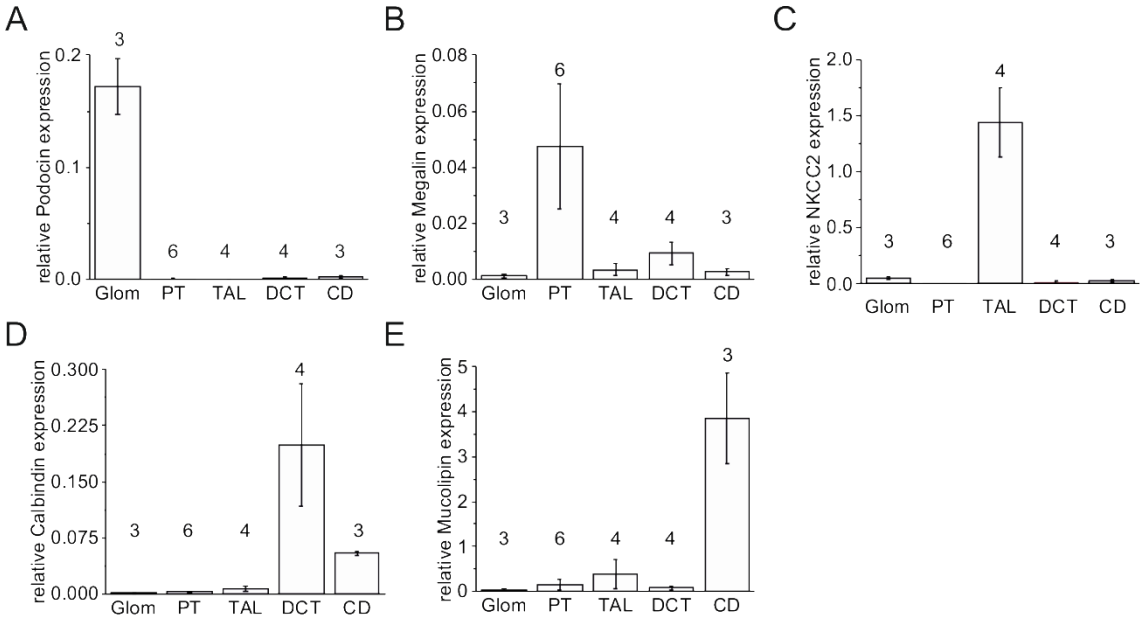

Figure S1. Relative expression of tubule markers.
Relative expression of tubule markers (A) podocin (glomeruli), (B) megalin (PT), (C) NKCC2 (TAL), (D) calbindin (DCT) and (E) mucolipin (CD) in sorted tubules to verify the correct sorting of each tubular segment. Abbreviations: Glom = glomeruli; PT = proximal tubule; TAL = thick ascending limb; DCT = distal convoluted tubule and CD = collecting duct. The numbers corresponds to the amount of idenpendent tubular preparations analyzed. Data is shown as mean±SEM.

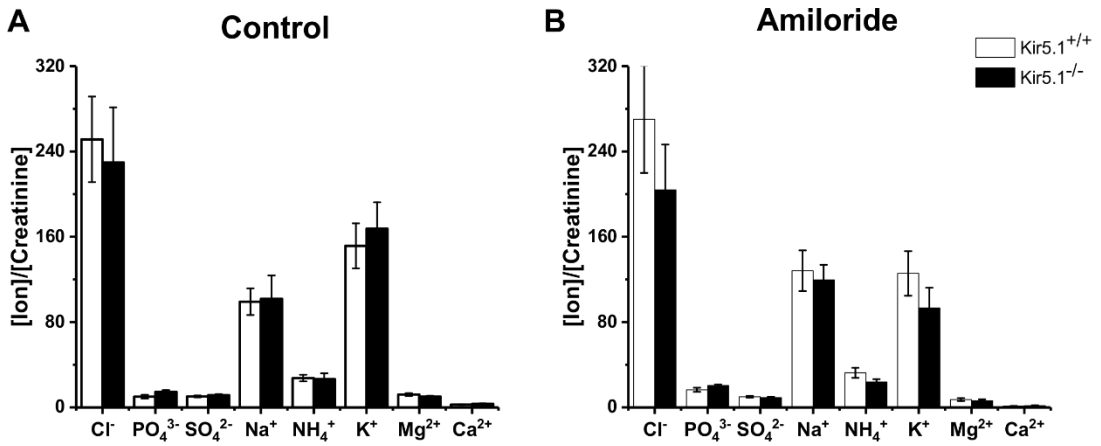

Figure S2. Effect of amiloride on normalized electrolyte excretion of Kir5.1$^{+/+}$ and Kir5.1$^{-/-}$ mice.
Electrolyte excretion of Kir5.1$^{-/-}$ (n = 19, ■) and control Kir5.1$^{+/+}$ (n=20, □) mice. All ions concentration were normalized to creatinine concentration in urine and presented as [mM ion/mM creatinine]. Statistical analysis was performed with an unpaired Student's t-test between the two groups or paired t-test between control and amiloride of each group. After Bonferroni corrections, p-values ≤ 0.006 were accepted as significantly different. Phosphate and Ca^{2+} were significantly different in Ki5.1$^{-/-}$ mice, while Ca^{2+} was significantly different for Kir5.1$^{+/+}$ between control and amiloride (paired t-test). Data was partially shown in Figure 18.

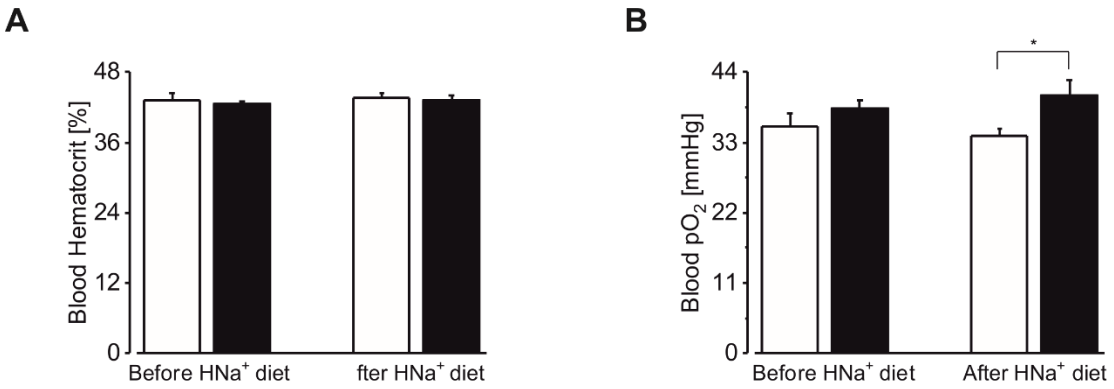

Figure S3. Effects of high salt diet on blood parameters of Kir5.1$^{+/+}$ and Kir5.1$^{-/-}$.
(A) Hematocrit and (B) pO_2 were analyzed by blood-gas analyzer of blood samples obtained from facial vein of conscious Kir5.1$^{+/+}$ (□) and Kir5.1$^{-/-}$ (■) mice Data represents mean values ± SEM. Statistical analysis was performed with a paired Student's t-test between before and after the diet for Kir5.1$^{-/-}$ and for Kir5.1$^{+/+}$. In addition, to an unpaired Student's t-test between Kir5.1$^{-/-}$ and Kir5.1$^{+/+}$ (*, p≤0.05).

Table S1. Normalized excretion of various electrolytes from Kir5.1$^{+/+}$ and Kir5.1$^{-/-}$ mice under high Na$^+$ diet.
Electrolyte excretion of Kir5.1$^{+/+}$ (n = 10) and Kir5.1$^{-/-}$ (n = 8) mice throughout the high salt diet. All ions concentrations were normalized to creatinine concentration in the urine and presented as [mM ion/mM creatinine]. Data represents mean±SEM. Statistical analysis was performed with unpaired Student's t-test between the two groups with Bonferroni corrections (p-value≤0.006) was considered statistically significant. Data was partially shown in Figure 19.

		Cl^-	PO_4^{3-}	SO_4^{2-}	Na^+	$NH4^+$	K^+	Mg^{2+}	Ca^{2+}
Control	**Mean Kir5.1$^{-/-}$**	72.9	13.0	17.0	38.3	39.3	134.4	21.7	3.8
	SEM	10.0	1.1	2.0	4.9	7.5	9.6	1.3	0.4
	Mean Kir5.1$^{+/+}$	50.1	10.0	12.5	21.6	14.9	90.2	11.1	1.1
	SEM	6.1	1.5	1.1	1.4	1.1	7.2	0.4	0.1
	p-value	0.10	0.15	0.10	0.01	0.02	0.004	≤0.001	≤0.001
Day 3	**Mean Kir5.1$^{-/-}$**	85.7	11.8	14.9	69.5	27.2	39.7	11.5	3.1
	SEM	21.1	0.9	1.7	14.7	5.5	6.1	1.4	0.5
	Mean Kir5.1$^{+/+}$	73.6	19.4	11.3	45.4	17.1	37.6	13.2	1.3
	SEM	15.7	2.1	2.2	7.7	2.6	9.0	1.1	0.2
	p-value	0.67	0.003	0.23	0.20	0.15	0.85	0.36	0.01
Day 8	**Mean Kir5.1$^{-/-}$**	448.4	29.8	29.0	292.8	62.1	131.5	16.1	2.7
	SEM	66.7	3.1	3.3	37.3	10.1	23.3	1.5	0.6
	Mean Kir5.1$^{+/+}$	181.3	12.4	15.4	129.3	24.3	39.2	9.9	0.9
	SEM	43.6	3.6	1.8	24.6	3.8	8.7	1.1	0.1
	p-value	0.007	0.003	0.005	0.004	0.006	0.004	0.005	0.015
Day 16	**Mean Kir5.1$^{-/-}$**	342.4	24.0	26.3	247.6	52.0	96.1	19.7	3.0
	SEM	84.7	4.4	4.7	49.8	10.6	23.5	2.2	0.4
	Mean Kir5.1$^{+/+}$	91.5	8.7	8.3	59.9	18.1	19.3	10.0	1.0
	SEM	22.9	1.7	1.7	14.5	3.5	6.7	1.1	0.1
	p-value	0.027	0.012	0.007	0.007	0.018	0.016	0.003	0.002

10. List of Figures

11. List of Tables

12. List of abbreviations

11-βHSD2	11-β hydroxysteroid dehydrogenase 2
AQP2	Aquaporin 2
ATP	Adenosine 5′-triphosphate
ATPase	Adenosine triphosphatase
BSA	Bovines Serum Albumin
BW	Body weight
Ca^{2+}	Calcium
CaSR	Ca^{2+} sensing receptor
CC	Current Clamp Modus
CC-0	Current Clamp Zero Modus
CD	Collecting duct
cDNA	complementary DNA
CHO	Chinese hamster ovary cells
Cl^-	Chloride
ClC_{KB}	Chloride channel Kb
CNT	Connecting tubule
DCT	Distal convoluted Tubule
EAST	Epilepsy, ataxia, sensorineural deafness and salt-wasting renal tubulopathy
EDTA	Ethylendiamintetraessigsäure
EGTA	Ethylene glycol-bis(2-aminoethylether)-N,N,N',N'-tetraacetic acid
ENaC	Epithelial sodium channel
FCS	fetal calf serum
FHHt	Familial hyperkalemic hypertension
GFR	Glomerular filtration rate
HEK	Human embryonic kidney cells
HEPES	4-(2-hydroxyethyl)-1-piperazineethanesulfonic acid
i.p.	Intraperitoneal
IC	Ion Chromatography
K^+	Potassium
Kir	Inwardly rectifying Potassium channel
LacZ	Operon lactose
Mg^{2+}	Magnesium

mRNA	messenger RNA
Na^+	Sodium
NCC	Sodium-chloride co-transporter
NCX1	Sodium-calcium exchanger
NH_4^+	Ammonium
PCR	Polymerase chain reaction
PE	Polyethylene
PFA	Paraformaldehyde
PMCA	Plasma membrane Ca^{2+}-ATPase
PO_4^{3-}	Phosphate
PT	Proximal tubule
PTH	Parathyroid Hormone
ROMK	Renal outer medullary potassium channel
SDS	sodium dodecyl sulfate
Sesame	Seizures, sensorineural deafness, ataxia, mental retardation and electrolyte imbalances
SNPs	Single nucleotide polymorphism
SO_4^{2-}	Sulfate
TAL	Thick Ascending Limb
TM	Transmembrane domain
TRPM6	transient receptor potential ion channel 6
TRPV5	Transient receptor potential cation channel subfamily V member 5
V_C	Voltage clamp
Vitamin D3	1,25-dihydroxyvitamin D3
V_m	Membrane potential
WNK	Serine-threonine kinase
X-Gal	5-bromo-4-chloro-3-indolyl-β-D-galactopyranoside

13. Attachment

13.1 Congresses

Quintanova C., Forst AL., Afonso S., Fischer A., Warth R. The role of the inwardly rectifying potassium channels Kir4.1 and Kir5.1 in the distal convoluted tubule. 96th Annual Meeting of the German Physiological Society March 2017 in Greifswald – Poster

Afonso S., Forst AL., Quintanova C., Ripper M., Reichold M., Warth R. A role of the inwardly rectifying potassium channel Kir4.1 in the regulation of water homeostasis? 96th Annual Meeting of the German Physiological Society March 2017 in Greifswald – Poster

Forst AL., Quintanova C., Afonso S., Fischer A., Reichold M., Warth R. The role of the inwardly rectifying potassium channels Kir4.1, Kir4.2 und Kir5.1 in the distal convoluted tubule. Kongress für Nephrologie September 2016 in Berlin – 8. Jahrestagung der Deutschen Gesellschaft für Nephrologie – Poster

Quintanova C., Afonso S., Forst AL., Konrad M., Warth R. Heteromeric KCNJ10 and KCNJ16 potassium channels: Functional consequences of the rare KCNJ16 variant p.R35Q. 95th Annual Meeting of the German Physiological Society March 2016 in Lübeck – Poster

Quintanova C., Sterner C., Afonso S., Meier C., Forst AL., Warth R. Expression and localization of KCNJ16 in various mouse tissues. 95th Annual Meeting of the German Physiological Society March 2016 in Lübeck – Poster

14. Acknowledgements

I would like to thank all the people that directly or indirectly contributed for the success of this work.

First, I would like to thank my supervisor Prof. Dr. Richard Warth for the opportunity to join this PhD. For all his help and supervision during this project that proved challenging but at the same time inspiring given the outdated difficulties. For the experience, that in science as in life not everything goes well at first attempt.

A special thanks to all my colleagues in the AG Warth lab group, Sascha, Ines, Christina, Anna-Lena, Markus, Sara and Julia W. for all the wonderful time and help. I want to thank Philipp and Markus for the introduction and valuable tips in the patch clamp and single channel. To Christina, for the kind introduction to the lab work and all the help in cloning and mice work. To Ines, for all the cell culture knowledge and for the analysis of many samples in the ion chromatography which were indispensable for my results. To my office companions, Sara, Julia S. and Julia W. for all the good time and funny conversations that lightened the mood. To Sara, for all the conversations in Portuguese and for making my life easier in the lab and in Regensburg. Not forgetting my partners in table football ─ Sara, Anna-Lena and Markus ─ for all the amazing and funny afternoons.
To Anna-Lena, in particular, for all the scientific support, companionship in all the mice experiments and mostly in the correction of this thesis whose advises were invaluable. Not to mention all the movie theatre Monday evenings.

I would like to thank to Prof. Dr. Martin Konrad for all the data available on the patients. To Prof. Dr. Markus Bleich and Nina Himmerkus for teaching me how to sort and perfused mouse renal tubules which was an important part of my work.

Um obrigado à Carina, Rui, Karina, Flávio, Inês, Helena e Hélio pela companhia e fantásticas conversas em todos os cafés, brunches, almoços e jantares que fizeram com que a minha estadia em Regensburg fosse muito mais divertida.

Dedico esta tese aos meus Pais, por tudo o que fizeram por mim ao longo de toda o meu percurso e por acreditarem sempre em mim. Agradeço ao meu irmão por toda a motivação e por estar sempre do meu lado.